

AD-A131 882

LASER VELOCIMETER MEASUREMENTS AND ANALYSIS IN  
TURBULENT FLOWS WITH COMBU... (U) PURDUE UNIV LAFAYETTE  
IN SCHOOL OF MECHANICAL ENGINEERING

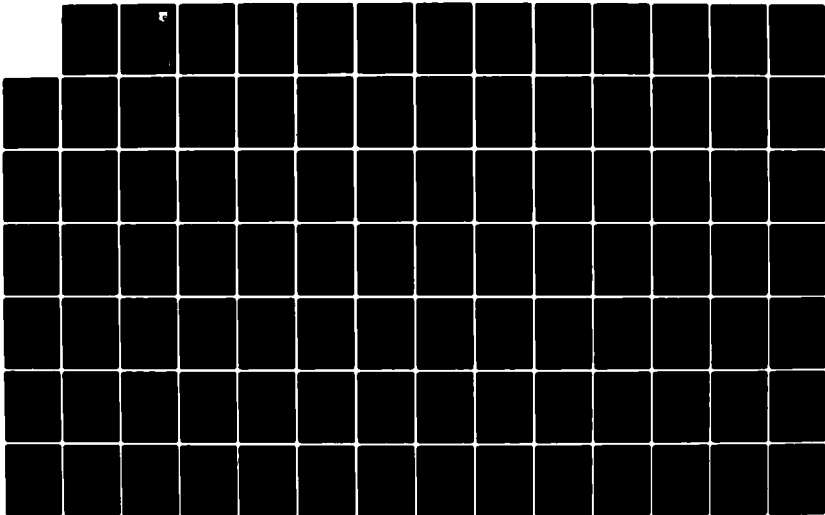
1/2

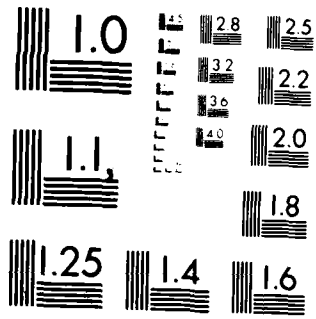
UNCLASSIFIED

W H STEVENSON ET AL. JUL 83

F/G 21/2

NL





MICROCOPY RESOLUTION TEST CHART  
NATIONAL BUREAU OF STANDARDS - 1963-A

2

ADA 131882

AFWAL-TR-82-2076  
Part II



LASER VELOCIMETER MEASUREMENTS AND ANALYSIS  
IN TURBULENT FLOWS WITH COMBUSTION  
PART II

W.H. STEVENSON  
H.D. THOMPSON  
R.D. GOULD

SCHOOL OF MECHANICAL ENGINEERING  
PURDUE UNIVERSITY  
WEST LAFAYETTE, INDIANA 47907

July 1983

Interim Report for Period January 1982 - December 1982

Approved for public release; distribution unlimited

DTIC FILE COPY

AERO PROPULSION LABORATORY  
AIR FORCE WRIGHT AERONAUTICAL LABORATORIES  
AIR FORCE SYSTEMS COMMAND  
WRIGHT-PATTERSON AIR FORCE BASE, OHIO 45433

DTIC  
UNCLASSIFIED  
AUG 30 1983  
E

83 08 26 084

NOTICE

When Government drawings, specifications, or other data are used for any purpose other than in connection with a definitely related Government procurement operation, the United States Government thereby incurs no responsibility nor any obligation whatsoever; and the fact that the government may have formulated, furnished, or in any way supplied the said drawings, specifications, or other data, is not to be regarded by implication or otherwise as in any manner licensing the holder or any other person or corporation, or conveying any rights or permission to manufacture, use, or sell any patented invention that may in any way be related thereto.

This report has been reviewed by the Office of Public Affairs (ASD/PA) and is releasable to the National Technical Information Service (NTIS). At NTIS, it will be available to the general public, including foreign nations.

This technical report has been reviewed and is approved for publication.

  
\_\_\_\_\_  
Roger R. Craig  
Project Engineer

  
\_\_\_\_\_  
Frank D. Stull, Chief  
Ramjet Technology Branch  
Ramjet Engine Division

FOR THE COMMANDER

  
\_\_\_\_\_  
James L. Radloff, Col. USAF  
Director, Ramjet Engine Division  
Aero Propulsion Laboratory

If your address has changed, if you wish to be removed from our mailing list, or if the addressee is no longer employed by your organization please notify AFWAL/PORT, WPAFB, OH 45433 to help us maintain a current mailing list. Copies of this report should not be returned unless return is required by security considerations, contractual obligations, or notice on a specific document.

UNCLASSIFIED

SECURITY CLASSIFICATION OF THIS PAGE (When Data Entered)

REPORT DOCUMENTATION PAGE		READ INSTRUCTIONS BEFORE COMPLETING FORM
1. REPORT NUMBER AFWAL-TR-82-2076	2. GOVT ACCESSION NO. Part II AD-A131552	3. RECIPIENT'S CATALOG NUMBER
4. TITLE (and Subtitle) LASER VELOCIMETER MEASUREMENTS AND ANALYSIS IN TURBULENT FLOWS WITH COMBUSTION PART II		5. TYPE OF REPORT & PERIOD COVERED Interim: 1 January 1982 31 December 1982
		6. PERFORMING ORG. REPORT NUMBER
7. AUTHOR(s) W.H. Stevenson, H.D. Thompson and R.D. Gould		8. CONTRACT OR GRANT NUMBER(s)  F33615-81-K-2003
9. PERFORMING ORGANIZATION NAME AND ADDRESS School of Mechanical Engineering Purdue University West Lafayette, Indiana 47907		10. PROGRAM ELEMENT, PROJECT, TASK AREA & WORK UNIT NUMBERS  2308-54-01
11. CONTROLLING OFFICE NAME AND ADDRESS Aero Propulsion Laboratory (AFWAL/PORT) Air Force Wright Aeronautical Lab. (AFSC) Wright-Patterson Air Force Base, Ohio 45433		12. REPORT DATE July 1983
		13. NUMBER OF PAGES 17
14. MONITORING AGENCY NAME & ADDRESS (if different from Controlling Office)		15. SECURITY CLASS. (of this report)  Unclassified
		15a. DECLASSIFICATION/DOWNGRADING SCHEDULE
16. DISTRIBUTION STATEMENT (of this Report)  Approved for public release; distribution unlimited		
17. DISTRIBUTION STATEMENT (of the abstract entered in Block 20, if different from Report)		
18. SUPPLEMENTARY NOTES		
19. KEY WORDS (Continue on reverse side if necessary and identify by block number)		
Turbulence measurements Laser velocimeter Bias errors (in laser velocimetry)		Recirculating flows Numerical Analysis Measurements in Combustion
20. ABSTRACT (Continue on reverse side if necessary and identify by block number)		
Laser velocimeter measurements in the highly turbulent flow field following an axisymmetric sudden expansion have been carried out for both isothermal and reacting flows. Mean streamwise velocity and turbulence intensity profiles covering the region from the sudden expansion to well beyond shear layer reattachment are presented. A study of velocity bias conducted as part of this investigation reconfirmed the effectiveness of the experimental bias elimination technique used in earlier studies. Numerical predictions of the		

UNCLASSIFIED

SECURITY CLASSIFICATION OF THIS PAGE(When Data Entered)

isothermal flow field using the  $k-\epsilon$  turbulence model were made and compared to experimental measurements. Significant differences in the mean velocity profiles were found to exist, with measured velocities in the central part of the flow being consistently higher than those predicted. Combustion was found to increase mean velocities in regions beyond the combustion zone as expected and to significantly alter the structure of the shear layer. Significant reductions in turbulence intensity were observed throughout most of the flow in the reacting flow case.

UNCLASSIFIED

FOREWORD

This interim technical report was submitted by the School of Mechanical Engineering of Purdue University under Contract No. F33615-81-K-2003 and covers the period 1 January 1982 - 31 December 1982. The research was sponsored by the Aero Propulsion Laboratory, Air Force Wright Aeronautical Laboratories, Wright-Patterson AFB, Ohio, under Project No. 2308 with Dr. Roger R. Craig AFWAL/PORT as Project Engineer. Warren H. Stevenson and H. Doyle Thompson of Purdue University were technically responsible for the work.

Accession For		
NTIS GRA&I	<input checked="" type="checkbox"/>	
DTIC TAB	<input type="checkbox"/>	
Unannounced	<input type="checkbox"/>	
Justification		
By _____		
Distribution/		
Availability Codes		
_____ and/or		
_____ Special		
A		



## TABLE OF CONTENTS

SECTION	PAGE
I. INTRODUCTION . . . . .	1
II. LITERATURE REVIEW . . . . .	4
1. Introduction . . . . .	4
2. Axisymmetric Sudden Expansions . . . . .	5
a. Past Experiments . . . . .	5
b. Separated Flow Regions . . . . .	7
c. Reattachment Length. . . . .	9
d. Mean Velocity and Turbulence Intensity. . . . .	13
e. Analytical Modeling of Axisymmetric Sudden Expansions. . . . .	15
3. Reacting Flows . . . . .	16
a. Introduction . . . . .	16
b. Comparison of Flows With and Without Combustion . . . . .	17
c. Effects of Axial Pressure Gradients. . . . .	23
d. Numerical Modeling . . . . .	26
4. LDV Measurement Accuracy . . . . .	28
a. Introduction . . . . .	28
b. LDV Measurement Errors . . . . .	28
c. Velocity Bias. . . . .	32
d. Bias Correction. . . . .	38
III. EXPERIMENTAL APPARATUS . . . . .	40
1. Introduction . . . . .	40
2. The LDV Optical System . . . . .	41

TABLE OF CONTENTS (cont'd)

SECTION	PAGE
3. The Flow System . . . . .	45
4. The Fuel System . . . . .	52
5. The Data, Collection, Storage and Processing System . . . . .	53
6. The Seeding Systems . . . . .	56
IV. EXPERIMENTAL TECHNIQUE . . . . .	58
1. Introduction . . . . .	58
2. Test Procedure . . . . .	59
3. Mean Velocities and Turbulence Parameter Measurements . . . . .	59
4. The Stream Function . . . . .	67
5. The Reattachment Length . . . . .	68
6. The Massflow Rate . . . . .	68
V. EXPERIMENTAL RESULTS. . . . .	70
1. Introduction . . . . .	70
2. Average Streamwise Velocity . . . . .	71
3. Streamwise Turbulence Intensity . . . . .	87
4. Skewness Coefficients . . . . .	109
5. The Reattachment Length . . . . .	115
6. The Stream Function . . . . .	115
7. The Massflow Rate . . . . .	118
8. Temperature Profiles . . . . .	119
VI. COMPARISON OF NUMERICAL ANALYSIS WITH ISOTHERMAL EXPERIMENTAL RESULTS . . . . .	123
1. Introduction . . . . .	123
2. Matching Reattachment Length . . . . .	128
3. Mean Streamwise Velocity . . . . .	128
VII. CONCLUSIONS AND RECOMMENDATIONS . . . . .	138
APPENDIX	
Experimental Data. . . . .	141
LIST OF REFERENCES . . . . .	151

## LIST OF ILLUSTRATIONS

FIGURE		PAGE
1	Separated Flow Regions in an Axisymmetric Sudden Expansion . . . . .	8
2	Corrected and Uncorrected Mean Streamwise Velocity Profiles in a Separated Region (from Ref. [47]) . . . . .	36
3	Corrected and Uncorrected rms Streamwise Velocity Profiles in a Separated Region (from Ref. [47]) . . . . .	37
4	LDV Optics Package . . . . .	42
5	Flow System . . . . .	46
6	Torch Ignitor . . . . .	49
7	Geometry of Axisymmetric Test Section . .	51
8	Fuel System . . . . .	54
9	Experimental Measurement Grid . . . . .	66
10	Measured Mean Streamwise Velocity Profile at $x/H = 1/3$ . . . . .	73
11	Measured Mean Streamwise Velocity Profiles at $x/H = 1$ . . . . .	74
12	Measured Mean Streamwise Velocity Profiles at $x/H = 3$ . . . . .	75
13	Measured Mean Streamwise Velocity Profiles at $x/H = 5$ . . . . .	76
14	Measured Mean Streamwise Velocity Profiles at $x/H = 7$ . . . . .	77
15	Measured Mean Streamwise Velocity Profiles at $x/H = 9$ . . . . .	78
16	Measured Mean Streamwise Velocity Profiles at $x/H = 11$ . . . . .	79

LIST OF ILLUSTRATIONS (cont'd)

FIGURE		PAGE
17	Measured Mean Streamwise Velocity Profiles at $x/H = 15$ . . . . .	80
18	Measured Mean Streamwise Velocity Profiles in Cold Flow . . . . .	81
19	Measured Mean Streamwise Velocity Profiles in Cold Flow and in Reacting Flow . . . . .	82
20	Measured Mean Centerline Velocity Decay. . . . .	85
21	Measured Normalized Streamwise Turbulence Intensity Profile at $x/H = 1/3$ . . . . .	88
22	Measured Normalized Streamwise Turbulence Intensity Profiles at $x/H = 1$ . . . . .	89
23	Measured Normalized Streamwise Turbulence Intensity Profiles at $x/H = 3$ . . . . .	90
24	Measured Normalized Streamwise Turbulence Intensity Profiles at $x/H = 5$ . . . . .	91
25	Measured Normalized Streamwise Turbulence Intensity Profiles at $x/H = 7$ . . . . .	92
26	Measured Normalized Streamwise Turbulence Intensity Profiles at $x/H = 9$ . . . . .	93
27	Measured Normalized Streamwise Turbulence Intensity Profiles at $x/H = 11$ . . . . .	94
28	Measured Normalized Streamwise Turbulence Intensity Profiles at $x/H = 15$ . . . . .	95
29	Measured Normalized Streamwise Turbulence Intensity Profiles . . . . .	96
30	Measured Local Streamwise Turbulence Intensity Profiles at $x/H = 1$ . . . . .	100
31	Measured Local Streamwise Turbulence Intensity Profiles at $x/H = 3$ . . . . .	101
32	Measured Local Streamwise Turbulence Intensity Profiles at $x/H = 5$ . . . . .	102

LIST OF ILLUSTRATIONS (cont'd)

FIGURE		PAGE
33	Measured Local Streamwise Turbulence Intensity Profiles at $x/H = 7$ . . . . .	103
34	Measured Local Streamwise Turbulence Intensity Profiles at $x/H = 9$ . . . . .	104
35	Measured Local Streamwise Turbulence Intensity Profiles at $x/H = 11$ . . . . .	105
36	Measured Local Streamwise Turbulence Intensity Profiles at $x/H = 15$ . . . . .	106
37	Measured Local Centerline Turbulence Intensity Profiles . . . . .	107
38	Measured Skewness Coefficient Profiles at $x/H = 3$ . . . . .	110
39	Measured Skewness Coefficient Profiles at $x/H = 7$ . . . . .	111
40	Measured Skewness Coefficient Profiles at $x/H = 11$ . . . . .	113
41	Measured Skewness Coefficient Profiles at $x/H = 15$ . . . . .	114
42	Normalized Stream Function Contours (Unbiased Cold Flow) . . . . .	116
43	Normalized Stream Function Contours (Biased Hot Flow) . . . . .	117
44	Temperature Contours at $x/H = 17.7$ . . . . .	121
45	Comparison of Predicted and Measured Mean Streamwise Velocity Profile at $x/H = 1$ . . . . .	129
46	Comparison of Predicted and Measured Mean Streamwise Velocity Profile at $x/H = 3$ . . . . .	130
47	Comparison of Predicted and Measured Mean Streamwise Velocity Profile at $x/H = 5$ . . . . .	131
48	Comparison of Predicted and Measured Mean Streamwise Velocity Profile at $x/H = 7$ . . . . .	132
49	Comparison of Predicted and Measured Mean Streamwise Velocity Profile at $x/H = 9$ . . . . .	133

LIST OF ILLUSTRATIONS (cont'd)

FIGURE		PAGE
50	Comparison of Predicted and Measured Mean Streamwise Velocity Profile at $x/H = 11$ . .	134
51	Comparison of Predicted and Measured Mean Streamwise Velocity Profile at $x/H = 15$ . .	135
52	Predicted Normalized Stream Function Contours . . . . .	137

LIST OF TABLES

TABLE		PAGE
1	Details of Previous Axisymmetric Annular Step Investigations . . . . .	6
2	Theoretical Review of Velocity Bias . . . . .	33
3	Experimental Review of Velocity Bias . . . . .	34
4	LDV System Parameter Settings . . . . .	61
5	Integrated Mass Flux in an Axisymmetric Sudden Expansion . . . . .	120
6	Conservation Equations Corresponding to Equation 10 . . . . .	125
7	Recommended Turbulence Constants from Ref. [20]. . . . .	126
A1	Experimental Velocity and Turbulence Data . . . . .	147
A2	Experimental Temperature Data . . . . .	154

## NOMENCLATURE

$A_R$	Area ratio
$C_1, C_2, C_D$	Turbulence constants
$D_1$	Inlet diameter of sudden expansion
$D_m$	Digital mantissa
$E$	Log law constant = 9.0 for smooth walls
$f$	Doppler frequency
$f_s$	Net frequency shift
$F_R$	Fringe spacing
$G_k$	See Table 6
$H, h$	Step height
$k$	Turbulent kinetic energy
$\dot{m}$	Mass Flux
$n$	Number of samples
$n$	Exponent on TSI processor
$N$	Number of cycles/burst on TSI processor
$r$	Radial coordinate direction
$R_1$	Inlet radius of sudden expansion
$R_2$	Outlet radius of sudden expansion
$S_\phi$	Source term for variable $\phi$
$[u'^2]^{1/2}$	RMS streamwise velocity
$u_i$	Individual velocity realization
$U_1$	Reference velocity 22.07 m/s

NOMENCLATURE (cont'd)

$\bar{u}$	Mean streamwise velocity
$x$	Streamwise coordinate direction
$x_r$	Reattachment point
<u>Greek Symbols</u>	
$\Gamma$	Exchange coefficient
$\epsilon$	Dissipation of turbulent kinetic energy
$\theta$	Angle between intersecting beams
$\kappa$	Log-law constant
$\lambda$	Laser wavelength
$\mu_{lam}$	Laminar viscosity
$\mu_t$	Turbulent viscosity
$\mu_{eff}$	Effective viscosity
$\rho$	Fluid density
$\sigma_\epsilon$	Turbulent Prandtl number for $\epsilon$
$\sigma_k$	Turbulent Prandtl number for $k$
$\tau_l$	Particle arrival time (validated)
$\tau_p$	Particle residence time in probe volume
$\tau_s$	Sampling time
$\tau_t$	Integral time scale of turbulence
$\tau_w$	Wall shear stress
$\omega$	Weighting function
$\Phi$	A general variable

NOMENCLATURE (cont'd)

$\psi$  Stream function  
 $\psi^*$  Normalized stream function

Math Symbols

$\Sigma$  Summation  
 $\frac{\partial}{\partial x}, \frac{\partial}{\partial r}$  Space derivatives  
 $\frac{\partial}{\partial t}$  Time derivatives  
 $\int$  Integral  
, ' Time average and its fluctuation

## SECTION I

### INTRODUCTION

Flows in which a separated turbulent shear layer reattaches after formation exist in many problems of engineering importance including external flows over structures and internal flows with sudden expansions. Axisymmetric sudden expansions are of particular interest because the region of recirculation can be used to advantage as a flame holder for a dump combustor. In spite of this importance and the large body of experimental data available for such flows, there is still an incomplete understanding of the problem. Part of the difficulty lies in the fact that these flows are highly turbulent with frequent velocity reversals which severely limits the quality of measurements made with conventional techniques such as pitot tube and hot wire anemometry. Reacting flows complicate the measurement problems even further. With the laser Doppler velocimeter (LDV), however, valuable information about such flows can be gained. This instrument has many desirable qualities: no physical probe to intrude on the flow, high spatial and temporal resolution, linear response, and the capability of determining the direction of the velocity being measured. A complete

description of the principles of laser Doppler velocimeters is given by Stevenson [1].<sup>1</sup>

Although the LDV is ideally suited for flow measurements in highly turbulent mixing flows with flow reversal, it is known that certain bias errors can occur [2]. Therefore one objective of the present study was to further verify a previously developed experimental technique for eliminating velocity bias [3,4,5]. In the present investigation three complete sets of LDV measurements were made in an axisymmetric sudden expansion. The three data sets consisted of mean streamwise velocity and turbulence intensity measurements, two of which were made in isothermal (cold) flow (unbiased and biased) and one of which was made in a reacting (hot) flow (biased). (Unbiased hot flow measurements could not be made because of seeder limitations.) The biased and unbiased cold flow measurements were compared to determine the effect of velocity bias on the flow measurements. The hot and cold flow measurements were compared to determine the effect of combustion on the turbulent structure of the flow field.

A review of the general flow characteristics of axisymmetric sudden expansions together with a review of LDV measurements in reacting flow fields are presented in Section II. A discussion of measurement errors which occur in laser

<sup>1</sup>. Numbers in brackets refer to references listed at the end of the report.

velocimetry is also given in Section II. Sections III, IV and V describe the apparatus, techniques and results for the experimental measurements. A description of the numerical code and a comparison of numerical predictions to the isothermal experimental results is given in Section VI. Conclusions and recommendations are presented in Section VII.

## SECTION II

### LITERATURE REVIEW

#### 1. INTRODUCTION

The general flow characteristics of axisymmetric sudden expansions are of great engineering interest and have been the focus of many recent experimental and analytical investigations. One purpose of this section is to describe the flow field of an axisymmetric sudden expansion and identify some of the relevant mechanisms responsible for the character of the flow field. A review of the recent literature pertaining to axisymmetric sudden expansions is also included.

Combustion significantly changes the character of the flowfield by introducing steep temperature gradients. The effects of combustion on the flow field and, in particular, on the turbulence in the flow has also been of great interest. Much work has been conducted in an effort to understand the turbulence-combustion interaction. Some recent literature dealing with LDV measurements in reacting flows will also be reviewed. Finally, a discussion of errors associated with LDV measurements will be presented.

## 2. AXISYMMETRIC SUDDEN EXPANSIONS

### a. PAST EXPERIMENTS

Several studies, both experimental and computational, have been conducted to determine the effect of such parameters as inlet flow characteristics on the shear layer in axisymmetric sudden expansions. Experimenters have used a variety of techniques to study the velocity field in flows of this type including flow visualization, hot wire and hot film anemometry, and, most recently, laser Doppler velocimetry. Air and water have been the basic fluids used, with only limited work conducted with reacting gases. Reynolds numbers based on average inlet velocity and inlet diameter typically range from 10 to  $10^7$ . The boundary layer at the point of separation has been either laminar or turbulent.

Table 1 is a compilation of recent investigations in axisymmetric sudden expansions. This is certainly not a complete list, but includes those studies pertinent to the discussion. Recent reviews of the related problem of two-dimensional step flows are given by Bremner, et al. [3] and by Eaton and Johnston [6,7].

TABLE 1. DETAILS OF PREVIOUS AXISYMMETRIC ANNULAR STEP INVESTIGATIONS.

<u>Model:</u>	<u>Axisymmetric annular step</u>		<u>Technique(s)</u>	<u>Fluid(s)</u>	<u>Inlet Velocity or Reynolds Number</u>	<u>Step Height or Area Ratio (h or <math>A_R</math>)</u>
<u>Year</u>	<u>Author(s)</u>					
1967	Macagno and Hung [8]		numerical, aluminum powder visualization	oil	$36 < Re_{D_1} < 4500$	$A_R = 2$
1972	Back and Roschke [10]		dye studies	water	$20 < Re_{D_1} < 4500$	$A_R = 2.6$
1974	Teyssandier and Wilson [23]		numerical	air	$Re_b = 114$	$1.43 < A_R < 3.33$
1975	Freeman [11]		LDV (one-component)	water	$Re_{D_1} = 3 \times 10^4$	$A_R = 2.1$
1977	Gosman, Khali and Whitelaw [22]		numerical	air	$Re_{D_1} = 5 \times 10^4$	$A_R = 2.6$
1977	Moon and Rudinger [12]		numerical, LDV (one component)	air	40 - 90 mps	$A_R = 1.43$
1978	Drewry [13]		pressure taps, gas-sampling, oil visualization	air	450 - 1010 fps	$A_R = 1.28, 1.536, 1.92$
1979	Kangovi and Page [14]		pressure taps, Pitot tube, hot wire	air	$0.12 < M < 0.95$	$h = 0.6, 1.3, 1.9, 2.5 \text{ cm}$
1982	Stevenson, et al. [15]		numerical, LDV (one-component)	air	$Re_{D_1} = 4.1 \times 10^4$	$A_R = 3.52$

## b. SEPARATED FLOW REGIONS

The separated flow downstream of a sudden expansion can be divided into two regions: 1) the mixing layer region and 2) the relaxation region as shown in Figure 1. The mixing layer region includes the flow from separation to reattachment. The mixing region may be further subdivided into four flow regions, namely I) The secondary recirculation zone (characterized by one or more vortices thought to be rotating about an axis perpendicular to the radial axis); II) The primary recirculation zone consisting of trapped eddies which rotate clockwise (in the bottom recirculation zone) in a meridional plane; III) The reattachment region where bifurcation of the shear layer occurs and part of the flow is deflected upstream into Region II to supply entrainment; and IV) A curved free shear layer with a varying velocity deficit across it, characterized by high turbulence and large intermittent eddies that promote the mixing process.

The relaxation region begins at flow reattachment and ends where full recovery of the turbulent boundary layer occurs. The low turbulence core and high turbulence shear layer lose their identity in this region and the mean velocity profile approaches that expected for a fully turbulent pipe flow. Studies have defined the turbulent structure of Regions II and III, but the structure in Region I has yet to be conclusively identified in axisymmetric sudden

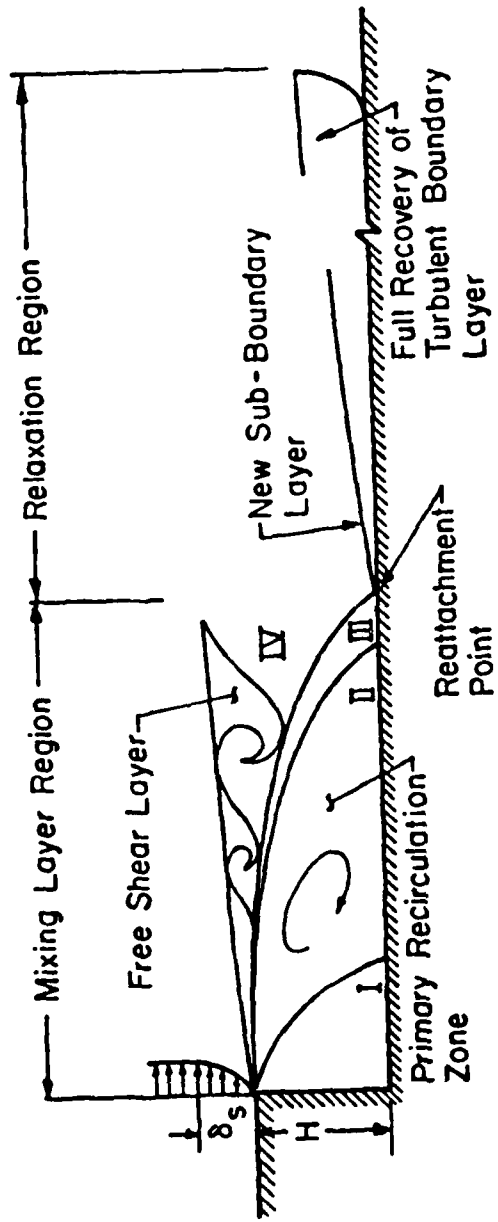


Figure 1. Separated Flow Regions in an Axisymmetric Sudden Expansion

expansions. This is probably due to the low velocities, typically 1% of the inlet velocity, present in this region.

One would expect symmetric flow patterns in axisymmetric sudden expansions for the following reason. An asymmetric flow would create an asymmetric pressure distribution in the separation region. This would be offset by a redistribution of pressure within this region leading to a symmetric flowfield. In a laminar<sup>1</sup> flow study. Macagno and Hung [8] showed that symmetric flow patterns are maintained over a wide range of Reynolds numbers for axisymmetric sudden expansions. Zemmanic and Dougall [9] did observe an asymmetric flow pattern (determined by heat transfer measurements) for turbulent<sup>2</sup> flow of air in an axisymmetric sudden expansion. The extent of asymmetry was small compared with that which occurs in a plane expansion, however. This is the only reference found which noted any asymmetry in an axisymmetric sudden expansion flow.

#### c. REATTACHMENT LENGTH

The streamwise distance between the point of separation and reattachment for axisymmetric sudden expansions has been the subject of many investigations. Functional relationships between reattachment length and Reynolds number, step

1. i.e. a flow with a laminar boundary layer at separation
2. i.e. a flow with a turbulent boundary layer at separation

height,  $H$  (or area ratio,  $A_R$ ), and inlet flow conditions have been postulated.

Back and Roscke [10] performed dye studies in an axisymmetric sudden expansion (oriented horizontally) using water as the working fluid for a Reynolds number (based on inlet pipe diameter and average inlet velocity) ranging from 20 to 4200. The purpose of the investigation was to study the effect of inlet Reynolds number on shear layer growth and reattachment length. Their results showed that laminar, transitional,<sup>3</sup> and turbulent separated flow occurred within the Reynolds number range of their study with reattachment length varying significantly. Reattachment length had a maximum value of 25 step heights for an inlet Reynolds number of 290. For Reynolds numbers greater than 290 laminar instabilities became visible in the inlet boundary layer and the reattachment length decreased very rapidly to about seven step heights at  $Re=1000$ . The reattachment length then slowly increased to a nearly constant value of approximately nine step heights for Reynolds numbers greater than 3000.

Freeman [11] measured streamwise velocities of water in the turbulent flow field of an axisymmetric sudden expansion (oriented vertically) using an LDV system. A frequency locked tracking processor along with a digital voltmeter and

<sup>3</sup> i.e. a flow with a laminar or transitioning boundary layer at separation which becomes turbulent by reattachment.

rms meter were used to measure mean and fluctuating velocities, respectively. Based on experimental stream function contours, reattachment was found to occur at 8.7 step heights. Maximum negative recirculation velocities were approximately 10% of the inlet centerline velocity.

Moon and Rudinger [12], in a turbulent axisymmetric sudden expansion experiment using air, found the reattachment length to be between 8 and 9 step heights. They located the reattachment point by interpolating mean velocity profiles obtained with an LDV at several cross-sectional planes. They found that the flow field downstream of the sudden expansion was symmetric, thus contradicting Zemmanic and Dougall [9]. They also concluded that reattachment length had no functional dependence on Reynolds number for turbulent flows.

An experimental study was performed by Drewry [13] on the axisymmetric sudden expansion in ramjet combustor models (cold flow) using flow visualization techniques, wall static pressure measurements, and gas sampling. Drewry found that reattachment length varied linearly with step height. The reattachment point occurred between 7.9 and 9.2 step heights for all geometries tested. He also found the flow to be symmetric with slight circumferential flow (swirl) downstream of the step. No explanation was given for this swirl component, but it may have been introduced by the inlet air facility.

Kankovı and Page [14], using static pressure taps and hot wire anemometry, found that reattachment occurred at about 8 step heights downstream of the sudden expansion. They also identified the presence of a weak secondary recirculation zone (Region I) located within one step height of the sudden expansion.

Stevenson, et al. [15], in a turbulent axisymmetric sudden expansion experiment with air, measured streamwise and tangential mean velocities and turbulence intensities using a one component LDV system. They also derived Reynolds stress correlations from independent measurements of velocity components. Logan's method [16] was used to derive the Reynolds stress from the individual component measurements. They found that reattachment occurred at 7.9 step heights downstream of the sudden expansion. The flow field was also found to be symmetric.

A review of the studies described above show that the observed reattachment length for axisymmetric sudden expansions varies between 7 and 10 step heights for turbulent inlet flow conditions. Although this was noted by the experimenters, little has been done to determine the reason for the variation. Eaton, et al. [17] suggested that part of the variation of reattachment length for similar geometries and inlet flow conditions may be the result of the recirculation zone slowly growing and shrinking causing the reattachment streamline to oscillate. The entrainment

rate balances the backflow rate, but only in the mean, not instantaneously. Limited observations suggest the oscillations to be of relatively low frequency (on the order of 50 Hz). Although there is some experimental evidence to support the unsteady reattachment postulate, the phenomena needs to be investigated in much more detail. Keuhn [16] suggested that part of the reattachment length variation can be attributed to differences in inlet conditions, but that most may be due to an adverse pressure gradient effect. He showed that superimposing different pressure gradients on the sudden expansion flow field, while keeping inlet conditions constant, led to large variations in reattachment length. The reattachment length for laminar and transitional flows has a strong dependence on the state of the boundary layer and the turbulence level in the free stream [10]. For turbulent flows the high degree of turbulence generated at separation overwhelms all other influences in the approaching flow.

#### d. MEAN VELOCITY AND TURBULENCE INTENSITY

Typically the maximum negative velocities in the primary recirculation zone are 10 to 15% of the inlet centerline value [11,12,15]. This is substantially lower than the maximum reverse flow velocities found in two-dimensional steps. Eaton and Johnston [6] quote values of  $.25U_1$  and Bremner, et al. [3] quote a maximum reverse velocity of

$.20U_1$ . The difference in these values may be due to step height differences in the experiments.

Centerline velocity decay following an abrupt axisymmetric expansion is similar to that for a free jet in the "core" region of the inlet flow. This "core" region is approximately five step heights long for a sudden expansion with an area ratio of 2. Beyond this point the similarity between the free jet and sudden expansion ceases to exist, since the free jet velocity decreases to zero while the sudden expansion flow decays to a fully developed turbulent pipe flow. The centerline velocity decay appears to be nearly independent of area ratio and inlet velocity profile when plotted against non-dimensional step height [15].

The centerline local turbulence intensity rapidly increases from a low value (typically 1-2%) at the sudden expansion to a value near 40% approximately 13 step heights downstream. Maximum turbulence intensities in the shear layer, normalized with respect to the inlet centerline velocity, are typically about 25% [3,6,15]. The reattachment length in an axisymmetric sudden expansion is normally between 7 and 9 step heights and appears to be independent of area ratio and inlet conditions for turbulent flows.

#### e. ANALYTICAL MODELING OF AXISYMMETRIC SUDDEN EXPANSION

Turbulent sudden expansion flows have received varied analytical treatment in recent years. Probably the most popular computer codes for this turbulent flow problem utilize the two-equation  $k-\epsilon$  model originally developed by Harlow and Nakayma [19] which has been modified by Launder and Spalding [20] and Launder, et. al [21]. Both Moon and Rudinger [12] and Stevenson, et al. [15] generated predictions for axisymmetric sudden expansions using codes of this type. The two dimensional, time averaged conservation equations in elliptic form were solved using refined finite difference techniques. The two-equation turbulence model requires "universal" turbulence coefficients. Moon and Rudinger demonstrated that these coefficients were not, in fact, universal, at least not for recirculating flows. Stevenson, et al. [15] found that although the  $k-\epsilon$  model was adequate for engineering purposes, it did not yield a precise representation of the flow field. Gosman, Khalil and Whitelaw [22] felt that the dissipation equation caused at least part of the deficiency in the model. More complex models (Reynolds stress), however, apparently do not result in any better representation of the flow field [22].

### 3. REACTING FLOWS

#### a. INTRODUCTION

The interaction between combustion and turbulence has been the subject of much research in the past few years. The effects of combustion on the structure of turbulence and the effects of turbulence on combustion (i.e. chemical reaction rates) is of great interest to the combustion engineer. Knowledge of these effects permit the design of more energy efficient combustion systems with low pollutant emission while minimizing costly test programs.

The objective of most recent experimental work in turbulent reacting flows is to obtain data for comparison with the numerical prediction codes that model turbulence, combustion and heat transfer. LDV measurements in reacting flows have been made in various geometries. The more common include: 1) co-axial jets, 2) diffusion flame jets, 3) bluff body flame holders in ducts, 4) industrial furnaces, and 5) two-dimensional rearward facing steps. All of these geometries have a common feature in that they induce a separated flow region which acts as an anchor for the flame front. High turbulence intensities and recirculation zones are characteristic features of these flows. Comparisons of mean velocities, turbulence intensities and recirculation zone sizes have been made in the above mentioned flow fields with and without combustion. These comparisons have been

made in an effort to understand the turbulence-combustion interaction. Turbulence structure parameters (i.e. skewness and flatness) are also often compared to give some insight to the interaction process. Results from these studies will be discussed in the following section. The effects of axial pressure gradient on the turbulent structure of reacting flows will also be discussed. Finally, a review of the current computer codes used to predict turbulent flow with combustion will be presented.

#### b. COMPARISON OF FLOWS WITH AND WITHOUT COMBUSTION

A comparative study of cold and reacting flow around a bluff body flame stabilizer in a duct was made by Fujii and Eguchi [24]. Mean streamwise velocities and turbulence intensities were measured downstream of the stabilizer. A homogeneous propane-air mixture was used in the reacting flow study. They found the recirculation zone to be 50% longer and 30% wider in the flow with combustion as compared to the isothermal flow. The recirculation zone varied from 5.4 to 7.5 bluff body half-widths downstream of the stabilizer. This recirculation zone length was found to be a function of the equivalence ratio, attaining a minimum value at stoichiometric fuel-air ratios and reaching a maximum value at the weak and rich limits. Local turbulence levels in the reacting flow were found to be much lower in the reacting flow, typically 50% of the values found in the

isothermal flow. Fujii and Eguchi proposed that this suppression of turbulence by combustion resulted from dilatation by heat release competing with turbulence energy production in the shear layer. The structure parameters, skewness and flatness, were found to be highly distorted in the reacting flow indicating highly anisotropic turbulence. Using spectrum analysis they also found that the distinct eddy formation and shedding mechanism, characteristic of isothermal separated flows, disappeared in the reacting flow. This was also observed previously by Williams, et al. [25]. The disappearance of eddy shedding in flows with combustion can be explained by considering the static pressure distribution downstream of the bluff body (flame holder). The minimum static pressure occurs at a point immediately downstream of separation. The static pressure then starts to rise as you proceed downstream in the wake region until a maximum is reached (where minimum gas velocity occurs). The distance between separation and the location of maximum static pressure approximately defines the eddy region length. With combustion, the eddy shedding process is stopped because the position of maximum static pressure shifts (due to the fundamental pressure loss associated with heat release) considerably closer to the bluff body as compared to the isothermal flow.

Durao and Whitelaw [26] measured the centerline axial mean velocity and corresponding normal stress in both disc

stabilized diffusion and premixed flames using an LDV. They found that the recirculation zone lengths in the isothermal flow, diffusion flame and premixed flame cases were similar. This is in disagreement with the results of Fujii and Eguchi and may be due to the fact that these flames were unconfined. This demonstrates the need for research to determine the effect of confinement on flames. The maximum reverse velocity in the recirculation zone was found to depend on initial velocity and reached a value approximately 40% of the inlet velocity for all flow cases. The normal stresses observed in the attached flames were generally found to be lower than in the isothermal jet. This suggests that the heat from the surrounding flame suppresses turbulence energy. The velocity probability distribution functions were found to be near Gaussian in shape along the flame centerline. This result would be expected due to the symmetry of the flow and the fact that the large gradients and flow intermittencies occur at the flame boundary.

In a study of enclosed turbulent diffusion flames, Hartmann [27] made LDV measurements in two different combustion chambers. In both chambers either propane or natural gas was introduced through a central orifice surrounded by air passing through an annular swirler. The mean axial velocities and rms fluctuations were measured using an LDV employing frequency shifting operating in the backscatter mode. The backscatter mode was used for two reasons: 1)

optical access was available on one side of the chamber only and 2) the backscatter mode was believed to minimize the problems of beam bending and optical alignment due to refractive index gradients in the flow field. Hartmann found that mean streamwise velocities increased in the flows with combustion, as expected, due to the reduction in gas density. The recirculation zone was found to be narrower (approximately 70% of the value found in the isothermal case) in the flow with combustion. The local turbulence intensity was typically found to be 15% lower in the combusting flow as compared to the isothermal flow. This is in agreement with both Fujii and Eguchi [24] and Durao and Whitelaw [26].

Baker, et al. [28] measured the three components of mean velocity and corresponding normal stresses in an axisymmetric coaxial jet furnace with and without combustion using a one component LDV. Comparisons of the flow field with and without swirl were also made. Profiles of the measured turbulent kinetic energy in the isothermal flows were presented and the regions of near-isotropic turbulence were identified. The study showed that the recirculation regions were substantially different in size for combusting flow as compared to isothermal flow and that the turbulence was significantly more anisotropic over most of the flow field as evidenced by the highly skewed velocity probability distribution functions. The recirculation zone in this

study was found to increase in length. This is contrary to the results of Fujii and Eguchi [24] when considering that the recirculation zones are toward the outside of the combustor in the present study (similar to an axisymmetric sudden expansion) but toward the center of the test section in the flow around a bluff body flame stabilizer. Integrating the rms velocity fluctuations across the radius of the furnace in both the isothermal and reacting flows indicated that the velocity fluctuations (turbulent kinetic energy) increased significantly (25%) as a consequence of the combustion. The explanation for this result, which is in disagreement with the four previously discussed studies, is not clear. The technique of integrating the rms fluctuations across the radius and directly comparing the two flow fields may be questionable, however. It would seem that the energy added from the heat input in the reacting case would have to be included in the turbulent kinetic energy balance in order to compare the two flow fields directly.

In an effort to evaluate the effect of combustion on the turbulent structure of a two-dimensional rearward facing step flow, Pitz [29] made extensive LDV measurements in such a flow with and without combustion. Detailed mappings of mean streamwise velocities and turbulence intensities were presented. The large scale turbulence structure was observed using high speed Schlieren photography and spectral analysis (LDV). A homogeneous propane-air mixture with an

equivalence ratio of 0.57 was used in the combustion study. The reattachment length in the flow with combustion was found to be 30% shorter than that found in the isothermal flow. The recirculation zone was also found to be thinner; that is, the shear layer boundary shifted towards the wall in the reacting flow. This was due to the increased velocity in the core flow at the top of the shear layer (due to combustion) which caused the upper boundary, as defined by the location of zero mean velocity, to shift toward the wall. Peaks in the turbulence intensity profiles confirmed this shift of the recirculation zone boundaries. It is of interest to note, however, that Schlieren visualization showed the flame boundary propagating further into the core region than the shear layer boundary (defined by the mean velocity profiles). The maximum normalized turbulence level in the reacting flow was found to be approximately 30% higher than that in the isothermal flow and was located in the shear layer one step height downstream of the step. Although the maximum normalized turbulence level was higher in the reacting flow case, local turbulence intensities were found to be lower due to the higher local velocities present in the reacting flow. Typically, the values of local turbulence intensity throughout the flow were a factor of three less in the reacting case as compared to the isothermal case at a plane in the vicinity of reattachment. This seems to suggest that more turbulence is generated in the shear layer in the reacting flow case, but is suppressed downstream due

to the combustion process. The reason for increased shear generation in the reacting flow case is not clear. In agreement with Fujii and Eguchi [24] and Williams, et al. [25], combustion was found to reduce the eddy coalescence in the reacting shear layer. The pairing process was nearly eliminated as a growth mechanism in the reacting layer.

### c. EFFECTS OF AXIAL PRESSURE GRADIENTS

It was mentioned earlier that axial pressure gradients are suspected of playing a large role in determining the location of reattachment in isothermal axisymmetric sudden expansions [4]. The effects of axial pressure gradients on turbulent diffusion flames were studied by Starner and Bilger [30]. In this study, various positive and negative pressure gradients were imposed on a coaxial jet configuration and LDV measurements were made. The measurements included axial and radial mean velocities and turbulence intensities. Reynolds stress correlations along with skewness and flatness parameters were also presented. It should be noted that the turbulence structure in confined coaxial jet flows is much more complex than that of the flow in an axisymmetric sudden expansion. However, the primary to secondary jet velocity ratio used in this experiment ( $u_p/u_s = 10$ ) causes the flow structure to approach that of a sudden expansion as opposed to an ejector. They found that local centerline turbulence intensities increased by

approximately a factor of two in flows with either positive or negative pressure gradients imposed on them (for different reasons) as compared with the zero pressure gradient case. This result is very interesting as Glass and Bilger [31] found that the normalized turbulence intensity was much the same for both isothermal and reacting flows with a near zero pressure gradient. This indicates that the normal shear-generated turbulence mechanism is dominant in both isothermal and reacting flows with near zero axial pressure gradient. The increase in turbulence intensity for adverse pressure gradient flows indicate that the advection term, i.e.  $\rho u \left( \frac{\partial k}{\partial x} \right)$ , is of the same order as the production term (at the radius of maximum shear stress) in the Favre averaged turbulent kinetic energy equation [32]. In accelerating flows it appeared that the turbulence was produced by the combustion process. This was suggested as the ratio of the source (or sink) term of turbulent kinetic energy, i.e.  $u'' \left( \frac{\partial p}{\partial x} \right)$ , to the production term (at radius of maximum shear stress) increased in the downstream direction. Further work in this area is indicated as there are significant implications for turbulence-combustion modelling. A detailed mapping of the complete flow field with a two-component LDV system may resolve more of the terms in the turbulent kinetic energy balance

These observations could explain why some experimenters found turbulence to increase with combustion while others found turbulence to be suppressed by combustion. One should be careful when stating that a complete reacting flow falls into one of these two broad categories (i.e. suppression or generation of turbulence due to the combustion process). Different turbulence mechanisms (i.e. production, dissipation, advection, etc.) dominate in different regions of the flow. For example, far downstream of the step in an axisymmetric sudden expansion turbulence production is insignificant, while turbulence production is very important in the turbulent kinetic energy balance immediately downstream of the step. When comparing turbulence characteristics of different flow geometries, one must be sure the fluid mechanisms in the two regions of concern are sufficiently similar.

The decay of centerline velocity was also found to depend strongly on pressure gradient. Typically the more positive the pressure gradient (diffusing flow) the faster the decay. Reacting flows were found to be more sensitive to imposed pressure gradients due to the low density of the hot gases. The structure parameters (skewness and flatness) and the correlation coefficients were found to be independent of pressure gradient. This would imply that the more complicated Reynolds stress turbulence models (that take into account the anisotropic nature of turbulence) may not be necessary [30].

#### d. NUMERICAL MODELING

One important motivation for making detailed LDV measurements in turbulent reacting flows is to generate experimental data which can be used to verify the predictions obtained from computer codes. Most measurements of this type have been aimed at obtaining mean velocity and turbulence intensity data throughout the flow field as mentioned in Section 3.1.

The most popular numerical prediction code in use today employs the two-equation turbulence model ( $k - \epsilon$ ) to complete closure for the time averaged Navier-Stokes equations. Typically one of three combustion models is used characterized by: 1) instant reaction, 2) instant reaction with scalar fluctuations, or 3) Arrhenius reaction or eddy-break up with scalar fluctuations.

Khalil, Spalding and Whitelaw [33] performed numerical predictions with a code as described above that used all three combustion models and obtained results that agreed with available experimental mean velocity data [28] to a good degree over most of the flow field. The maximum disagreement occurred at the centerline of the flow which is also where prediction problems occurred in isothermal flows [15]. The instant reaction with scalar fluctuations combustion model was found to give marginally better predictions than the other two models. The relatively simple ( $k - \epsilon$ )

turbulence model, as compared to the more complicated turbulence stress model, was found to predict the flow sufficiently well in view of the additional complexities involved in employing the more accurate stress model [33]. They found, in fact, that anisotropic turbulence models will not be useful until improvements are made in the existing combustion models. Additional numerical predictions in combusting flows were made by Hutchinson, Khalil and Whitelaw [34] and Gosman, Lockwood and Salooja [35] with similar results.

Bray [32] has questioned the common practice of using constant density-empirical closures and modeling equations in reacting flow situations. Use of these models is hard to justify theoretically when it is realized that many closures originated from simple dimensional analysis, while combustion introduces additional dimensionless groups such as density ratio. These arguments are valid from the theoretical standpoint, but until better combustion models are developed constant density closure models seem adequate. The most important need of the combustion modeler at the moment is reliable measurements of velocity, temperature, species concentration and the corresponding correlations in well defined turbulent reacting flows.

#### 4. LDV MEASUREMENT ACCURACY

##### a. INTRODUCTION

The LDV has many desirable qualities, as noted in Section I, which make it a useful diagnostic tool in highly turbulent flows. In reacting flows it is especially advantageous due to the hostile environment present in these flows which prohibits the use of conventional velocity measuring instruments.

The individual realization LDV is, in principle, an absolute instrument; that is, it requires no calibration. However the finite size of the probe volume, the fact that the measured velocity is actually the velocity of a small particle as it passes through the probe volume (as opposed to the true gas velocity), and the requirements of statistical averaging, especially in highly turbulent flows, may introduce errors into the measurements. The primary sources of error introduced by this instrument are discussed in more detail below. A discussion of velocity bias and guidelines for the correction of biased velocity data are also presented.

##### b. LDV MEASUREMENT ERRORS

Several sources of error have been discovered which are inherent in LDV measurements. These errors can result from

particle seeding effects, probe volume effects, the data sampling method used, and signal processor operating characteristics. Many of these errors have been fully analyzed and are easily eliminated or reduced to an insignificant level. A brief review of the more significant errors is presented below. The effect of refractive index gradient effects in reacting flows is also discussed.

Two primary sources of error can affect the accuracy of LDV measurements made in highly turbulent flows. These are velocity bias and incomplete signal bias. Velocity bias occurs when the velocity data are obtained at unequal time intervals as controlled by random particle passages through the probe volume. Since more particles per unit time pass through the probe volume during time intervals when the velocity is high, the mean velocity calculated by a simple averaging of the data is higher than the true mean. Turbulence intensity and the higher order moments are also affected. Although several correction schemes have been proposed for the reduction of velocity bias, no one method has yet been selected as a standard. Sampling techniques have been proposed that eliminate velocity bias, but these techniques require high seeding densities which may not be achievable in some flows. Since the velocity bias error can be significant in flows of the type under consideration

here, it is important to account for it. A brief review of the status of velocity bias will be presented in the following section.

Incomplete signal bias occurs when particles traverse the fringes of the probe volume at large angles of attack and generate an insufficient number of fringe crossings to allow signal validation by the processor. This also leads to an incorrectly high mean velocity. A detailed discussion of other bias errors which may occur in LDV measurements is given by Thompson and Flack [2]. These errors include frequency broadening, directional ambiguity, clock errors in high speed counters, particle distribution bias resulting from non-uniform seed distribution, particle lag bias and particle acceleration bias. There can also be a bias if there is a steep velocity gradient in the probe volume. Usually these errors are small. For the measurements of interest here, only incomplete signal bias and velocity bias need to be considered and, as shown in Ref. [4] incomplete signal bias is easily eliminated by appropriate frequency shifting.

Refractive index gradients generated by the large density, temperature and species concentration gradients in reacting flows can be a concern when using an LDV system. These gradients not only cause the incoming laser beams to bend due to refraction, but also cause the beams to diverge and lose spatial coherence giving rise to optical alignment

problems and poor signal-to-noise ratio. To date, no criteria exist to analytically predict whether refractive index gradients will cause problems. However, there is empirical evidence on the length of a combustion chamber that the beams can pass through and still yield good signals.

In a large industrial furnace (2 m. square) Baker, Hutchinson and Whitelaw [36] measured velocities and turbulence intensities using an LDV. They found that the beam waist diameter increased by about a factor of four as the beams passed through the furnace. The beams also fluctuated approximately 2.5 mm about a mean position due to the fluctuating refractive index in the flow. Therefore the beams crossed intermittently, causing severe signal distortion. This is, in fact, the only published literature that identifies refractive index gradients as being a serious problem.

Typically the signals are of good enough quality to give accurate LDV measurement, especially in small diameter furnaces [29]. Careful alignment of the probe volume image on the pinhole of the photomultiplier tube after the beams have passed through the combusting flow field will ensure good signal quality. Operating in the backscatter mode has been suggested [27] to minimize the path length traveled by the beams. Another advantage of this method is that the scattered light is transmitted back along approximately the

same path the incoming beams traverse. This means that refraction occurring as the beams go into the flow happens in the reverse order as the signal comes out.

As a final note, Barlow [37] demonstrated in a 1.2 meter diameter furnace that photon correlation methods are well suited to measure signals that are intermittent or weak. From these and other experimental observations it appears that the refraction problem is not serious in combustion studies near atmospheric pressure for test zones of 0.5 meters or less and that measurements, albeit of lower quality, can be made in flows up to about 1.5 meters in cross-section.

#### c. VELOCITY BIAS

McLaughlin and Tiederman [38] proposed in 1973 that measurements with an individual realization LDV would contain a bias commonly referred to as velocity or sampling bias. They proposed a weighting factor correction using the reciprocal of the velocity components. Since that time there have been several analytical studies with a variety of proposed corrections for velocity bias. Those are summarized in Table 2. Some recent experimental work related to the velocity bias problem is summarized in Table 3. The tables indicate that researchers use four characteristic time scales in an effort to quantify the biasing effect.

TABLE 2. THEORETICAL REVIEW OF VELOCITY BIAS

Author	Study Mathematical Formulation	Assumptions	Comments
McLaughlin and Tiederman [38] (1973)	Bias due to the dependence of burst generation rate on velocity $\langle U \rangle = \frac{\sum U_i}{N} \frac{\sum \left( \frac{1}{ U_i } \right)}{N \left( \frac{1}{ U_i } \right)}$	-Spherical Control Volume -Uniform Seeding -Predominant velocity direction	-Postulated the existence of velocity bias -Proposed 1-D correction -Errors up to 10% in U, 15% in U' <sup>2</sup> for 30% turbulence intensity
Barnett and Bentley [39] (1974)	Bias elimination by harmonic averaging $\langle U \rangle = \frac{1}{T} \sum \frac{1}{N} U_i \Delta t_i$	-Spherical Control Volume -Uniform Seeding	-Proposed the removal of velocity bias by harmonic averaging over the total sampling interval
Buchhave [41] (1975)	Response of LDA system to large $u/\bar{U}$ , 3-D Gaussian turbulence	-No frequency shift -Spherical Control Volume -Monodispersed particles -No velocity gradients in the control volume	-Generalized M-T correction to more dimensions by using 3-D gaussian probability distributions -1-D analysis by $1/ U_i $ overcompensates biased data.
Dimotakis [40] (1976)	Data reduction techniques for low and high particle arrival rates $\langle U \rangle = \left( \frac{\sum U_i \tau_i}{N \tau_i} \right)^{-1}$	-Monodisperse particles -Velocity vector enclosed by an elliptic cone -No frequency shift	-At low particle concentrations use time integrals -At high particle concentrations use ensemble averages weighted by the probability of particle occurrence
Edwards and Jensen [42] (1981)	Sampling of velocity at regular-fixed time intervals: Weighting with $\langle \tau_s \rangle$ and particle density	-Measurement intervals should be less than $1/2f_{max}$ and longer than $\langle \tau_p \rangle$	-Statistical bias is a function of particle density and sampling interval, time scale of turbulence -Minimum when detector obtains one measurement every sample period

TABLE 3. EXPERIMENTAL REVIEW OF VELOCITY BIAS

Author	Study	Conditions	Comments
Hoesel and Rodi [43] (1976)	Removal of velocity bias/Air-jet	Uniform Seeding	Weighted-average with $\langle \tau_p \rangle$ : $U = \left( \frac{\sum U_i \Delta \tau p_i}{\sum \Delta \tau p_i} \right)^{-1}$ Weighted average with $\langle \tau_i \rangle$
Durao, Later, Whitelaw [44] (1980)	Combined effect of velocity and amplitude bias	$\tau_t > \tau_i > \tau_s$ $\tau_i > \tau_t > \tau_s$	-Velocity bias can be removed by weighting with $\langle \tau_i \rangle$ . -Postulated that amplitude bias may partially compensate for velocity bias when $\tau_i > \tau_t$ .
Roesler, et al. [4] (1980)	Velocity bias at high particle concentrations, controlled by sampling times	$\tau_i > \tau_t > \tau_j$ $\tau_s \gg \tau_i$	Removed by slow sampling. Experimentally verified that velocity bias does exist and can be eliminated by controlling the sampling rate in a highly seeded flow.
Johnson, et al. [46] (1982)	Velocity bias at low particle concentrations	Weighting with $\tau_i$ $\bar{U} = \frac{\sum U_i \tau_i}{\sum \tau_i}$	Velocity bias increases with turbulence levels and is independent of particle occurrence rate for low seeding. Corrections with 2-D weighting function was effective.
Erdmann and Tropea [45] (1981)	Velocity bias at high particle concentrations, controlled by sampling times	$\tau_s \sim \tau_t$ $\tau_s \gg \tau_t$ $\tau_s \ll \tau_t$	Velocity bias high at low particle density increases with turbulence. Reduced to zero at very large and very small particle rates. Velocity bias depends on turbulence intensity.

They are: 1) the time between particle arrivals,  $\tau_1$ , 2) the residence time of the particles in the probe volume,  $\tau_p$ , 3) the sampling time,  $\tau_s$ , and 4) the characteristic time scale of turbulence,  $\tau_t$ .

Attempts to experimentally verify that velocity bias does in fact exist were largely unsuccessful until the work of Roesler, et al. [4] in 1980 in which the existence of both incomplete signal bias and velocity bias were clearly shown experimentally. More recently Johnson, et al. [46] have also experimentally verified the existence of velocity bias, and have proposed a two dimensional velocity weighting factor to correct it. They also tried using a residence time weighting factor but had little success. No reason was given for the failure of this technique, but the data processing is suspected as the problem. The two-dimensional velocity weighting factor appears to be the best method of correcting for velocity bias when 2-D measurements are available and unbiased data cannot be obtained using the equal time interval sampling method of Roesler, et al. [4].

In an effort to determine the potential errors induced by biased sampling, Tiederman [47] applied both one-dimensional and two-dimensional correction factors to biased two-dimensional LDV data obtained from the 1T wind tunnel at Arnold Engineering Development Center. Figures 2 and 3 show the biased ( $\omega = 1$ ) and corrected mean velocity and rms fluctuating velocity profiles respectively in a separated region

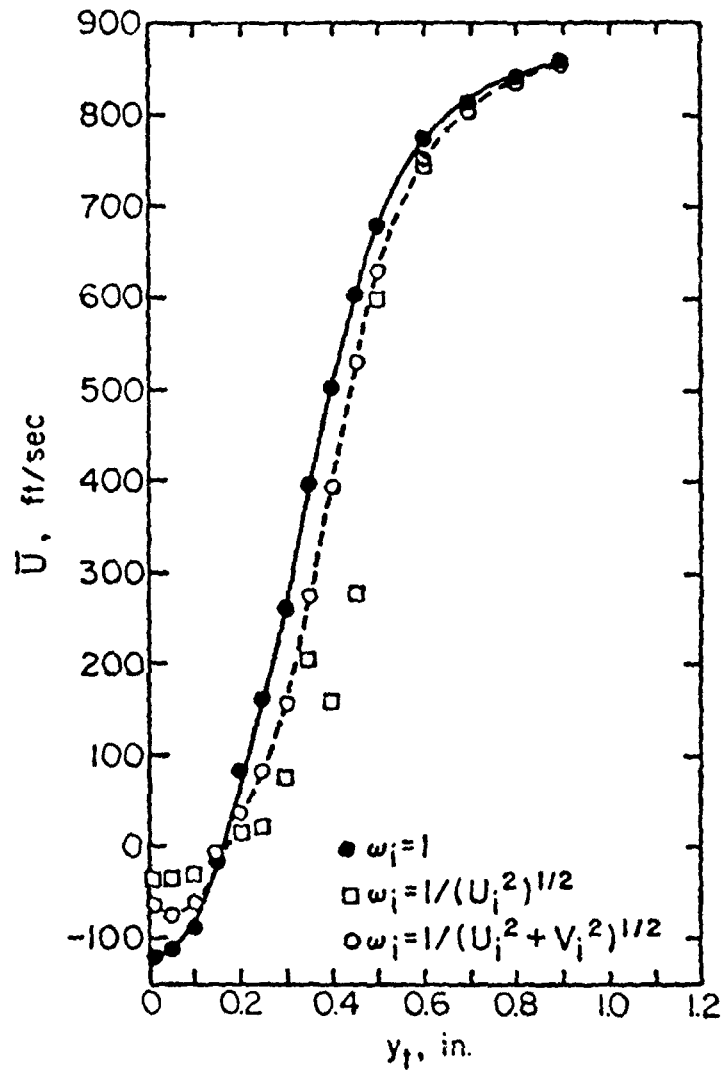


Figure 2. Corrected and Uncorrected Mean Streamwise Velocity Profiles in a Separated Region (from Ref. [47]).

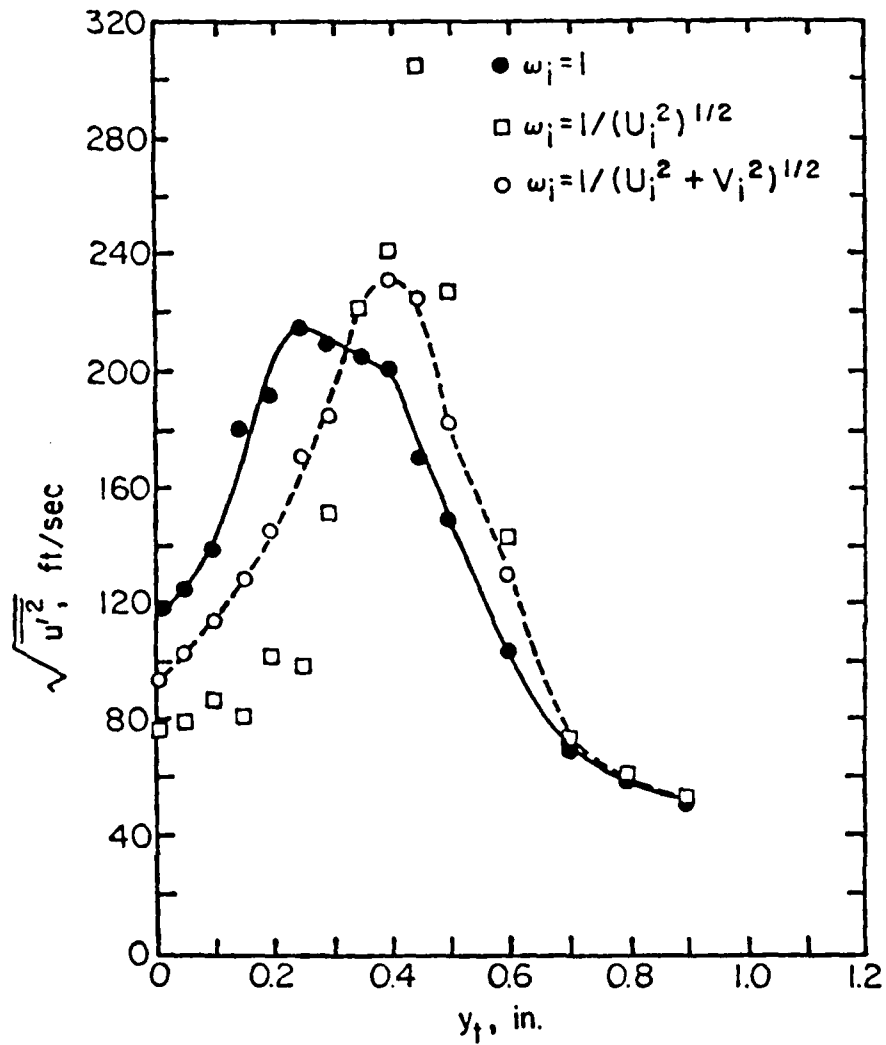


Figure 3. Corrected and Uncorrected rms Streamwise Velocity Profiles in a Separated Region (from Ref. [47]).

downstream of a hump. The trends of the mean velocity data (biased vs. 2-D correction) are as expected. The 1-D correction scheme was found to give spurious results due to the singularities that occurred when the velocity component equaled zero. These singularities were found to be absent when using the 2-D correction scheme. The profiles (biased vs. 2-D correction) of rms fluctuating velocity were found to be significantly different as shown in Figure 3. This result is important as the spatial distribution of turbulence intensity is altered by a sizable amount when biased velocity data is used. It appears, however, that the maximum rms fluctuation velocity is not significantly changed.

#### d. BIAS CORRECTION

Based on the experimental and theoretical findings to date, a set of guidelines for velocity and incomplete signal bias elimination or correction can be formulated.

- a. Velocity and incomplete signal biases are only important in highly turbulent flows. Therefore, no correction is needed for flows with local turbulence intensity levels below about 10%.
- b. Incomplete signal bias can be virtually eliminated by frequency shifting, and since frequency shifting is essential in highly turbulent flows to resolve the flow direction, that bias is of little concern in most applications.
- c. The easiest way to eliminate velocity bias is to heavily seed the flow and control the processor sampling rate such that nearly time averaged data are collected. This sampling technique is recommended whenever it is possible to use it. The

seeding density should provide a particle arrival rate two orders of magnitude or more greater than the sampling rate. The technique is described in Ref. [4].

- d. Velocity bias corrections of data at local turbulence intensity levels up to 20% should be made only if high levels of accuracy are required. For flows in which the mean velocity is not near zero and the local turbulence is of the order of 25% or less, the one-dimensional McLaughlin-Tiederman correction appears to work well for the main velocity component. If two-component measurements are made the two-dimensional correction scheme should be used.
- e. Unless velocity bias is eliminated by equal time interval sampling (at high seed density) or the velocity sampling is controlled by particle arrival statistics such that "completely biased" data is obtained, the amount of bias in a data set is unknown. Obviously it is inappropriate to use any of the proposed bias correction methods on a "partially biased" data set, since the resulting error may exceed that in the original data. Unfortunately much of the data in the published literature is ill-defined in this sense and must be used with this limitation in mind.

## SECTION III

### EXPERIMENTAL APPARATUS

#### 1. INTRODUCTION

The experimental mapping of the flow field in the axisymmetric sudden expansion required various types of instrumentation and hardware. The LDV used in this experiment was designed specifically to allow investigation of the effect of data acquisition methods and optical parameters on measurements in highly turbulent flows. The system allowed for variation in LDV optical parameters, seeding particle arrival rate and data sampling conditions. This section describes the experimental apparatus which may be divided into five major subsystems:

1. the LDV optical system
2. the flow system
3. the fuel system
4. the data collection, storage and processing system
5. the seeding systems

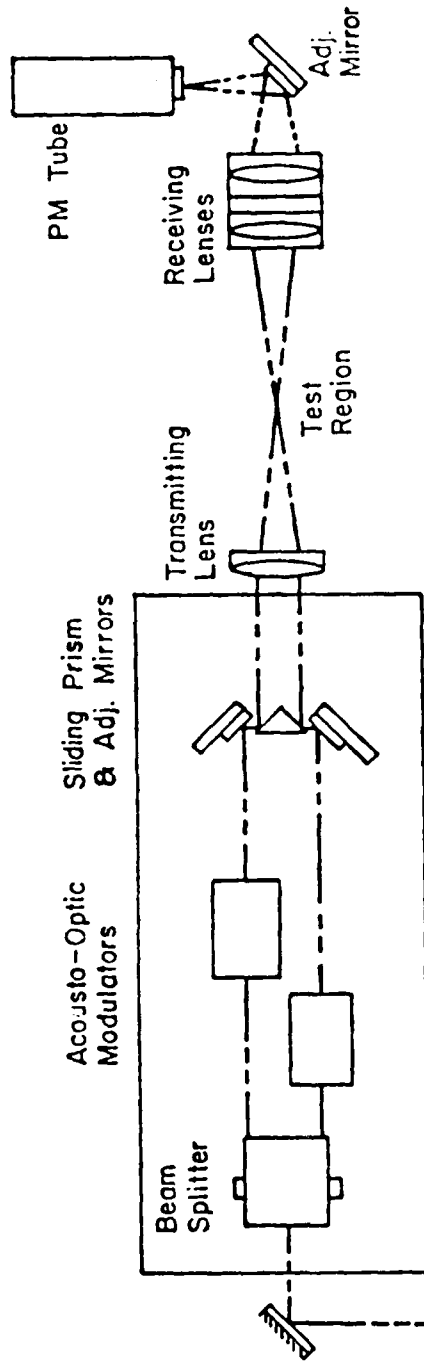
## 2. THE LDV OPTICAL SYSTEM

The LDV used is a one component system operating in the dual-beam forward scatter mode. It has the capability of changing probe volume size, fringe spacing, and angular orientation. Frequency shifting one or both beams and traversing the probe volume in three-dimensional space are also possible. A schematic drawing of the general layout of the LDV system is shown in Figure 4.

Laser light for the system is provided by a five watt Coherent Radiation Model 52 argon ion laser normally operated on the green line ( $0.5145 \mu\text{m}$ ). (The laser power was set between 100 and 200 mW for all experimental runs in the present study.) The beam exits the laser and enters a polarization rotator (Spectra-Physics, Model 310-21). Rotating the plane of polarization of the beam perpendicular to the beam dividing prism insures that the beam is split into two equal intensity beams. This produces maximum fringe contrast in the probe volume. Upon leaving the polarization rotator, the beam passes through a beam expander telescope composed of a 44 mm lens and a 68 mm lens. Traversing the second lens over a 7.5 mm range varies the beam waist diameter from 60 to  $500 \mu\text{m}$ .

Following the telescope, two broadband all-dielectric mirrors (Newport Research Corp.) direct the beam to the beam splitter (TSI, Model #916-1) on the upper table of the

UPPER OPTICS PACKAGE



Optics Table

LOWER OPTICS PACKAGE

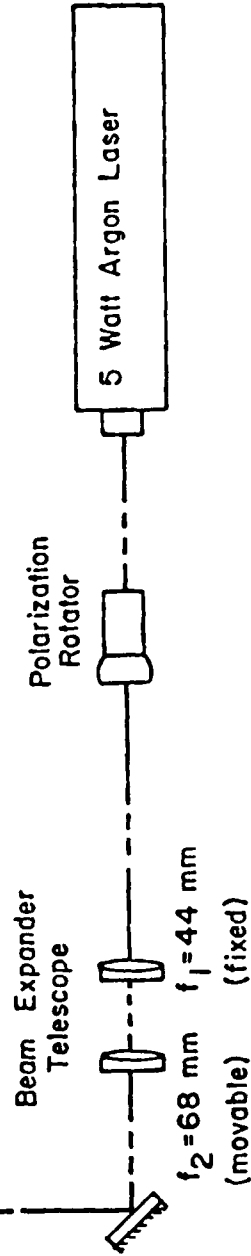


Figure 4. LDV Optics Package

optics package. The beam splitter divides the entering beam into two parallel equal intensity beams which enter two acousto-optic modulators (Intra-Action Corp., Model #ADM-40). The modulators shift the frequency of the incoming beam by an amount equal to the frequency of the driver. The frequency shift may be either up or down allowing for a wide range of net frequency shifts between the two beams. A net frequency shift of 10 MHz was used in the present study. This allowed unambiguous measurement of negative velocities up to approximately 40 m/s.

Upon leaving the modulators, the beams are reflected by adjustable mirrors (Newport Research Corp., Model #600-2) to a sliding prism. Adjustment of the prism changes the beam separation and therefore the converging beam angle, thus controlling the fringe spacing and the number of fringes in the probe volume. The adjustable mirrors are used to position the beams such that they cross at their waists on the optical axis after passing through the transmitting lens. The transmitting lens (TSI, Model #918) has a focal length of 250 mm.

Scattered light from particles passing through the probe volume is collected, collimated and focused by a pair of receiving lenses (TSI, Models #917 and #918) mounted several centimeters apart. The focal lengths of the receiving lenses are 250 mm and 120.6 mm, respectively. The focused light is reflected by a mirror mounted on an

adjustable fixture (Newport Research Corp., Model #600-2). This allows fine lateral adjustment of the focused spot, insuring that it is located on the 200  $\mu\text{m}$  pinhole. The receiving optics package may be moved along the optical axis for coarse adjustment of the probe volume image on the pinhole with fine adjustment provided by the threaded pinhole mounting. Beam stops on the initial receiving lens block the direct laser beams and allow only scattered light to pass into the PM tube.

The upper transmitting optics table is mounted on bearings which allow angular rotation about the optical axis and thus permit any velocity component in a perpendicular plane to be measured. The entire optics package (including laser) is mounted on a 3-axis milling machine table. Three Bodine DC gearmotors with variable speed control are used to drive the mill table. Linear potentiometers (New England Instruments) with a linearity of 0.25% are used to obtain an electrical readout of position on digital panel meters which read directly in millimeters to an accuracy of  $\pm 0.1$  mm. The traverse range is 254 mm (10 in.) in the vertical (y) direction and 152 mm (6 in.) in the x and z directions. A more detailed description of the entire optical system including the individual components is given by McVey [48].

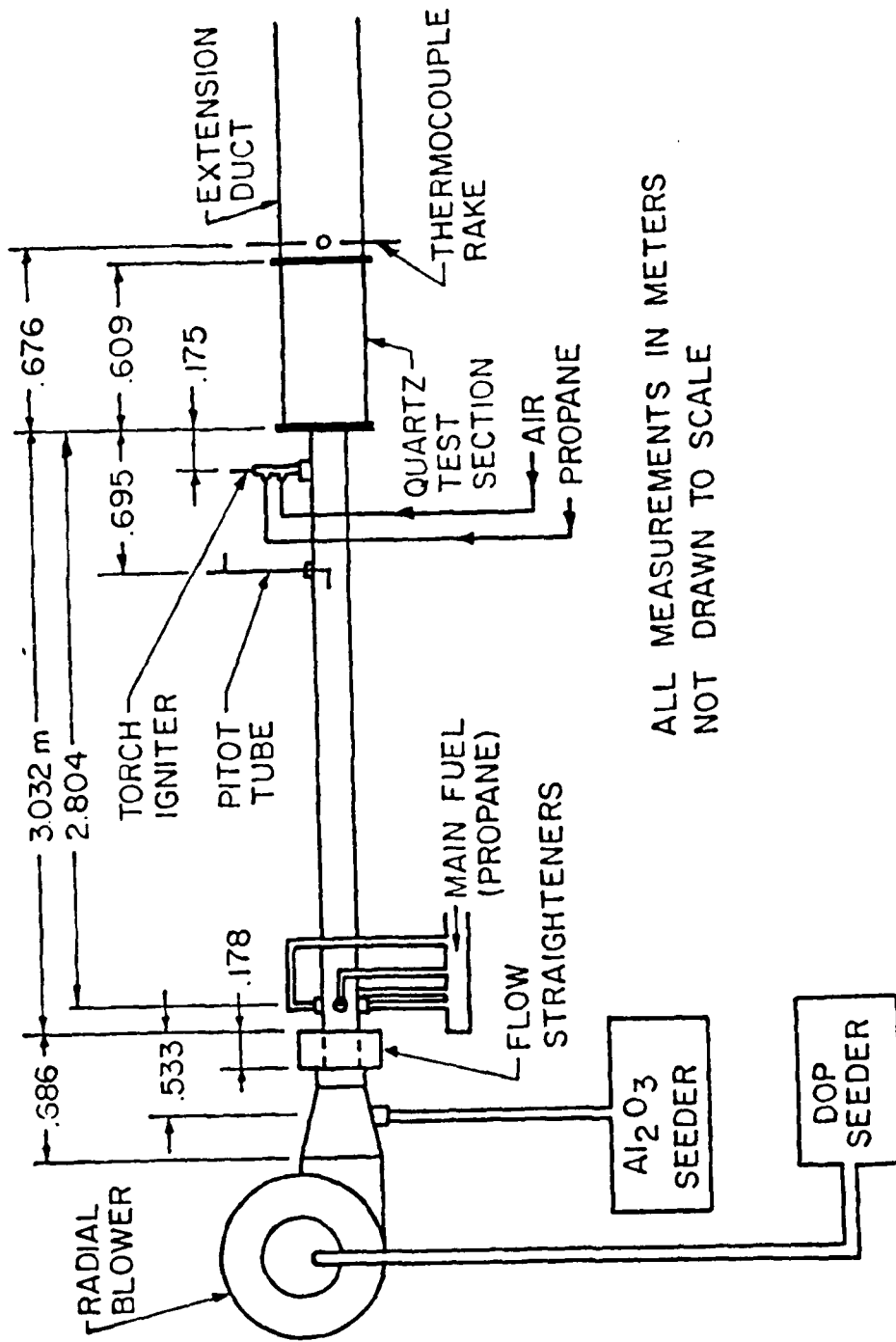
### 3. THE FLOW SYSTEM

The flow system was designed to provide a flexible system allowing easy optical access, while fitting within the diagnostic range of the LDV for both isothermal and reacting flows. The geometry used in this study is that of an axisymmetric sudden expansion. One unique feature of the test rig is that a cylindrical quartz tube was used as the test section. This eliminated the flow field perturbation induced by inserting flat windows in a cylindrical pipe. More will be said about the test section later. The flow system consisted of eight major parts, as shown in Figure 5.

1. a radial vane blower
2. a flow conditioning section
3. a connecting duct
4. main fuel injection
5. torch ignitor
6. a cylindrical quartz test section
7. a thermocouple rake
8. an extension duct

The radial vane blower was a Peerless Model PWB4GA driven by a variable speed direct current motor. The blower-motor combination allows a flow capacity of 1100 cfm.

The flow conditioning section consisted of a set of flow straighteners 76.2 mm (3 in.) in diameter. The elements of this section included wire window screen followed



ALL MEASUREMENTS IN METERS  
NOT DRAWN TO SCALE

Figure 5. Flow System

by a honeycomb of 6.35 mm (0.25 in.) diameter plastic soda straws 25.4 mm (1 in.) in length. This section exited into a series of four window screens spaced 25.4 mm (1 in.) apart. The conditioning section was 178 mm (7 in.) in length and was connected to the blower via a convergent adapter.

The connecting duct, fabricated from 76.2 mm (3 in.) diameter standard schedule 40 steel pipe, was 3.032 m (10 ft.) in length. This length was chosen to give a fully developed velocity profile as an inlet boundary condition to the axisymmetric sudden expansion.

The main fuel (gaseous propane) was injected through four plain hole orifices, located 90° apart circumferentially, in a plane located 2.804 m (110 in.) upstream of the sudden expansion. This allowed sufficient mixing for flame stabilization in the dump-section. A completely premixed fuel-air mixture was not desired at the dump plane as this mixture would lie outside the burning limits for the lean overall fuel-air mixture used in this experiment. Using a lean fuel-air mixture allowed for steady state operation by keeping the test section walls below the annealing temperature for quartz (1070°C).

A pitot tube was inserted in the connecting duct 695 mm (27 in.) upstream of the sudden expansion. This was used

to set and monitor the inlet centerline flow velocity. The pitot tube remained inserted in the duct during all test runs.

A propane-air torch ignitor was used to ignite the fuel-air mixture. The ignitor was mounted flush to the connecting duct wall to minimize flow field disturbances and was located 175 mm (6.9 in.) upstream of the sudden expansion. The torch ignitor was fabricated from stainless steel tubing and is shown in Figure 6. The propane flows down the annulus formed by the 3/8" tube and the 1/4" ceramic insulator. The air flows down the annulus formed by the 1/2" tube and the 3/8" tube. The 3/8" tube is approximately 1 inch shorter than the 1/2" outer tube in order to allow the two gases to mix before they reach the exit plane. The mixture is ignited by arcing a spark across the tungsten wire and the 1/2" outer tube. Spark energy is supplied by a neon light high voltage coil. The primary coil voltage is supplied by a 120 vac outlet followed by a VARIAC reostat. Spark energy is controlled by the VARIAC setting (typically 170vac). The torch ignitor was extinguished as soon as the flame was stabilized in the dump section.

The test section was extruded from optical quality quartz (Supersil) by Heraeus-Amersil, Inc. The cylindrical test section has a 152.4 mm (6 in.) inside diameter with 3 mm (0.120 in.) walls and is 609 mm (24 in.) in length. Although the quartz itself was optical quality,

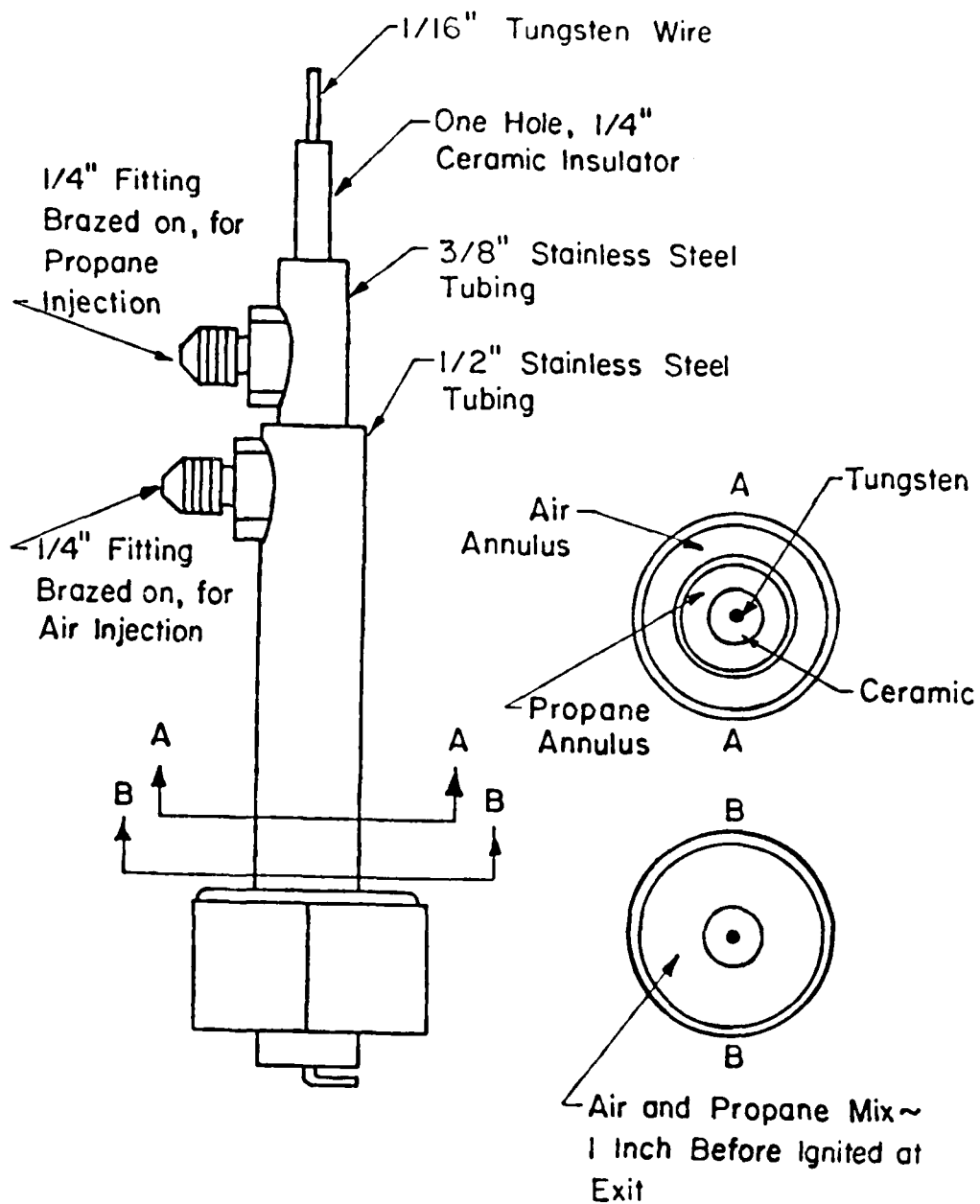


Figure 6. Torch Ignitor

(i.e. no bubbles, inclusions or striae) the surface finish was not. Circumferential "waves" due to the extruding process were present. These waves had a period in the axial direction of approximately 6.3 mm (0.25 in.) and had peaks and valleys of 0.1 mm (.004 in.) that were visible to the eye. These surface irregularities did not deviate the laser beams to any major extent for the majority of data points. However, it was necessary to examine the beam intersection at the pinhole of the PMT to assure that the beams were not distorted. If they were, the measurement location was shifted slightly to give a good quality signal. The quartz section was mounted between two steel flange plates which were compressed by a set of four springs. This allowed for relative thermal expansion of the steel rig and quartz tube without the generation of large stresses. Asbestos rope was used as the gasket material between the steel flanges and the quartz tube. Figure 7 shows the test section assembly.

A set of chromel-alumel thermocouples (Omega # CAIN-14#-12) located 676 mm (26.6 in.) downstream of the sudden expansion allowed the symmetry of the flow to be monitored. The thermocouple beads were located  $90^{\circ}$  apart circumferentially. It should be noted that the temperatures measured were equilibrium temperatures and not true gas temperatures. No effort was made to shield the thermocouples from radiation losses and no temperature correction for radiation, convection or conduction heat transfer effects was made. A

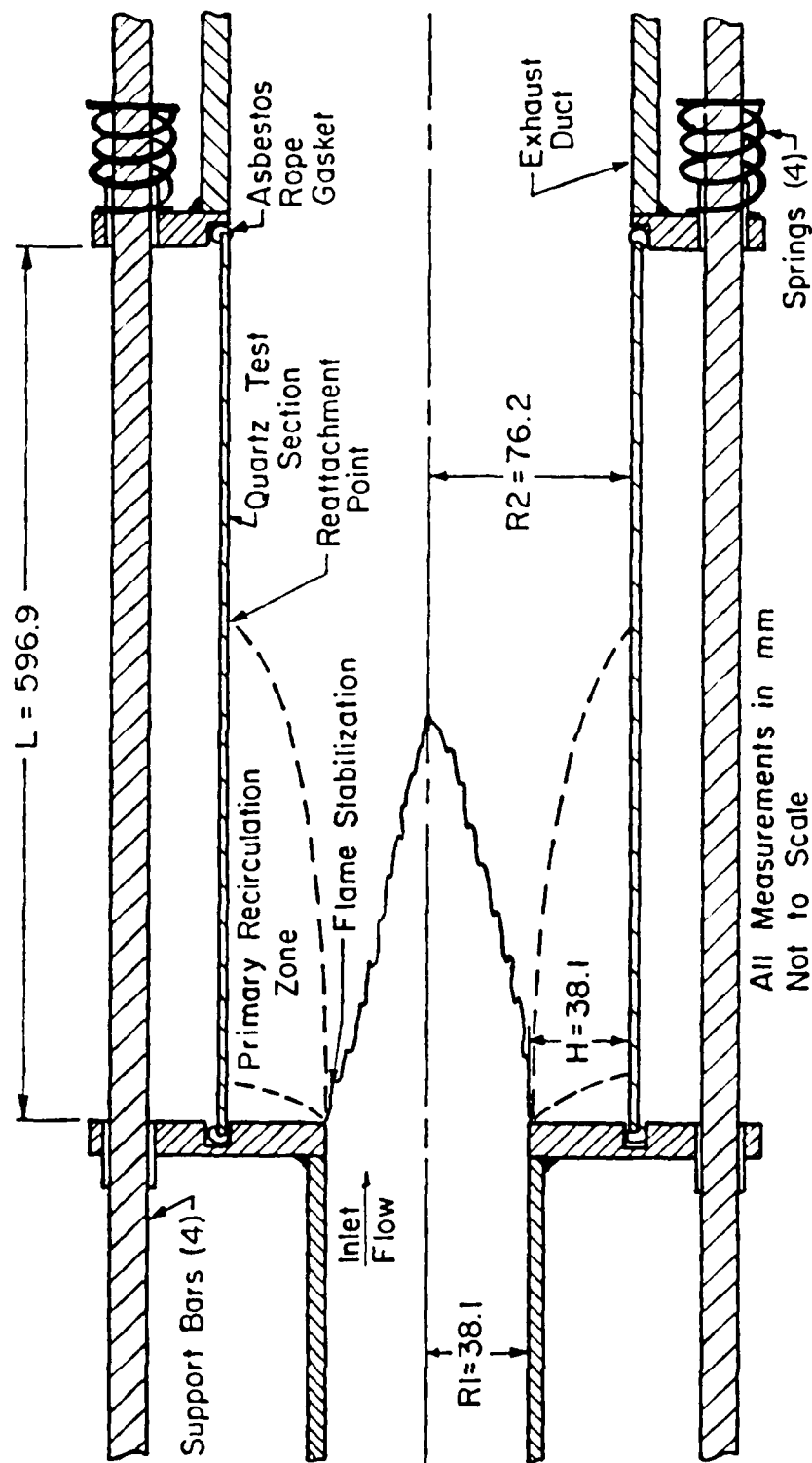


Figure 7. Geometry of Axisymmetric Test Section

thermocouple rake with ten thermocouples was used to measure the temperature profile at a location 676 mm downstream of the sudden expansion. A ten channel digital thermometer (Omega, Model 2176A) accurate to  $\pm 0.01^{\circ}$  C was used to convert the electrical output of the thermocouples into a digital temperature reading.

The extension duct was fabricated from 152.4 mm (6 in.) standard schedule 40 steel pipe and was approximately 1.83 m (6 ft.) long. The length of this extension duct was found to govern the range of fuel-air mixture ratios over which a flame could be stabilized within the dump. If the extension duct was too long the flame would be very unstable with explosions and blowout occurring. Shortening the duct widened the stability loop and produced quiet, stable combustion.

#### 4. THE FUEL SYSTEM

Four 100 lb. bottles of liquid propane connected in parallel were used to supply fuel to the test rig. The propane was kept at  $33^{\circ}$  C ( $90^{\circ}$ F) with a small electrical heater. This increased the propane tank pressure to approximately 170 psig, which allowed an experimental run time of approximately one hour before tank pressure dropped significantly ( $< 40$  psig), causing the run condition to drift.

The propane flowed out of the tank manifold into a regulator set at 40 psig. This maintained a constant flow rate even though tank pressure was decreasing due to the latent heat of vaporization. This regulated flow was next split into two paths. One path went to the torch ignitor and the other went to the main fuel orifices.

A gas stove regulator was used to regulate the torch ignitor propane flowrate while a single stage regulator was used to control the air flowrate. An electrically controlled solenoid valve (normally closed) was placed in the propane line directly upstream of the torch ignitor for safety reasons. The main fuel branch consisted of a shut-off valve, a rotometer (Brooks, Model 1100), a two-stage regulator and an electrically controlled solenoid valve (normally closed) directly upstream of the main fuel manifold. Figure 8 schematically shows the fuel system.

## 5. THE DATA COLLECTION, STORAGE AND PROCESSING SYSTEM

The LDV photomultiplier tube output was connected to a TSI Model 1980 signal processor [49]. This unit features a 250 MHz clock with two nano-second resolution and capability for either digital or analog output. Only the digital output was used in this investigation. In the absence of external control the processor data rate (number of validated velocity measurements per second) depends on the rate

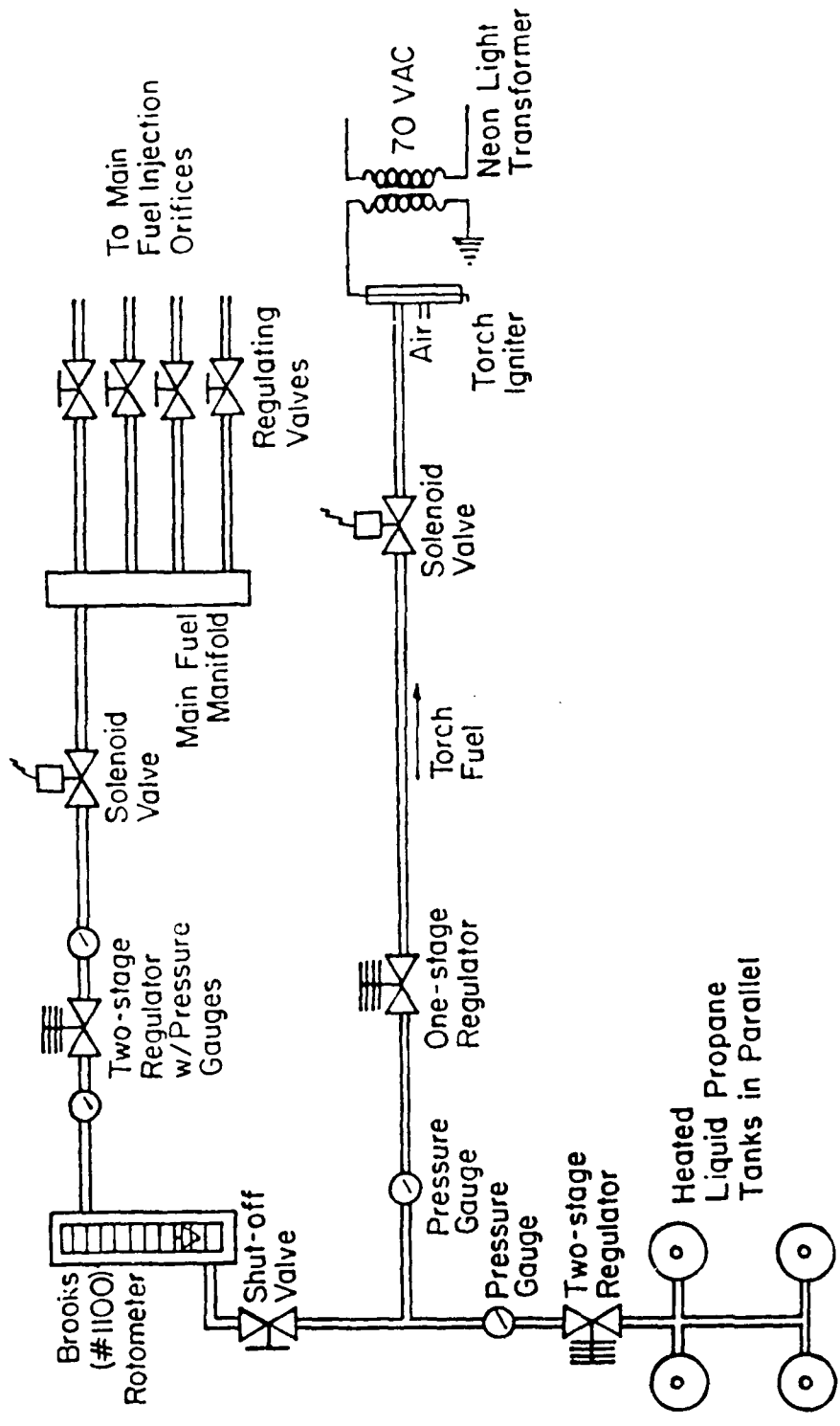


Figure 8. Fuel System

at which seeding particles enter the probe volume, the processor gain setting (which effectively sets the trigger level) and the number of cycles per Doppler burst required for validation. Data rates as low as a few per second to in excess of 20,000 per second were obtained. The rate at which particles enter the test section was controlled by the particle seeder.

Data acquisition and short term storage were performed by an IMSAI 8080 microcomputer and Micropolis floppy disk system. Data could be sampled (by microcomputer control) from rates as low as 0.1 sample per second to approximately 4800 samples per second. The microcomputer had the capability of storing 15,600 data points in its memory.

After sampling, the data were written onto a floppy disk for temporary storage. Each disk is capable of storing 100,000 data points. The microcomputer also interfaced with Purdue University's CDC 6500 and 6600 computers. Data may be transferred from the floppy disk to magnetic tape for permanent storage. The CDC 6500 and 6600 were used for all data reduction.

The microcomputer and TSI processor were also interfaced so that velocity sampling was jointly controlled by the processor and the microcomputer. When the TSI processor has a data point ready, it transmits a data ready pulse to the microcomputer. Upon reception of the data ready pulse

the microcomputer returns a data inhibit pulse to the TSI processor. The inhibit stops the processor from accepting more data and causes it to hold the present data until it can be read. The microcomputer waits a fixed amount of time, chosen by the operator, before reading the data point. After the data is read the data inhibit is removed by the microcomputer and the cycle continues until the desired number of samples has been taken. The rate at which data is actually acquired is therefore controlled by the slower of the two instruments. When seeding density is high and the sampling time interval is large, the data will be acquired at essentially equal time intervals and an unbiased velocity distribution will result [4,5].

## 6. THE SEEDING SYSTEMS

Two flow seeders were used in this experiment. One for the isothermal flow and one for the reacting flow. The seeder used for the unbiased cold flow was one which is commercially built by TSI. It consisted of a Model 3074 air supply, a Model 3076 liquid atomizer and a Model 3072 evaporation-condensation monodisperse aerosol generator. This system produced seeding particles about one micron or less in diameter using a solution of 100% Dioctyl Phthalate (DOP). The seeder was operated at constant pressure, normally 60 psi, while the evaporation-condensation unit was operated at a constant voltage, 60 volts. The seed density

inside the flow section was sufficient to give particle arrival rates in excess of 20,000 per second at the LDV probe volume over most of the test region.

Hot flow measurements were made with  $1\ \mu\text{m}\ \text{Al}_2\text{O}_3$  seeding particles supplied by a TSI Model 3400 fluidized bed particle generator. The maximum particle number density generated by the aluminum oxide fluidized bed seeder was much lower than the particle density generated by the DOP seeder. Particle arrival rates of 5,000 per second in the central part of the test region were the maximum obtainable with the present fluidized bed particle generator. The aluminum oxide seeder was also used for making biased measurements in the cold flow so that a comparison between cold flow and reacting flow results using the same type of seeding could be made.

SECTION IV  
EXPERIMENTAL TECHNIQUE

1. INTRODUCTION

Experimental mapping of the axisymmetric sudden expansion flow field consisted of direct measurements in both isothermal and reacting flows. Both biased and unbiased velocity measurements were made in the isothermal flow case, while only biased measurements were made in the reacting flow case. More will be said about this later. This section presents the techniques used to obtain the following flow field parameters:

1. mean streamwise velocity,  $\bar{u}$
2. streamwise turbulence intensity,  $\sqrt{\overline{u'^2}}$
3. stream function,  $\psi$
4. reattachment length,  $x_r$
5. integrated mass flow rate

Also included in this section are the appropriate values of the various LDV system and flow system parameters used in the study.

## 2. TEST PROCEDURE

As noted previously, three sets of data were taken at each measurement location consisting of two data sets for cold flow (biased and unbiased) and one data set for hot flow (biased). These data are presented in Section V. Comparisons between the unbiased and biased cold flow results illustrate the effect of velocity bias while comparisons between the biased hot and cold flow data show the effect of combustion on the flow field. (Unbiased hot flow data could not be obtained directly because of seeder limitations.)

All flow conditions were maintained at near constant values throughout the testing procedure. The inlet centerline velocity was 22.07 m/s  $\pm$  0.08m/s. The fuel flow was maintained at 0.0038 lbm/s  $\pm$  0.0002 lbm/s. This gives an overall fuel-air ratio of 0.018 and an overall equivalence ratio of 0.28. The hot flow run condition was controlled by monitoring the inlet centerline velocity and the fuel flow reading on the rotometer. Four exit thermocouples were also used to monitor the hot flow run condition. Typically, the exit temperatures were maintained constant to within  $\pm 10^{\circ}\text{C}$ .

## 3. MEAN VELOCITIES AND TURBULENCE PARAMETER MEASUREMENTS

The mean velocities and turbulence parameters are calculated from LDV measurements at various grid points in the flow field. System parameters were set and held constant

throughout the series of measurements to insure continuity of technique and minimize sources of error. Table 4 is a listing of the system parameters used for all measurements.

The techniques employed to obtain the beam waist diameter and position can be found in Ref. [49]. The beam half angle was measured and found to be  $3.52 \pm 0.03$  degrees.

The fringe spacing,  $F_R$ , can be determined from

$$F_R = \frac{\lambda_0}{2 \sin \left( \frac{\theta}{2} \right)}. \quad (1)$$

Substitution of the measured half angle  $\frac{\theta}{2}$  into Equation (1) yields a fringe spacing of  $4.19 \pm 0.04 \mu\text{m}$ . The seed particle size was approximately  $1 \mu\text{m}$  in diameter for both the DOP and aluminum oxide particles.

The net frequency shift employed,  $f_s$ , was  $10 \text{ MHz} \pm 1 \text{ KHz}$ . The positive frequency shift indicates that the fringes are moving upstream against the mean flow direction, in this case with a velocity of  $41.9 \text{ m/s}$ . This was adequate for the identification of negative velocities at all points in the flow and eliminated incomplete signal bias as noted earlier.



The output signal of the photomultiplier tube was filtered to remove the "pedestal" and any high frequency noise. A 30 MHz low pass filter and a 3 MHz high pass filter were used. A 16 to 8 fringe comparison ( $N = 16$ ) was used with the accuracy of this comparison set at 3.1 percent (comparator = 3). This means that the time for a particle to cross 16 fringes is compared with twice the time for the same particle to cross 8 fringes. An error in the comparison of more than 3.1 percent results in the measurement being rejected. The exponent,  $n$ , was allowed to float (variable) and was an output of the TSI processor.

For unbiased cold flow measurements the liquid atomizer followed by the evaporation-condensation unit supplied DOP particles at a number density sufficient to give particle arrival rates (number of valid data points per second available for sampling by the TSI processor) in excess of 20,000 per second at the probe volume over most of the test region. Hot flow measurements were made with  $Al_2O_3$  seeding particles supplied by the fluidized bed seeder. Seeding number density was lower in this case, with maximum particle arrival rates of 5,000 per second in the central core of the test region. The particle arrival rate was actually maintained at between 500-1500 particles per second throughout the entire test section during hot flow runs by varying the gain on the TSI processor and the laser power. This was done to reduce variability in the measurements due to seeding

density variations. The fluidized bed seeder was also used for making biased measurements in the cold flow case for later comparison to the reacting flow results.

The method of velocity bias elimination suggested by Roesler, et al. [4,5] was employed in the cold flow studies due to the high seeding density obtainable with the liquid aerosol seeder. Unfortunately, the fluidized bed seeder used for the hot flow study did not have a capacity large enough to produce the seed density required for full velocity bias elimination. The processor was free running (limited only by the maximum cycling rate of the microcomputer in this case) so that validated Doppler signals were recorded as fast as they could be read into the microcomputer. The rate at which the microcomputer was able to sample the available data was at its maximum of 4800 samples per second. In all cases each velocity measurement was constructed from 4500 samples. The sample size was large enough to give valid results without using excessively large computer storage. A maximum validation rate of 1500 particles per second (biased data only) allows the sampling to take place over a three second interval. This interval was believed long enough to contain the major part of the turbulence spectrum in the present flow field. Using statistical analysis and assuming gaussian distributions and local turbulence intensity values of 70% (defines standard deviation of histogram) gives the expected sampling error for

this sample size. Mean velocities and turbulence intensities were found to be statistically accurate to  $\pm 1\%$  and  $\pm 3\%$ , respectively for a 95% confidence level [50].

Each sampled output of the TSI processor consisted of three digital numbers namely  $N$  (cycles/burst),  $n$  (exponent) and  $D_m$  (digital matissa). This data was converted into a frequency  $f$  and then a velocity,  $u_1$ , by the following equations [48]:

$$f = \frac{N \times 10^8}{D_m \times 2^{n-2}} \quad (2)$$

and

$$u_1 = [f - f_s] F_R \quad (3)$$

Where  $f_s$  is the frequency shift and  $F_R$  is the fringe spacing calculated from Equation (1). The mean, variance and skewness coefficient of the 4500 individual velocities were then computed from Equations (4), (5) and (6) below.

$$\bar{u} = \frac{1}{n} \sum_{i=1}^{4500} u_i \quad (4)$$

$$\overline{u'^2} = \frac{1}{n} \sum_{i=1}^{4500} [u_i - \bar{u}]^2 \quad (5)$$

$$S = \frac{1}{n} \sum_{i=1}^{4500} \frac{[u_i - \bar{u}]^3}{[u'^2]^{3/2}} \quad (6)$$

In computing values from Equations (4), (5) and (6) any individual measurements deviating more than  $\pm 3\sigma$  from the mean were discarded as noise. The number of discarded points was typically about 10 to 15 and always less than 50 per data set.

The experimental grid consisted of 70 grid points divided into 7 radial grid lines as shown in Figure 9. Each grid point was spaced approximately 7.62 mm (0.300 in) apart in the radial direction while the grid line separation was two step heights starting at  $x/H = 1$ . The grid line at  $x/H = 13$  was excluded. The "inlet" velocity and turbulence intensity profiles were measured at  $x/H = 1/3$ . This measurement plane was as close to the sudden expansion plane as the LDV system could be used due to physical obstruction.

Although the system geometry was axially symmetric the flow downstream of the sudden expansion may not be. Thus it was necessary to determine if symmetry existed in the downstream flow. Symmetry was tested for the cold flow by two means. As a coarse check static pressure measurements were

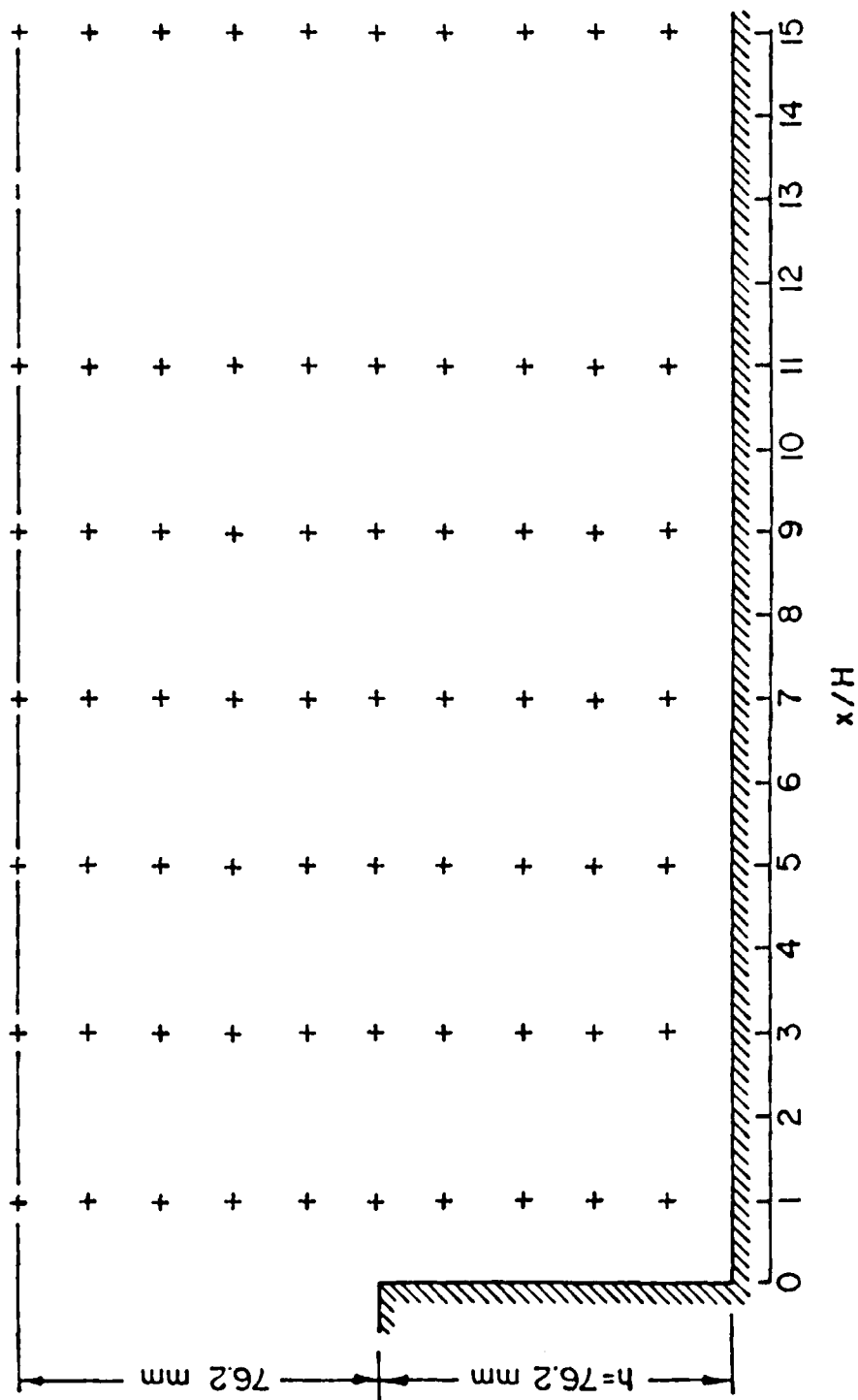


Figure 9. Experimental Measurement Grid

taken circumferentially at six streamwise locations in a steel test section of the same geometry as that of the quartz test section. These measurements showed no asymmetry in the flow. The second more sensitive technique involved taking LDV measurements on both sides of the centerline of the test section. The results showed that the mean flow and rms velocities were indeed axially symmetric. Because of this, only measurements along a radius in the horizontal plane were required to map the flow field. The hot flow was also believed to be symmetric as the fuel was injected well upstream of the sudden expansion at four circumferential locations. Also, the amount of fuel added to the flow was very low ( $f/a = 0.018$ ) and did not change the flow field appreciably.

#### 4. THE STREAM FUNCTION

The stream function,  $\psi$ , for an axisymmetric incompressible flow is defined by

$$\bar{u} = \frac{\partial \psi}{\partial r} \quad (7)$$

Using second order central differencing about the points  $i$  and  $i + 1$ , Equation (7) can be approximated by

$$\frac{\bar{u}_{1+1} + \bar{u}_1}{2} = \frac{\psi_{1+1} - \psi_1}{r_{1+1} - r_1} + F(x) \quad (8)$$

At any given x-plane  $F(x)$  will be a constant and can be arbitrarily set to zero. Because of this, Equation (8) becomes

$$\psi_{1+1} = \psi_1 + (r_{1+1} - r_1) \left[ \frac{\bar{u}_{1+1} + \bar{u}_1}{2} \right] \quad (9)$$

The stream function values, calculated from equation (9), were then tabulated and contours of the stream function were determined for specific values of this parameter.

#### 5. THE REATTACHMENT LENGTH

The reattachment length,  $x_r$ , was determined by linearly extrapolating a  $\bar{u} = 0$  curve to the wall. The  $\bar{u} = 0$  curve was located by linear interpolation between adjacent grid points at which  $\bar{u}$  changed sign.

#### 6. THE MASSFLOW RATE

Since the flow was axisymmetric, it was possible to compute the mass flux at each measurement plane. This

permitted a further check on the accuracy of the velocity data. Both the biased and unbiased cold flow mean velocity data were integrated using piecewise integration of a polynomial fit. The mass flux at each grid line was normalized with the inlet mass flux, which was calculated using a 1/7 power law velocity profile for fully developed pipe flow. This power law profile gave an integrated mass flux that agreed with the experimental integrated mass flux at grid lines located at  $x/H = 5$  and  $7$  to better than one percent (see Table 5). Mass flux was not computed for the hot flow case due to the lack of temperature and therefore density information.

SECTION V  
EXPERIMENTAL RESULTS

1. INTRODUCTION

In this section the results of the LDV velocity measurements in both the isothermal (cold) flow and reacting (hot) flow cases are presented. Cold flow data in the biased and unbiased modes will be compared. As previously noted, only biased hot flow measurements could be made. The Reynolds number for the axisymmetric sudden expansion based on step height and inlet centerline velocity was  $5.5 \times 10^4$ , which corresponds to an inlet centerline velocity,  $U_1 = 22.07 \text{ m/s}$ . Measurements with combustion occurring were made using gaseous propane and air at an overall equivalence ratio of  $\phi = 0.28$ . A lean mixture was employed to keep the temperature in the test section at levels which allowed steady state operation. The propane was injected well upstream of the sudden expansion as noted in Section III. Thus the propane and air were reasonably well mixed at the sudden expansion. However, a completely premixed mixture

was not obtained, since stable combustion was achieved at an overall fuel-air mixture ratio well below the lean burning limit.

Representative plots of mean streamwise velocity, streamwise turbulence intensity normalized with the inlet centerline velocity and the local streamwise turbulence intensity for both cold flow (biased and unbiased) and hot flow (biased) are presented. Skewness coefficient profiles at four grid lines are also presented. Flow streamlines and reattachment lengths are derived from the experimental data. Integrated mass flux comparisons of the biased and unbiased cold flow velocity data are made at different grid lines and the measured temperature profile at  $x/H = 17.7$  is presented. The comparison of the cold flow measurements with numerical predictions is contained in Section VI. The reduced experimental velocity data is tabulated in Appendix A1. The tabulated data include mean velocities, normalized turbulence intensities and local turbulence intensities for each measurement point. Temperature data at the exit plane is tabulated in Appendix A2.

## 2. AVERAGE STREAMWISE VELOCITY

The inlet velocity profile was measured experimentally at  $x/H = 0.33$ . This measurement plane was as close to the plane of the sudden expansion as the LDV setup would permit.

Figure 10 shows the experimental unbiased streamwise velocity measurements at  $x/H = 0.33$  along with a  $1/7$  power law velocity profile. As the figure shows, the agreement between the measurements and a  $1/7$  power law profile was very good. This allowed one to obtain the inlet mass flow rate by analytically integrating the power law velocity profile across the inlet pipe radius. The power law profile was also used as an inlet boundary condition in the numerical prediction code described in Section VI.

Figures 11 through 17 show the normalized mean streamwise velocity profiles at measurement planes located 1, 3, 5, 7, 9, 11, and 15 step heights downstream of the sudden expansion. The data sets presented in each of the figures are for biased and unbiased cold flow and for biased hot flow. Figure 18 summarizes the normalized mean streamwise velocity data presented in Figures 11 through 17 (cold flow only) in one plot. The computational predictions described in Section VII are also shown on this figure. Figure 19 summarizes biased hot and unbiased cold flow normalized mean streamwise velocity data in one plot. Although the statistical error was found to be rather small ( $\pm 1\%$  for mean velocities and  $\pm 3\%$  for turbulence intensities), there can be additional experimental error due to the problem of defining the probe volume location exactly and run condition drift. The experimental error can be identified roughly by noting

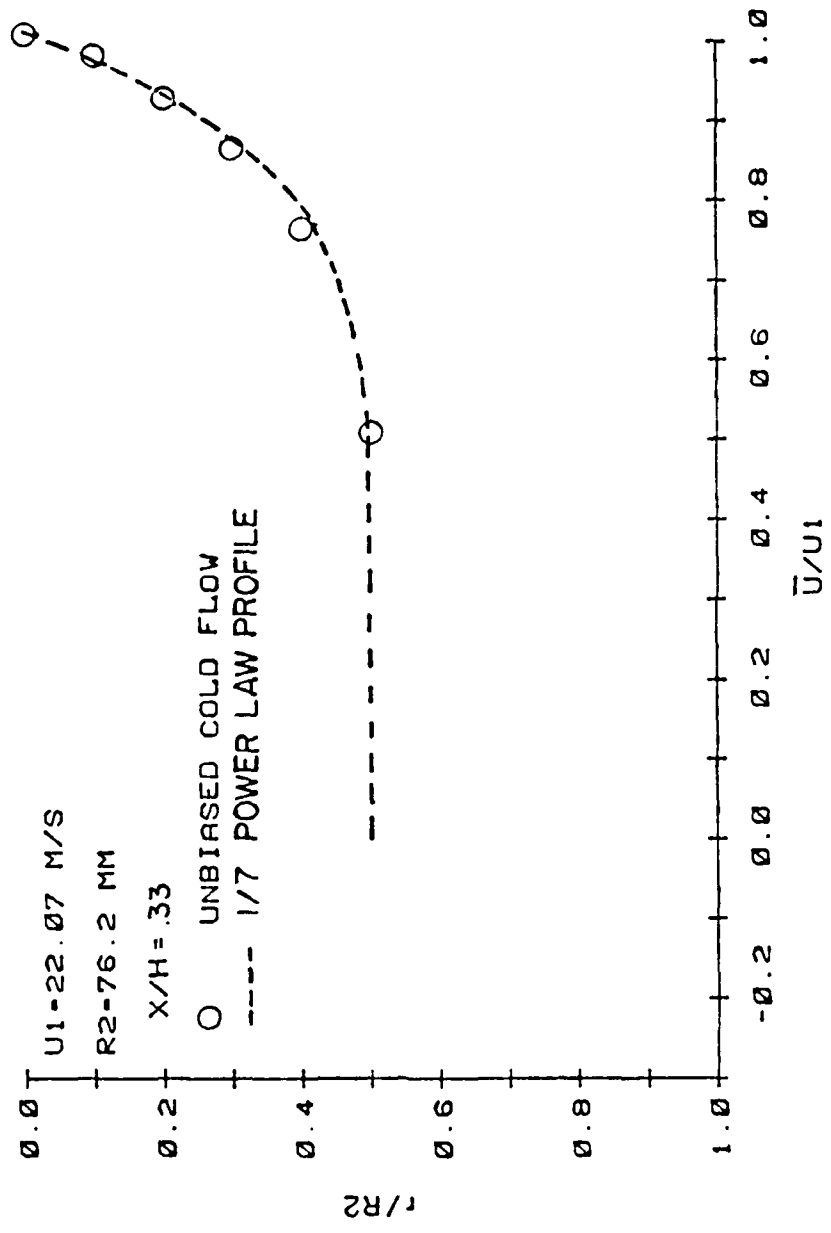


Figure 10. Measured Mean Streamwise Velocity Profile at  $x/H = 1/3$

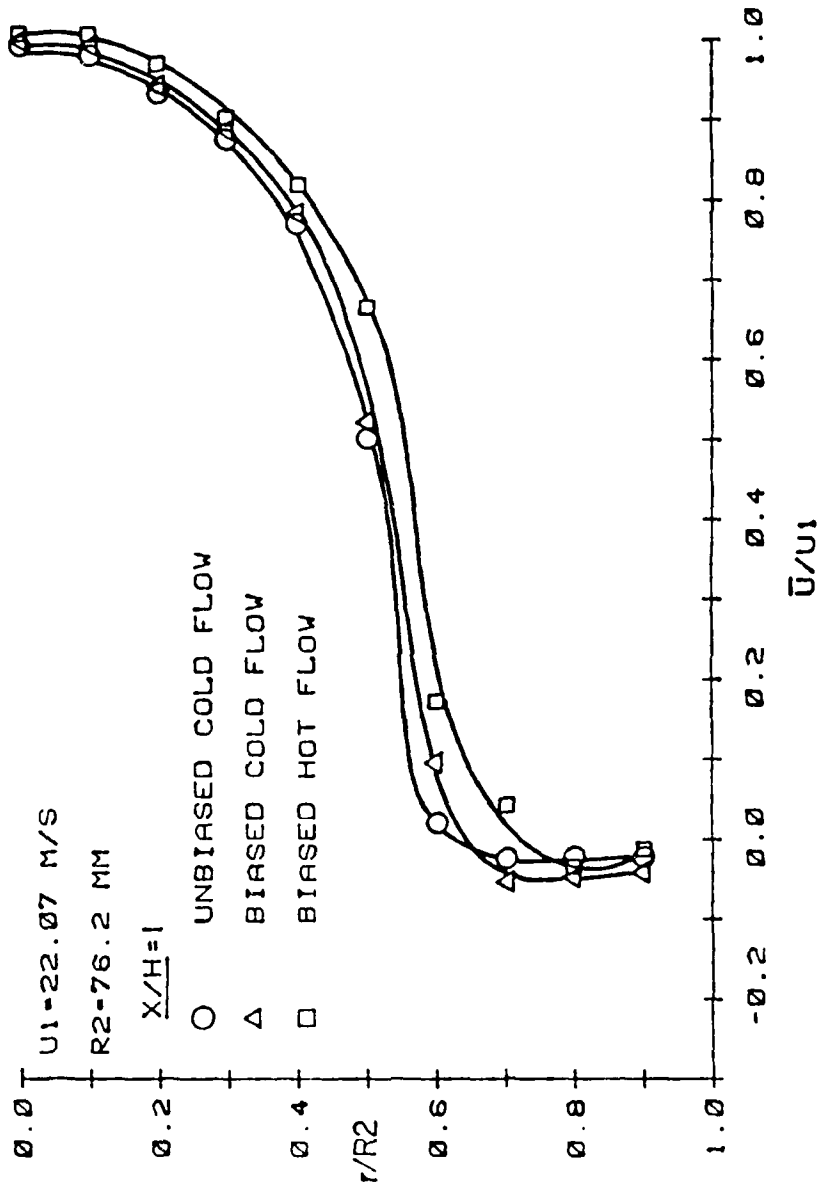


Figure 11. Measured Mean Streamwise Velocity Profiles at  $x/H = 1$

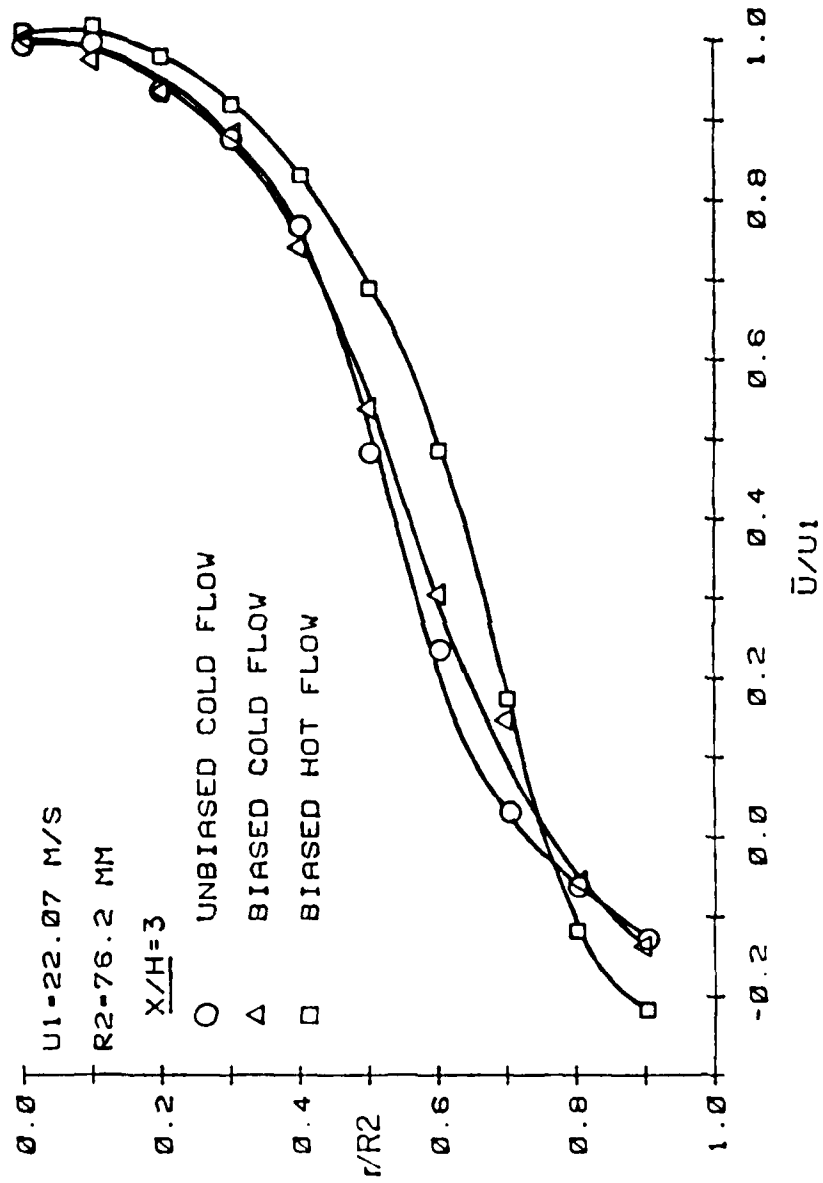


Figure 12. Measured Mean Streamwise Velocity Profiles at  $x/H = 3$

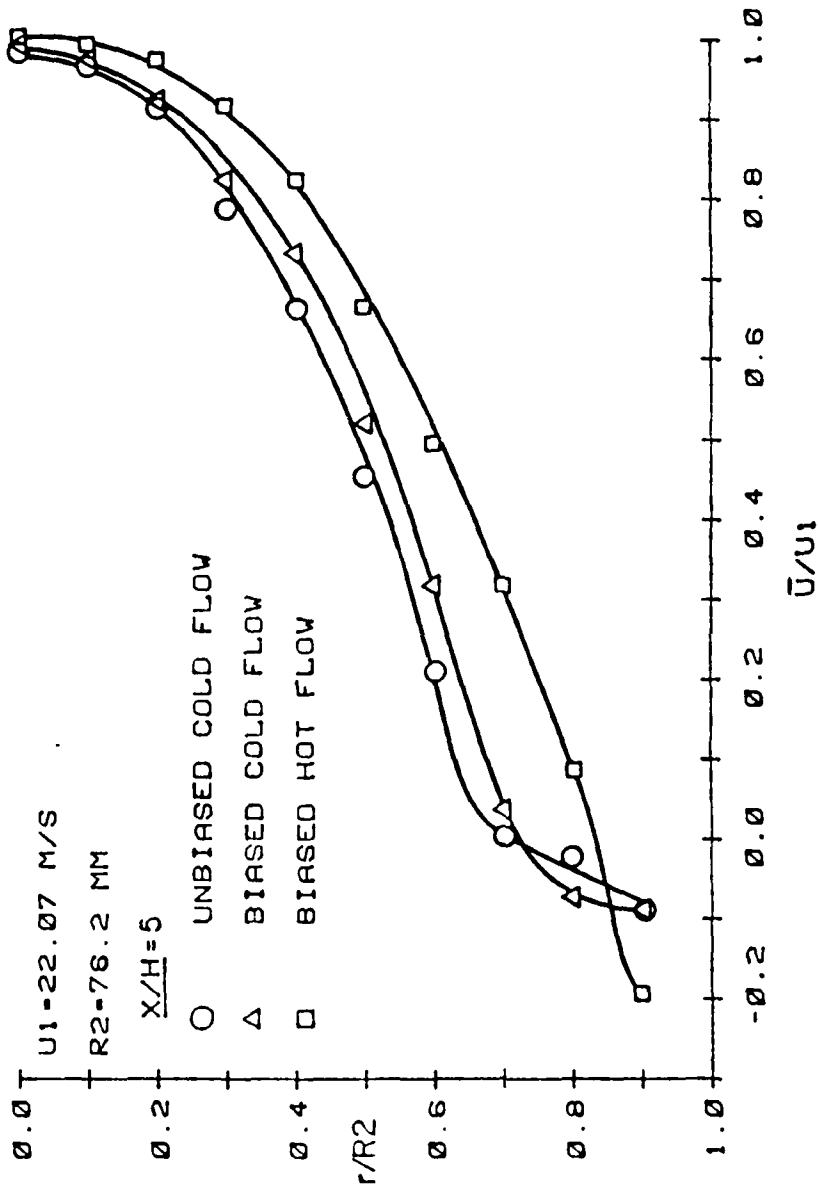


Figure 13. Measured Mean Streamwise Velocity Profiles at  $x/H = 5$

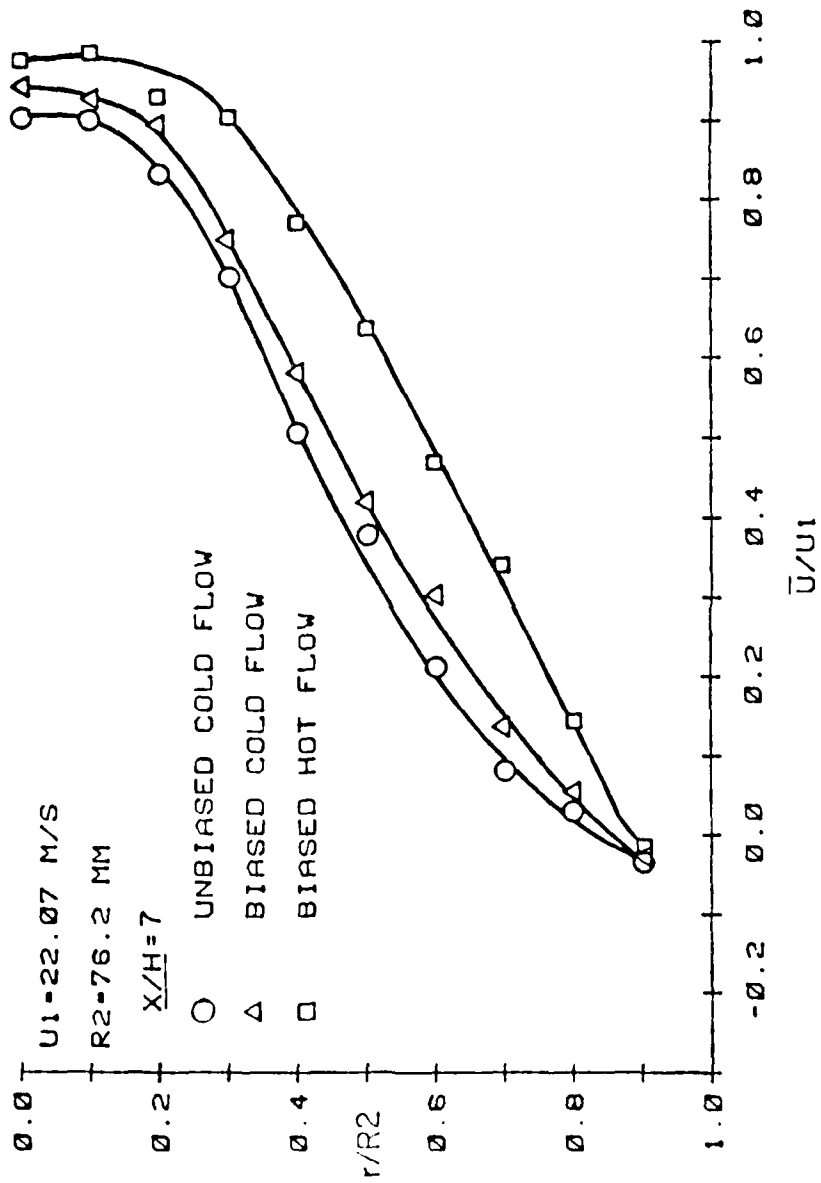


Figure 14. Measured Mean Streamwise Velocity Profiles at  $x/H = 7$

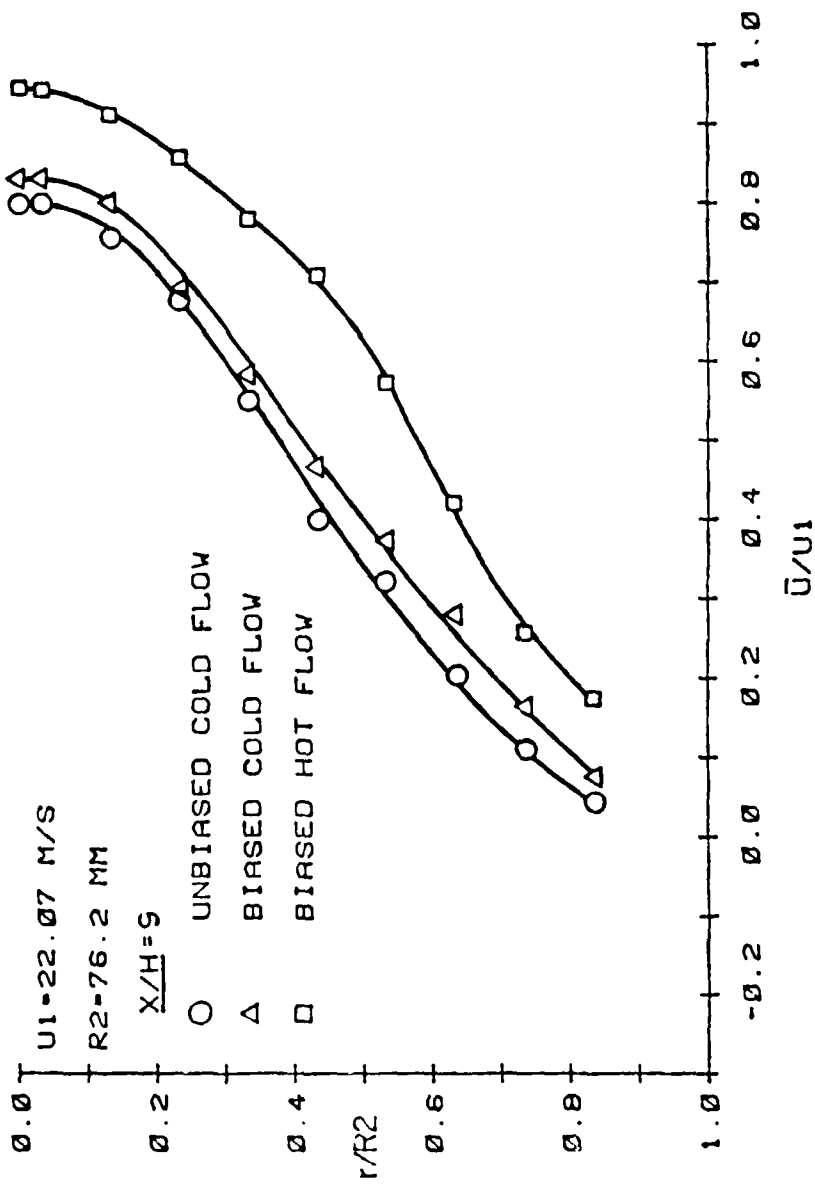


Figure 15. Measured Mean Streamwise Velocity Profiles at  $x/H = 9$

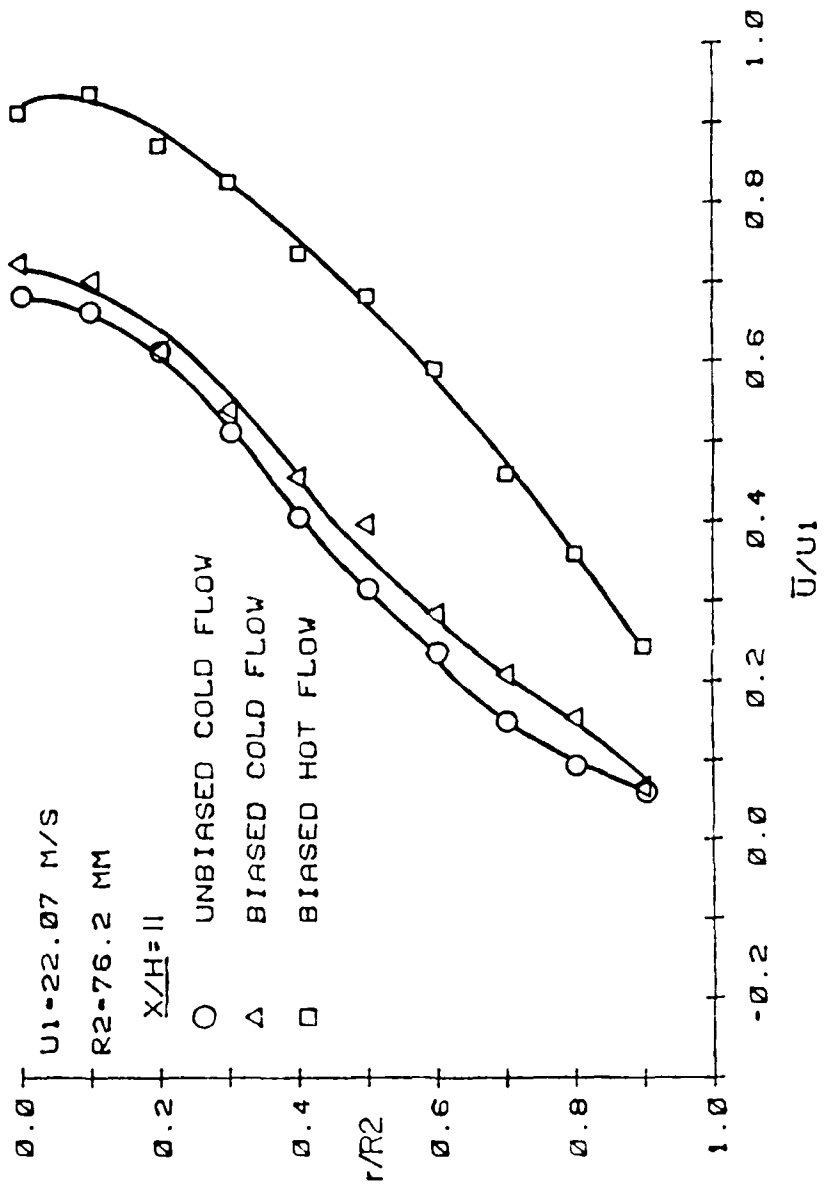


Figure 16. Measured Mean Streamwise Velocity Profiles at  $x/H = 11$

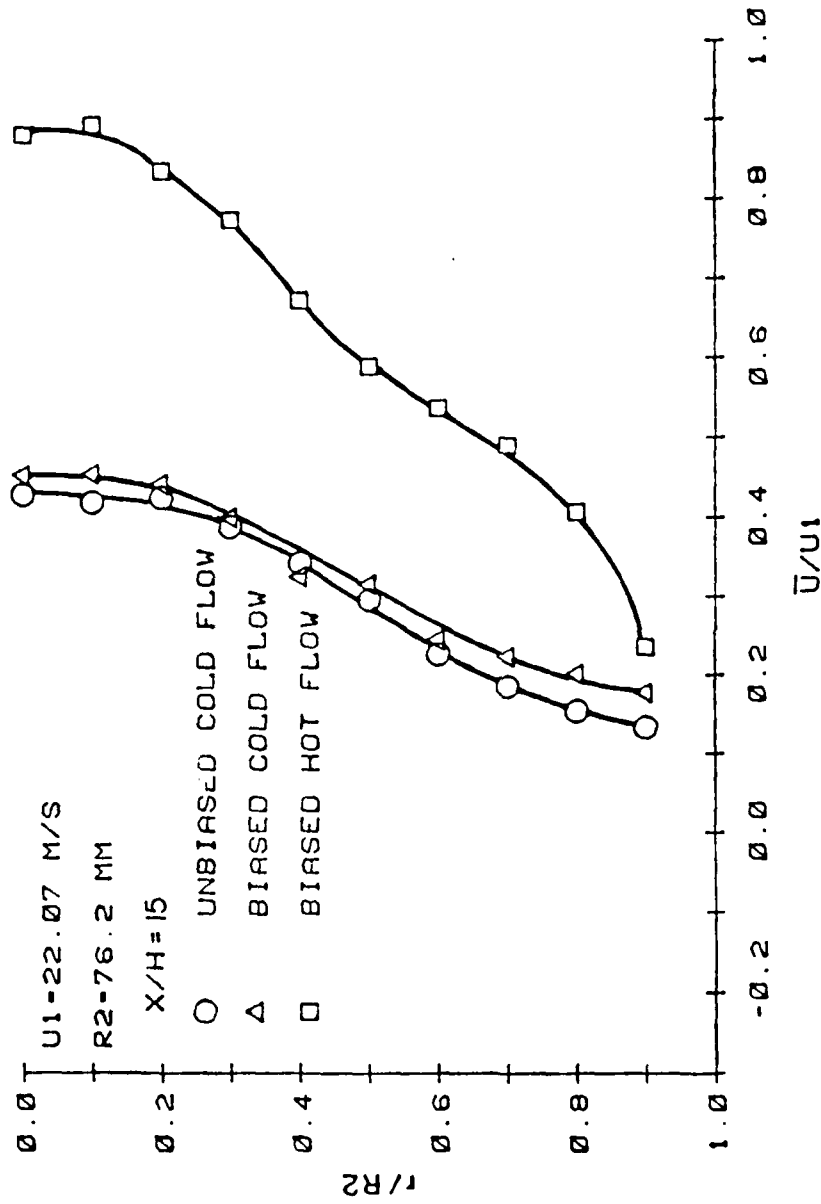


Figure 17. Measured Mean Streamwise Velocity Profiles at  $x/H = 15$

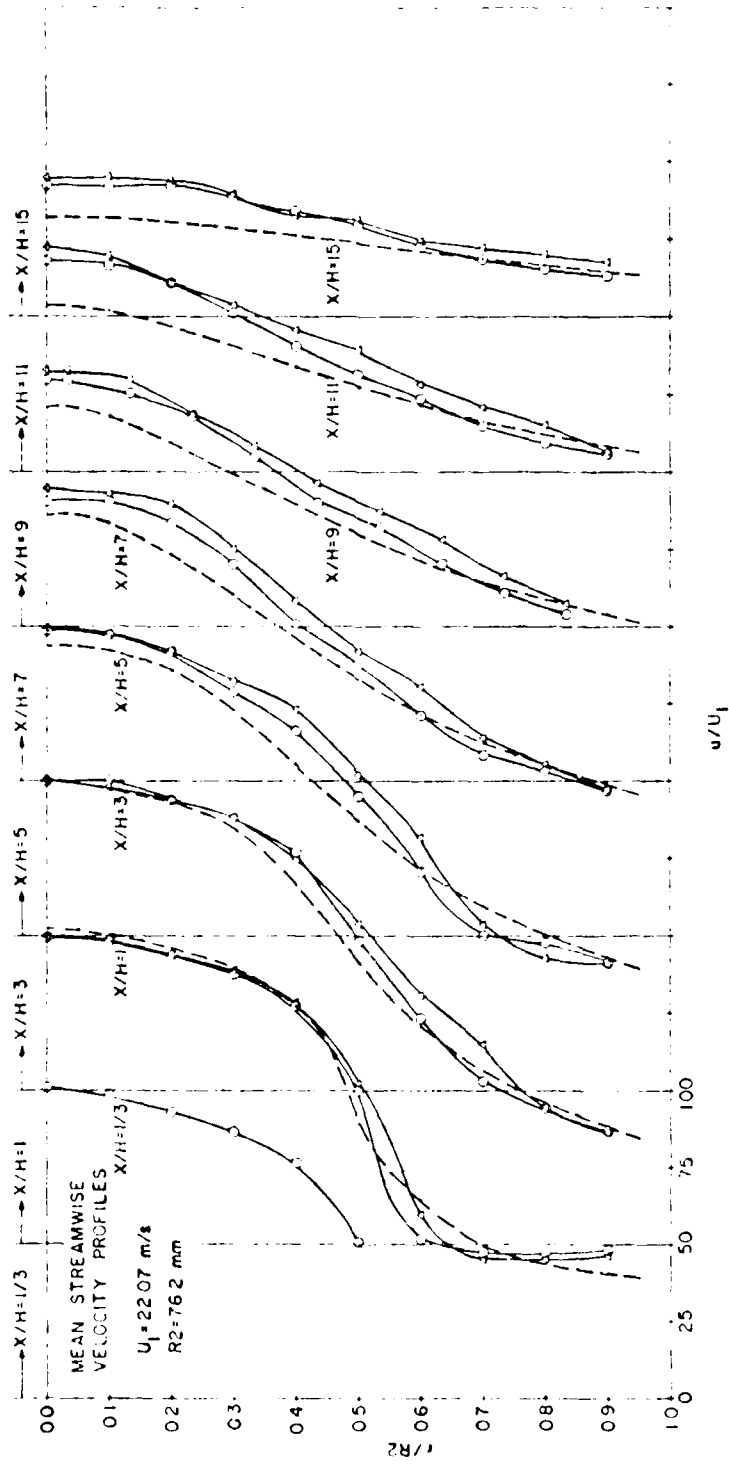


Figure 16. Measured Mean Streamwise Velocity Profiles in Cold Flow  
 (o - unbiased cold flow, Δ - 2/E/FIX prediction)

AD-A131 882

LASER VELOCIMETER MEASUREMENTS AND ANALYSIS IN  
TURBULENT FLOWS WITH COMBU. (U) PURDUE UNIV LAFAYETTE  
IN SCHOOL OF MECHANICAL ENGINEERING  
W H STEVENSON ET AL. JUL 83

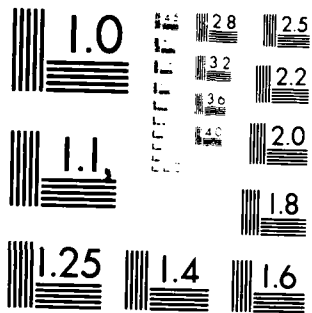
2/2

UNCLASSIFIED

F/G 21/2

NL

END
DATE
FILMED
9 83
DIC



MICROCOPY RESOLUTION TEST CHART  
NATIONAL BUREAU OF STANDARDS-1963-A

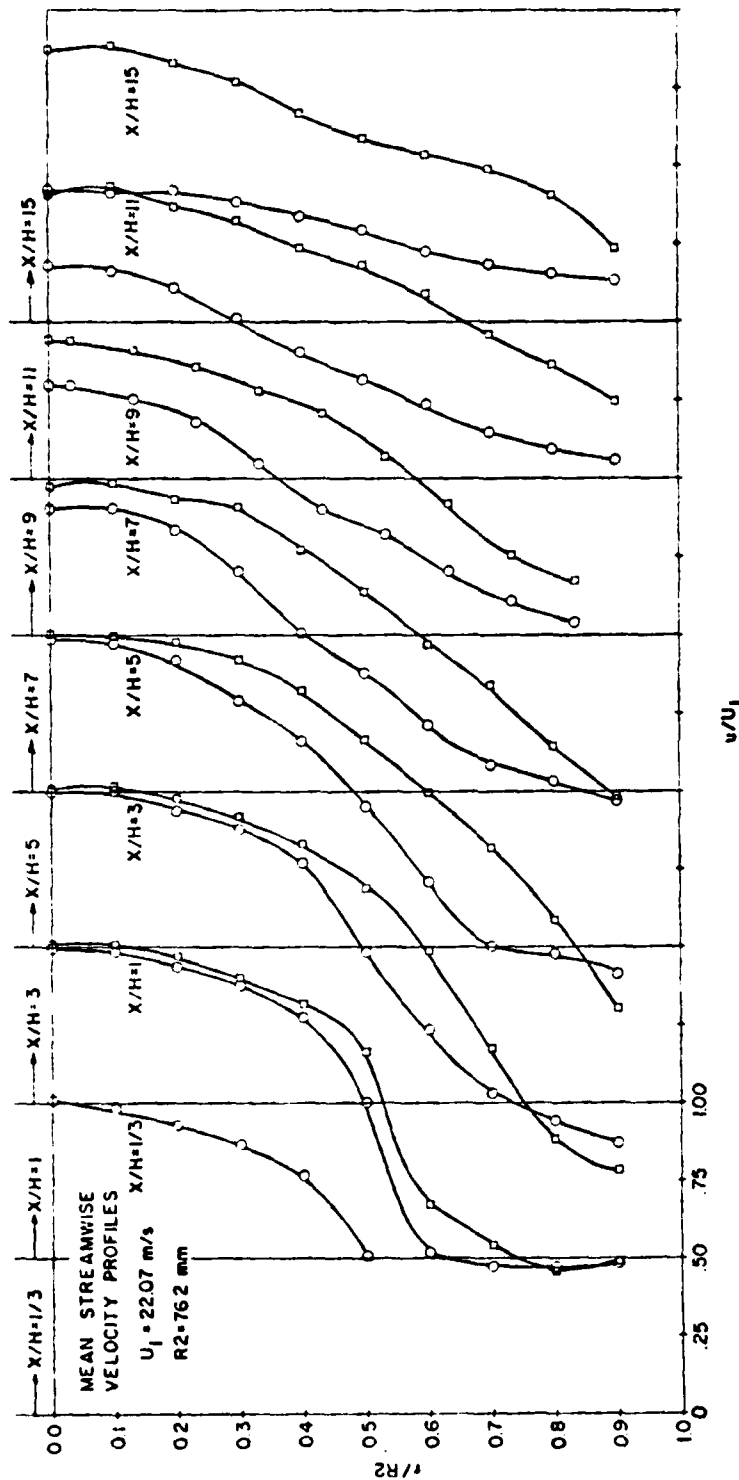


Figure 19. Measured Mean Streamwise Velocity Profiles in Cold Flow and in Reacting Flow  
 (o - unbiased cold flow, □ - biased hot flow)

the deviation between individual data points and the solid line drawn through the data. The solid lines represent a "best fit" profile.

Several observations can be made from the mean stream-wise velocity data. The trends of the biased versus unbiased mean velocities are as one would expect. That is, the absolute value of the biased mean velocity is higher than the absolute value of the unbiased mean velocity throughout the flow field. The differences are largest in the regions of high turbulence intensity and are insignificant in regions of low turbulence intensity. There is a crossover of the mean velocity profiles as you pass from a positive flow region into a negative flow region as shown in Figures 11 through 13. Typically, the biased cold flow data was less than 1 m/s higher than the unbiased cold flow data throughout the flow field. Velocity differences in the biased and unbiased cold flow data are almost indistinguishable in the core of the inlet jet, but show a difference of from 0.4 to 0.6 m/s in the turbulent region at axial distances greater than five step heights.

Maximum negative velocities in the recirculation zone were -2.9 m/s and -4.8 m/s for the cold flow and hot flow cases, respectively. These values convert to -13% and -22% of the inlet centerline velocity. Although the recirculation zone was found to be somewhat stronger in the hot flow case it was also found to be thinner and shorter than the

cold flow recirculation zone. Pitz also observed this effect in Ref. [29] where LDV measurements were made in isothermal and reacting flows behind a rearward facing step. The profiles in Figure 19 show that reattachment occurs between 7 and 9 step heights downstream of the sudden expansion in the cold flow case and at approximately 7 step heights downstream of the sudden expansion in the hot flow case. The effects of combustion (i.e. higher velocities due to higher temperatures) are not seen until axial distances are greater than three step heights. Note the inflection point present in the velocity profiles at  $x/H = 15$  in Figure 17. This characteristic was also found by Stevenson, et al. [15] and indicates that the flow is far from fully developed.

Figure 20 shows the centerline velocity decay for the unbiased cold flow and the biased hot flow cases. Also shown in this figure are the corresponding cold flow data obtained by Stevenson, et al. [15], Moon and Rudinger [12] and Freeman [11]. The cold flow data obtained in the present study show very good agreement with that of Stevenson, et al. [15], Moon and Rudinger [12] and Freeman [11] when plotted as a function of downstream distance normalized with step height. This is in spite of the fact that the expansion area ratios of the various test sections were different by as much as a factor of two. Also, inlet boundary conditions were different, varying from an almost flat inlet

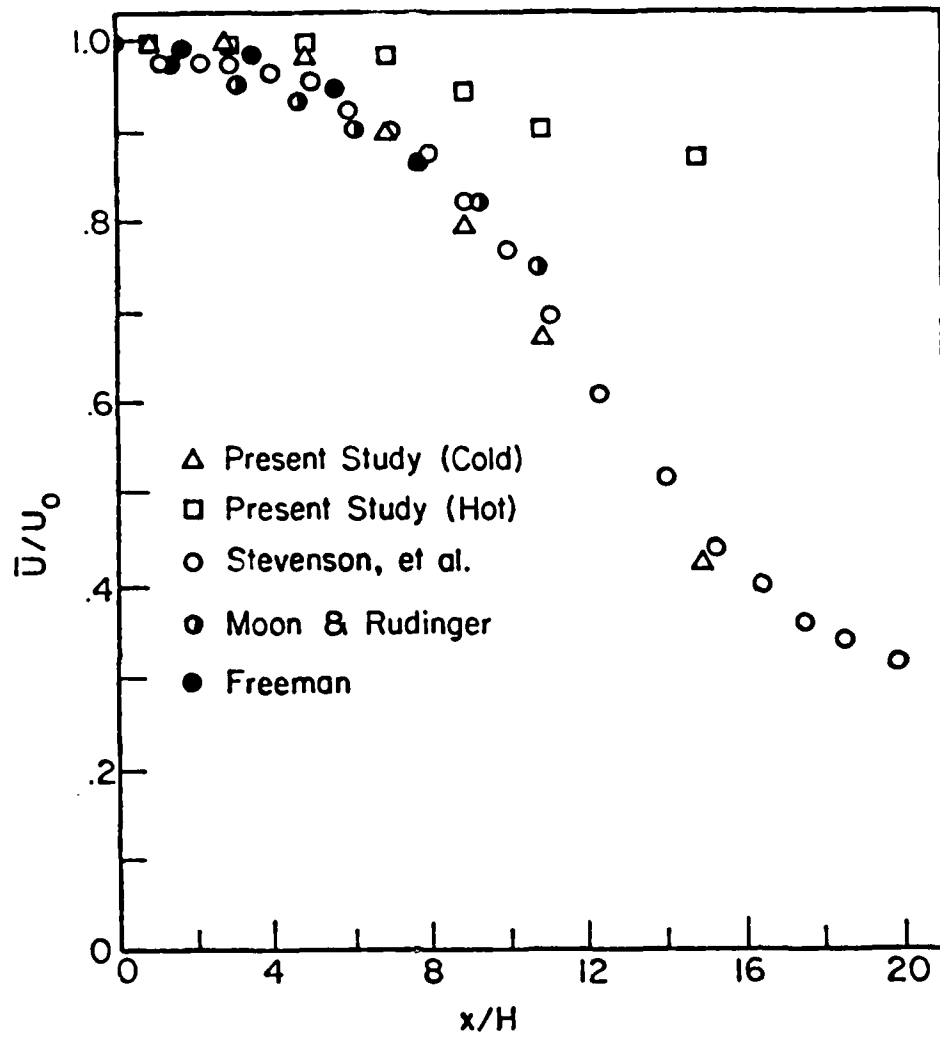


Figure 20. Measured Mean Centerline Velocity Decay

velocity profile in [15], to fully developed pipe profiles. This figure also indicates that the flow has not relaxed to fully developed pipe flow at 15 step heights downstream of the sudden expansion, since  $U/U_1 = 0.41$  instead of 0.25 as would be obtained from an area ratio argument.

Measurement inaccuracies due to steep velocity gradients can be a problem when using an LDV system. The errors in high velocity gradient regions can be large, especially if there are fluctuations (instabilities) in the flow field. This error is primarily due to the finite probe volume size. For the geometry used in this study, the highest velocity gradients occur in the shear layer at a radius equal to the inlet pipe radius close to the sudden expansion plane. Using the velocity profile at  $x/H = 1$  to calculate the velocity gradient across the shear layer gives  $\delta u/\delta R = 140s^{-1}$ . This converts to a velocity gradient of 0.14 m/s per millimeter. In this study the probe volume (length of 2 mm) would therefore have a 0.28 m/s velocity gradient across it. This does not effect the mean velocity calculation, but does effect the turbulence intensity calculation. Using the procedure given by Karpuk and Tiederman [51], which assumes a cylindrical probe volume and a linear velocity gradient across the probe volume, the maximum error in turbulence intensity due to the finite size of the probe volume was found to be 0.08 m/s. Thus velocity gradient

error was deemed insignificant for the present investigation, since this calculation is a worst case example.

### 3. STREAMWISE TURBULENCE INTENSITY

The normalized inlet turbulence intensity profile at  $x/H = 0.33$  is shown in Figure 21. As expected fairly low levels of turbulence are present in the central core of the inlet "jet" flow, whereas large levels of turbulence are present in the shear layer at the edge of the inlet pipe. This figure shows that the turbulence intensity normalized to the inlet centerline velocity varies from 3.5% in the core region to 15% in the shear layer. Since the local average velocity decreases as you move toward the shear layer the local inlet turbulence intensity varies from 3.5% at the centerline to 31.3% in the shear layer at  $x/H = 0.33$ .

Figures 22 through 28 show the streamwise turbulence intensity normalized with the inlet centerline velocity at measurement planes located 1, 3, 5, 7, 9, 11, and 15 step heights downstream of the sudden expansion plane. Again, results from the three data sets mentioned earlier are presented here. Figure 29 summarizes the normalized streamwise turbulence intensity data presented in Figures 22 through 28. These figures all show a peak in the normalized turbulence intensity which broadens as the mixing zone spreads in the downstream direction. The peak turbulence

U1-22.07 M/S  
 R2-76.2 MM  
 X/H = .33  
 ○ UNBIASED COLD FLOW

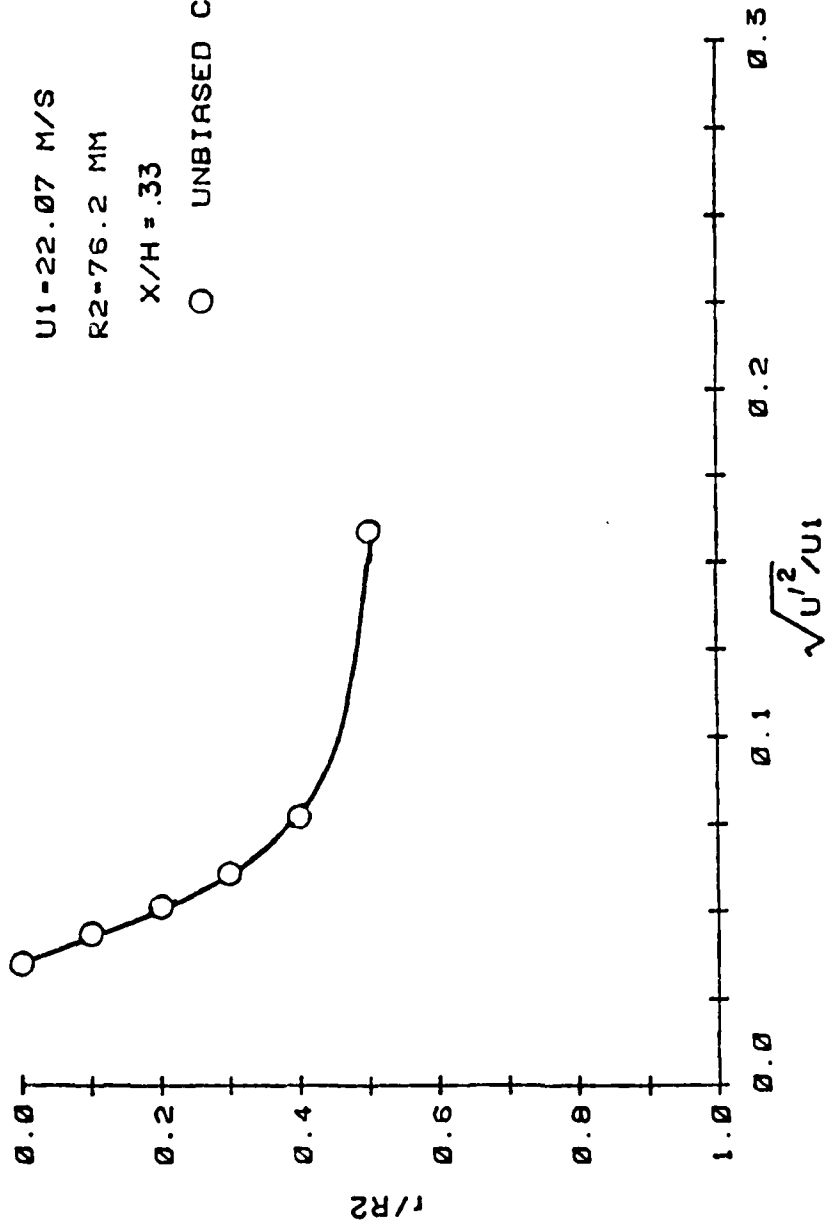


Figure 21. Measured Normalized Streamwise Turbulence Intensity Profile at  $x/H = 1/3$

U1=22.07 M/S  
 R2=76.2 MM

$X/H=1$

- UNBIASED COLD FLOW
- △ BIASED COLD FLOW
- BIASED HOT FLOW

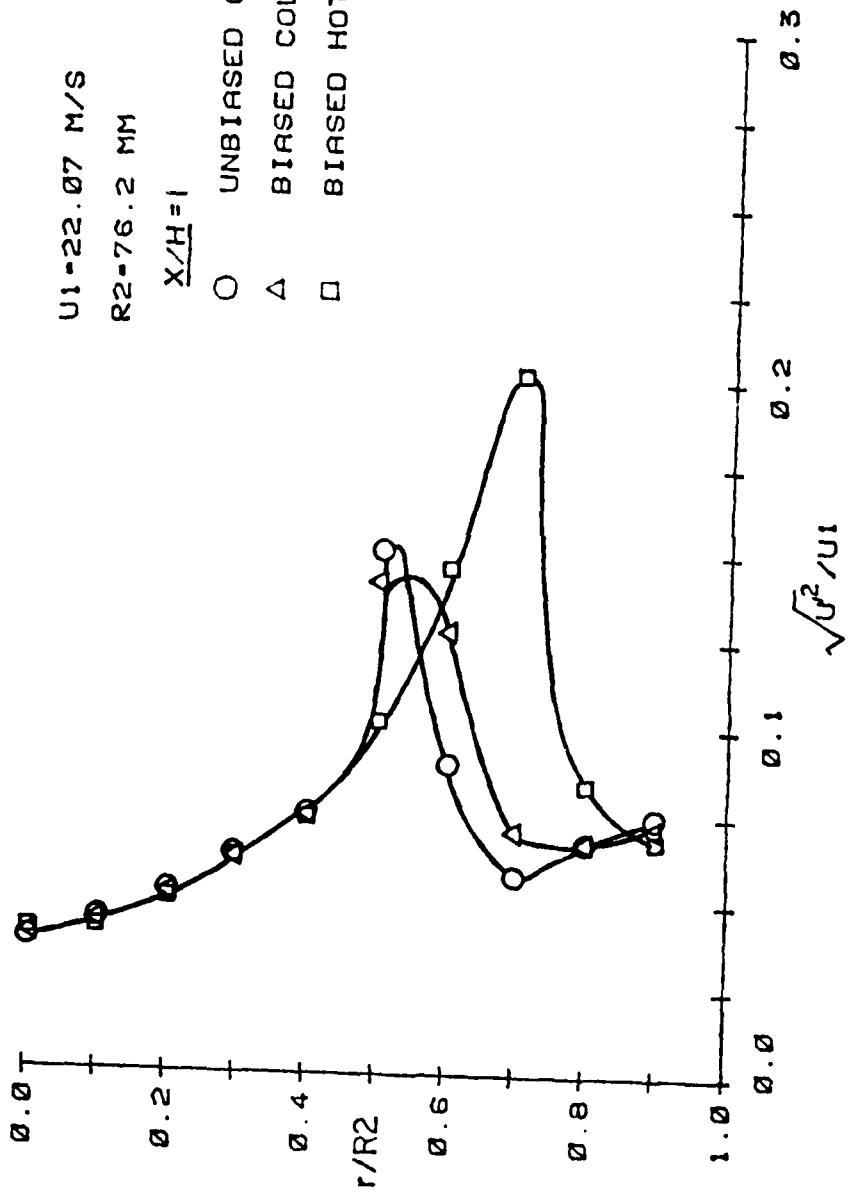


Figure 22. Measured Normalized Streamwise Turbulence Intensity Profiles at  $x/H = 1$

U1=22.07 M/S

R2=76.2 MM

X/H=3

O UNBIASED COLD FLOW

Δ BIASED COLD FLOW

□ BIASED HOT FLOW

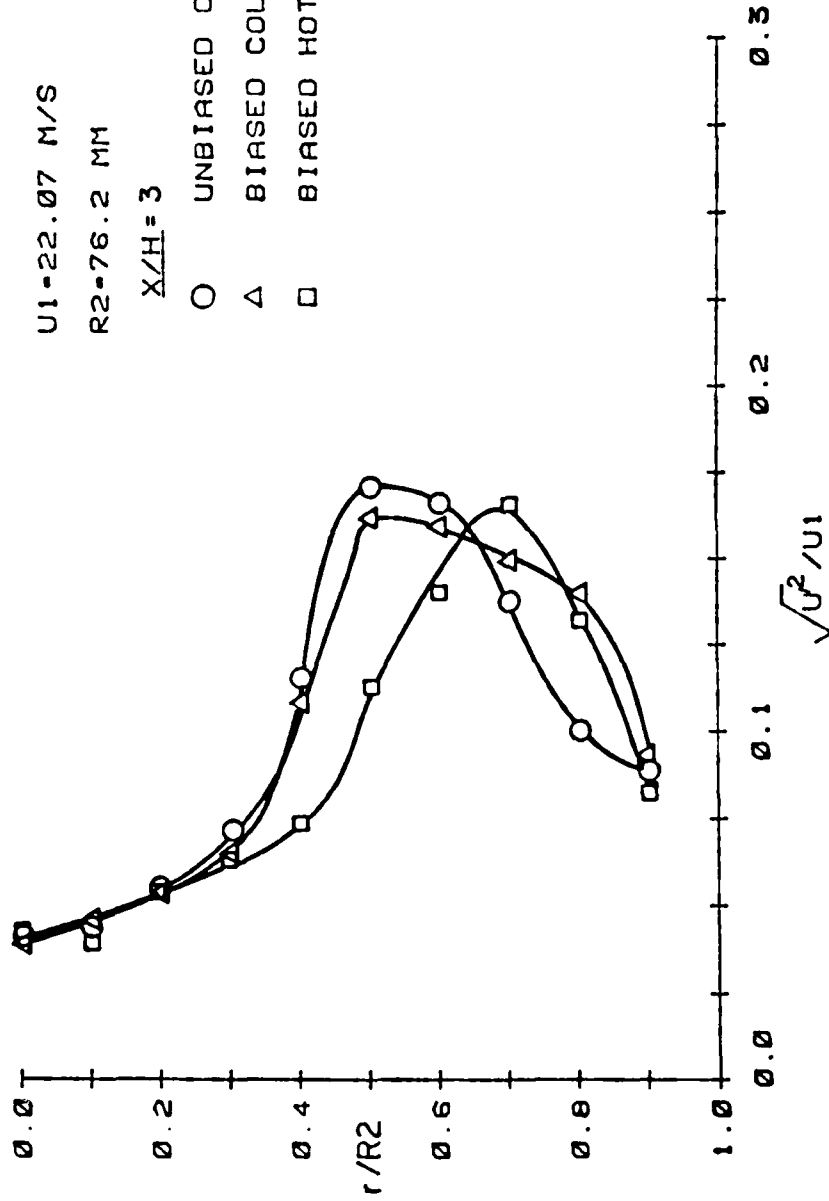


Figure 23. Measured Normalized Streamwise Turbulence Intensity Profiles at  $x/H = 3$

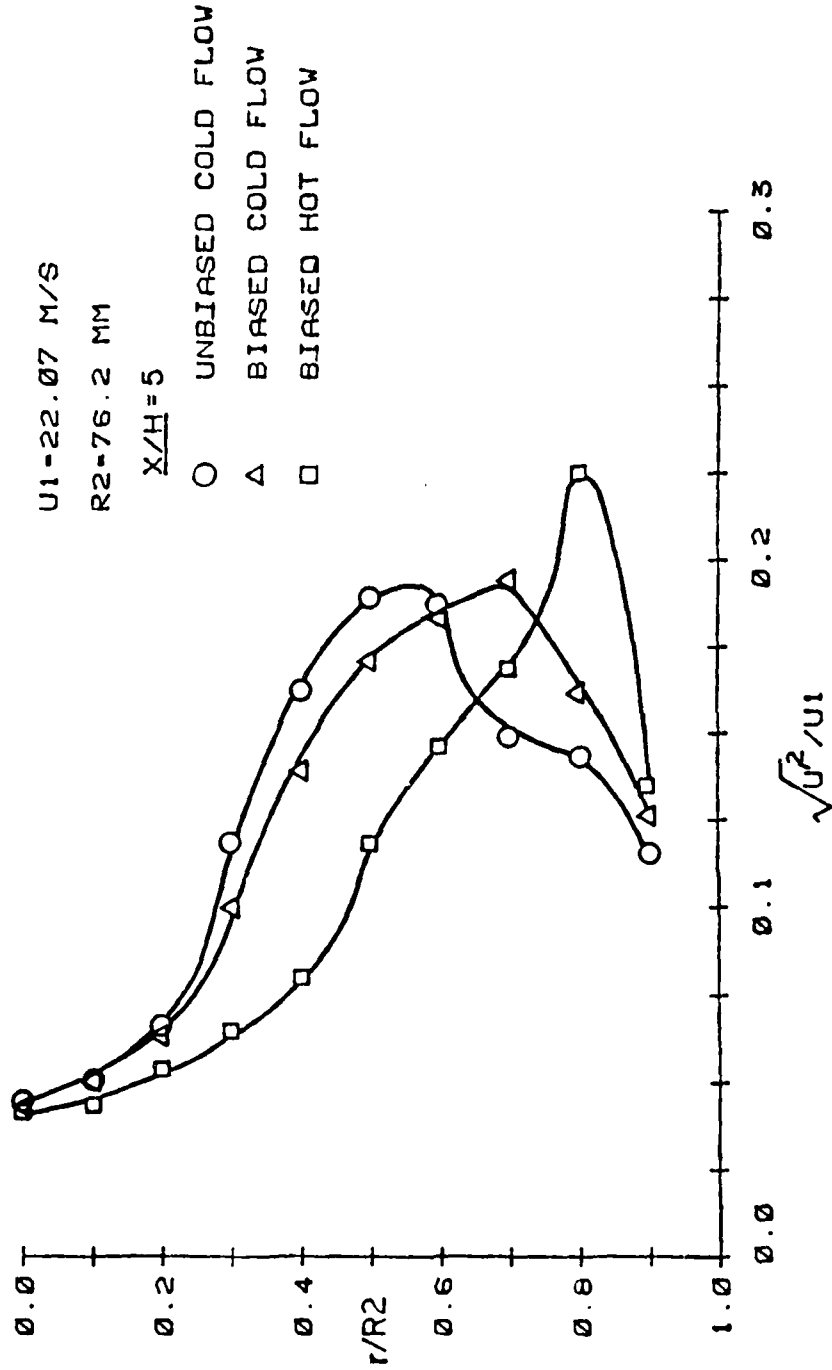


Figure 24. Measured Normalized Streamwise Turbulence Intensity Profiles at  $x/H = 5$

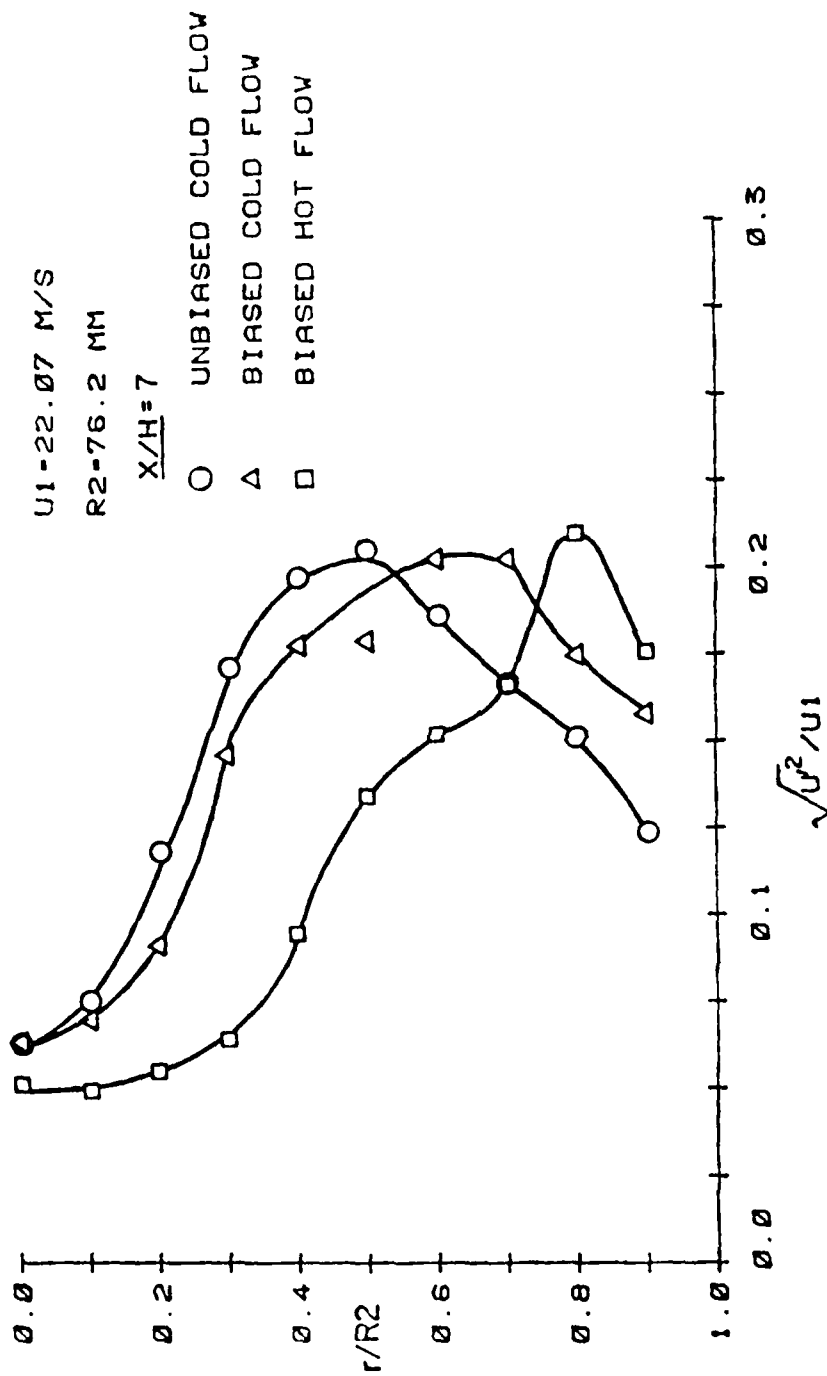


Figure 25. Measured Normalized Streamwise Turbulence Intensity Profiles at  $x/H = 7$

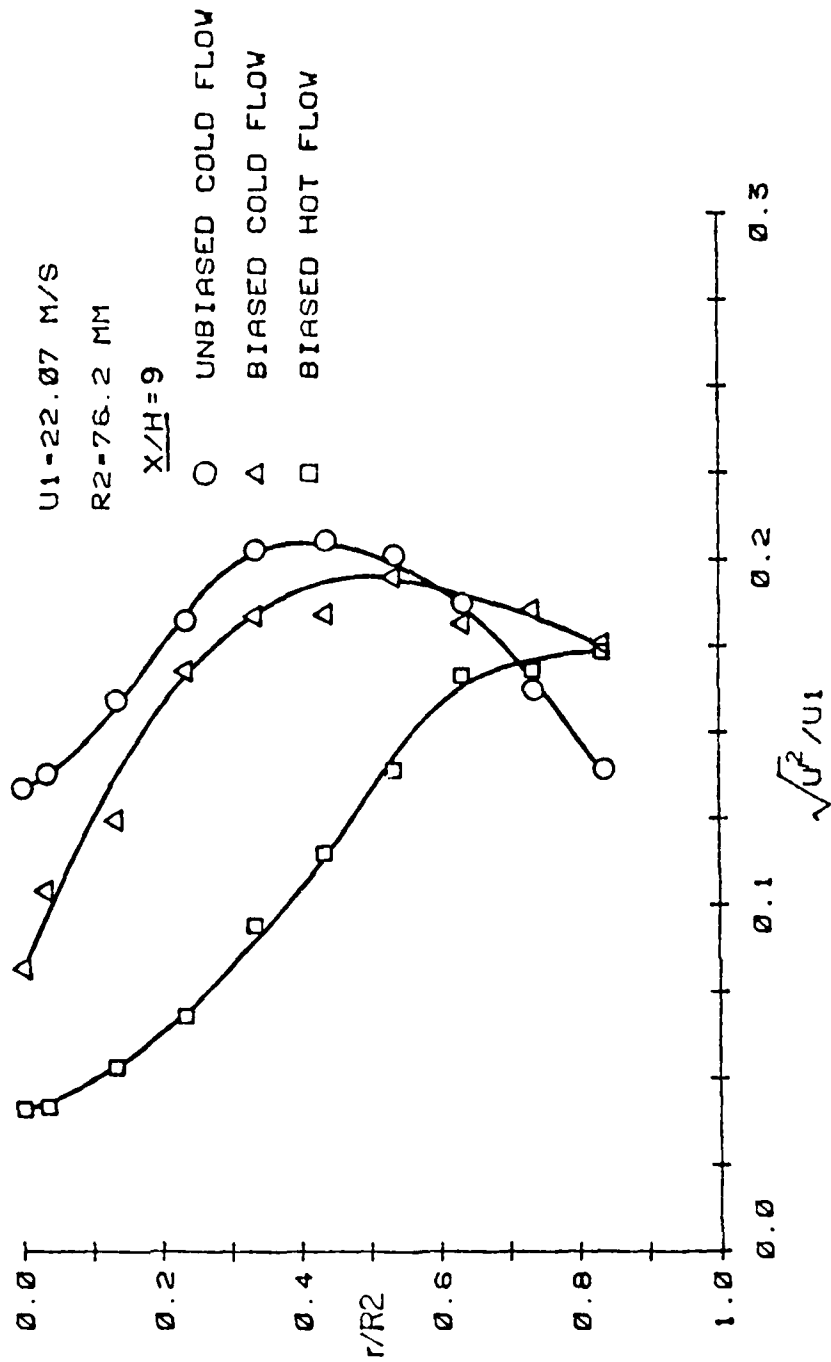


Figure 26. Measured Normalized Streamwise Turbulence Intensity Profiles at  $x/H = 9$

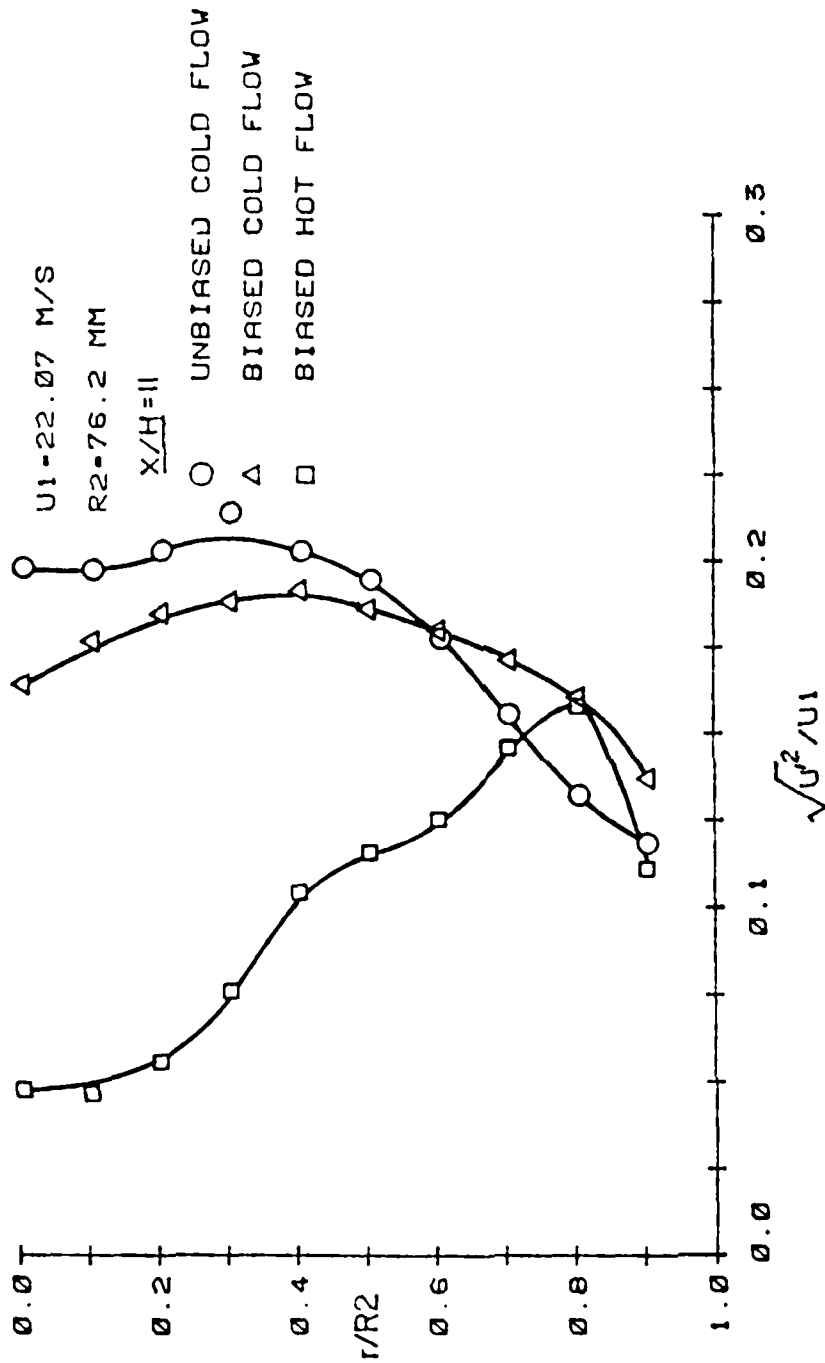


Figure 27. Measured Normalized Streamwise Turbulence Intensity Profiles at  $x/H = 11$

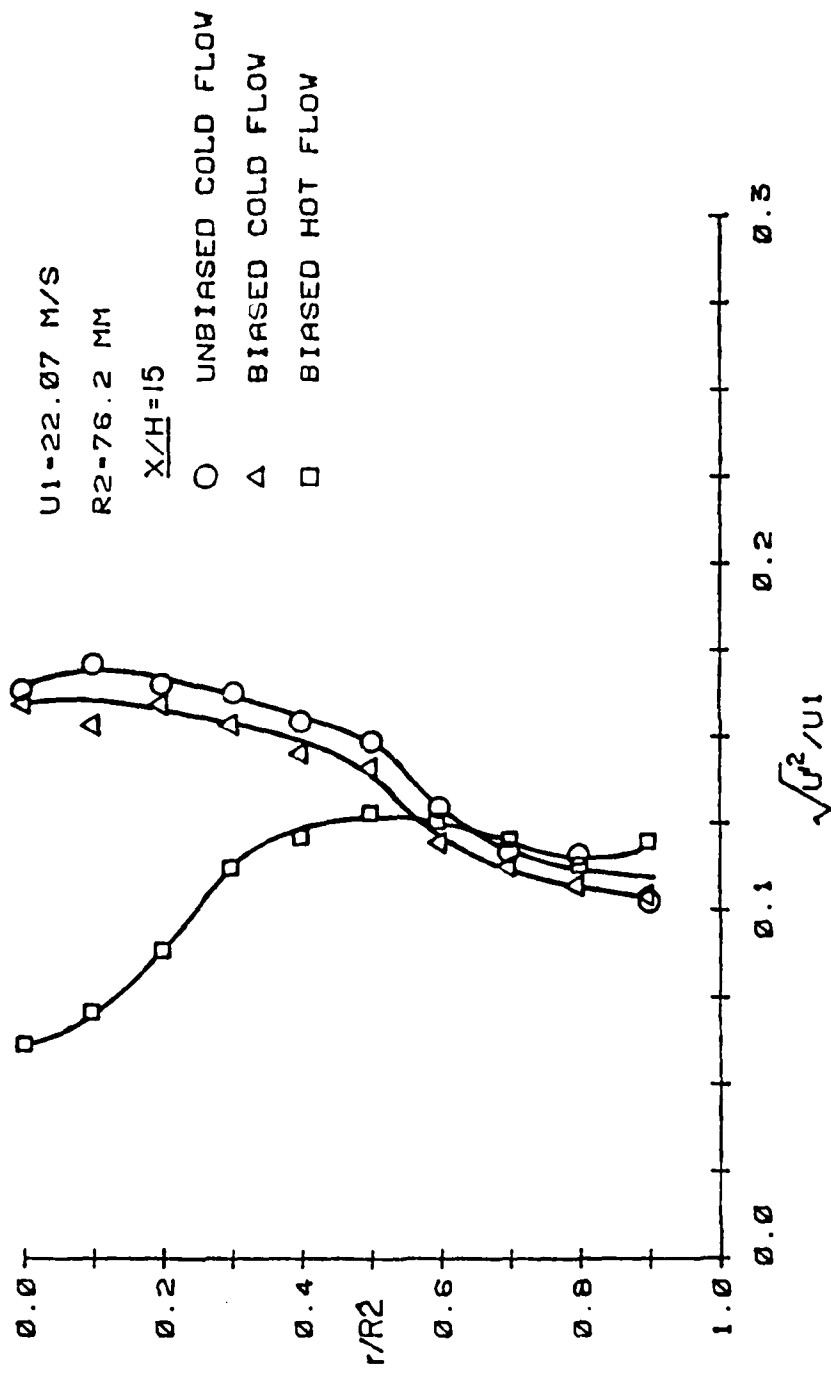


Figure 28. Measured Normalized Streamwise Turbulence Intensity Profiles at  $x/H = 15$

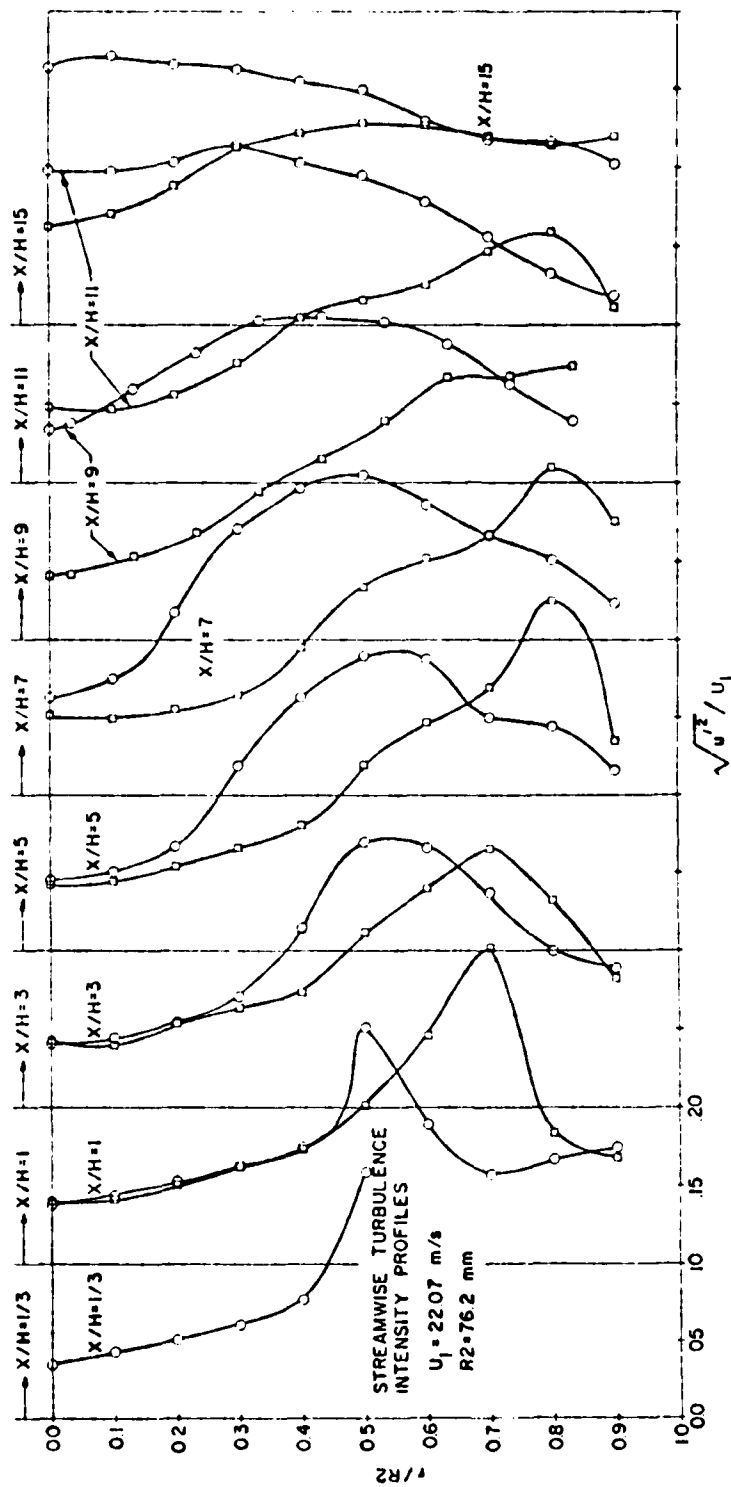


Figure 29. Measured Normalized Streamwise Turbulence Intensity Profiles  
 (o - unbiased cold flow, □ - biased hot flow)

intensities identify regions of high shear and mixing. Maximum normalized streamwise turbulence intensities were found to be approximately 22% for both the hot and cold flows. By comparison, maximum values of normalized turbulence intensity reported for backward facing step flows are 28% by Pitz [29], 21% by Eaton and Johnston [5,6] and 19% by Bremner, et al. [3]. These results are in good agreement with the present study. Downstream of the recirculation zone, at  $x/H = 15$ , the streamwise turbulence intensity profile was found to be almost flat with normalized turbulence intensities of approximately 15%.

One interesting result found in the cold flow study was the change in shape of the normalized turbulence intensity profiles as a result of velocity bias as shown in Figures 22 through 27. These changes in profile were found to be insignificant in the low turbulence core region where biasing effects were small, and significant in regions of high turbulence. Most notably, the location of maximum shear was found to differ significantly for the biased and unbiased data sets. The value of normalized turbulence intensity obtained at a given location in a highly turbulent region was also found to differ (by as much as 35%). It should be noted that these differences were due only to the sampling technique, as the fluid structure of the flow remained the same. This indicates that the probability distributions constructed from the individual velocity realizations were

controlled not only by the turbulence in the flow, but by the sampling technique. These trends agree with the trends of the biased and two-dimensional corrected data of Tiederman [47] as previously shown in Figure 3. This indicates that the two-dimensional correction scheme appears to change the velocity probability distribution toward an unbiased one.

Because biased data gives a higher mean velocity than unbiased data (more high velocity particles pass through the probe volume per unit time than low velocity particles), one would expect biased data to give lower local turbulence intensities than unbiased data. This is because the variance, as defined by Equation 5, is divided by a larger local mean velocity in the biased case as opposed to the unbiased case. This assumes, of course, that there is no change in the variance due to the sampling technique. In the outer regions of the flow the biased mean velocities were found to be approximately 1 m/s higher (in positive flow regions) than the unbiased mean velocities as mentioned in Section 4.2. Although the variance of the biased measurements was found to be larger (higher normalized turbulence intensity) in this same region, the effect of the higher local mean velocities (biased) was to reduce the local turbulence intensity for biased measurements. This overriding effect was because the 1 m/s mean velocity offset due to bias was a major portion of the absolute local mean velocity in this

outer region. Figures 30 through 36 show the local stream-wise turbulence intensity profiles for the biased and unbiased cold flow on a semi-log scale and verifies this result. It should be noted that values of local turbulence intensity greater than 100-200% can be deceiving, because they reflect regions of near zero mean velocity. Typically, in non-zero mean velocity regions, the biased local turbulence intensity is 25-35% less than the unbiased local turbulence intensity. In the potential core region, at axial distances less than five step heights, the difference was found to be insignificant as expected.

It is interesting to note that the centerline local turbulence intensity increases rapidly as you move downstream from the potential core. Figure 37 shows the local centerline turbulence intensity for the unbiased cold flow data from this study along with data from Stevenson, et al. [15]. Good agreement was obtained considering the different inlet boundary conditions used in the two studies. The local turbulence intensity increases from 14% for  $0 < x/H < 5$  to a maximum value of 38% at  $x/H = 15$ .

This again indicates the complex turbulent structure in the region downstream of the potential core. Local values of centerline turbulence intensity in a fully developed pipe flow are approximately 4%. The values obtained here, however, are of the same magnitude as those found in the near wall region of turbulent pipe flow.

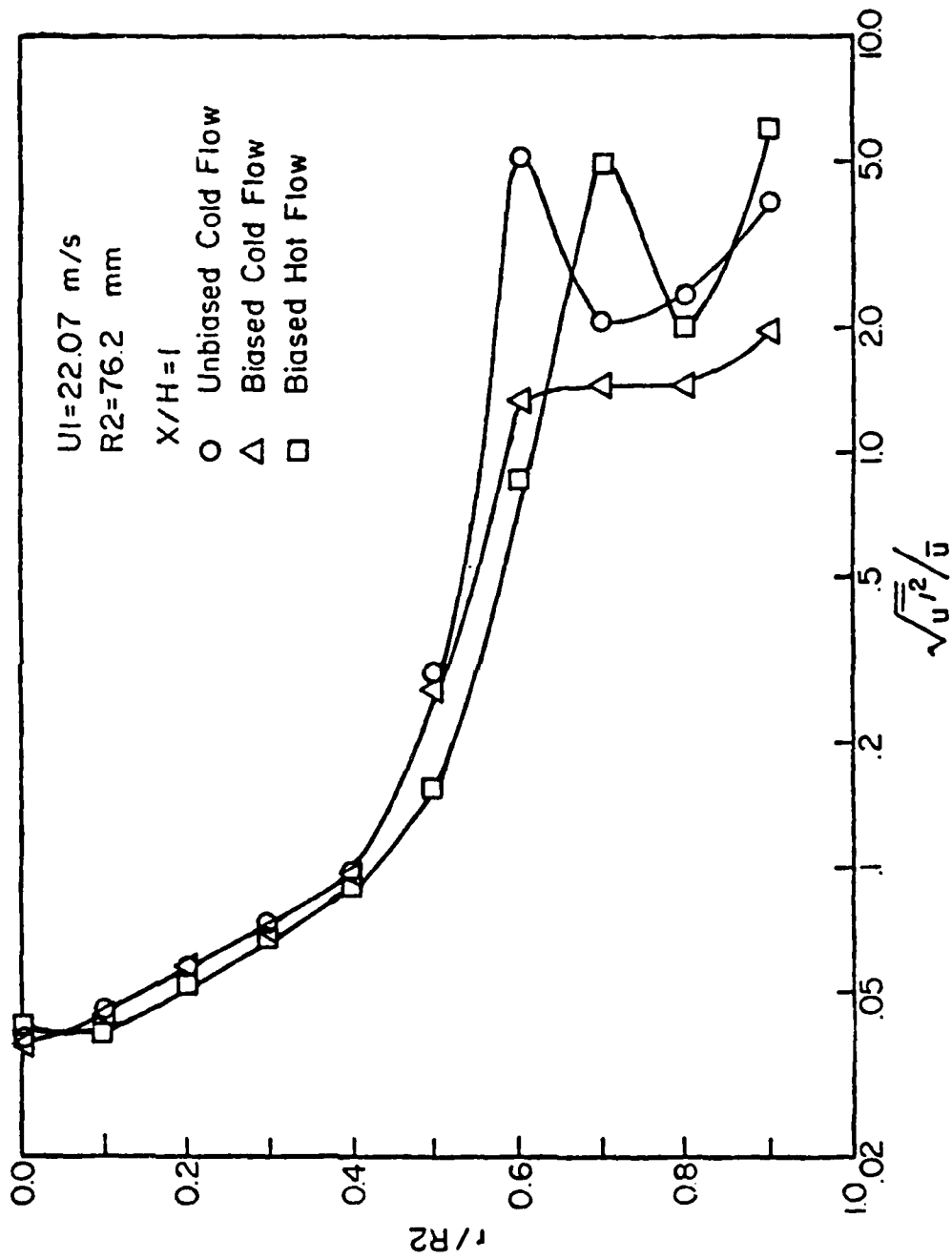


Figure 30. Measured Local Streamwise Turbulence Intensity Profiles at  $x/H = 1$

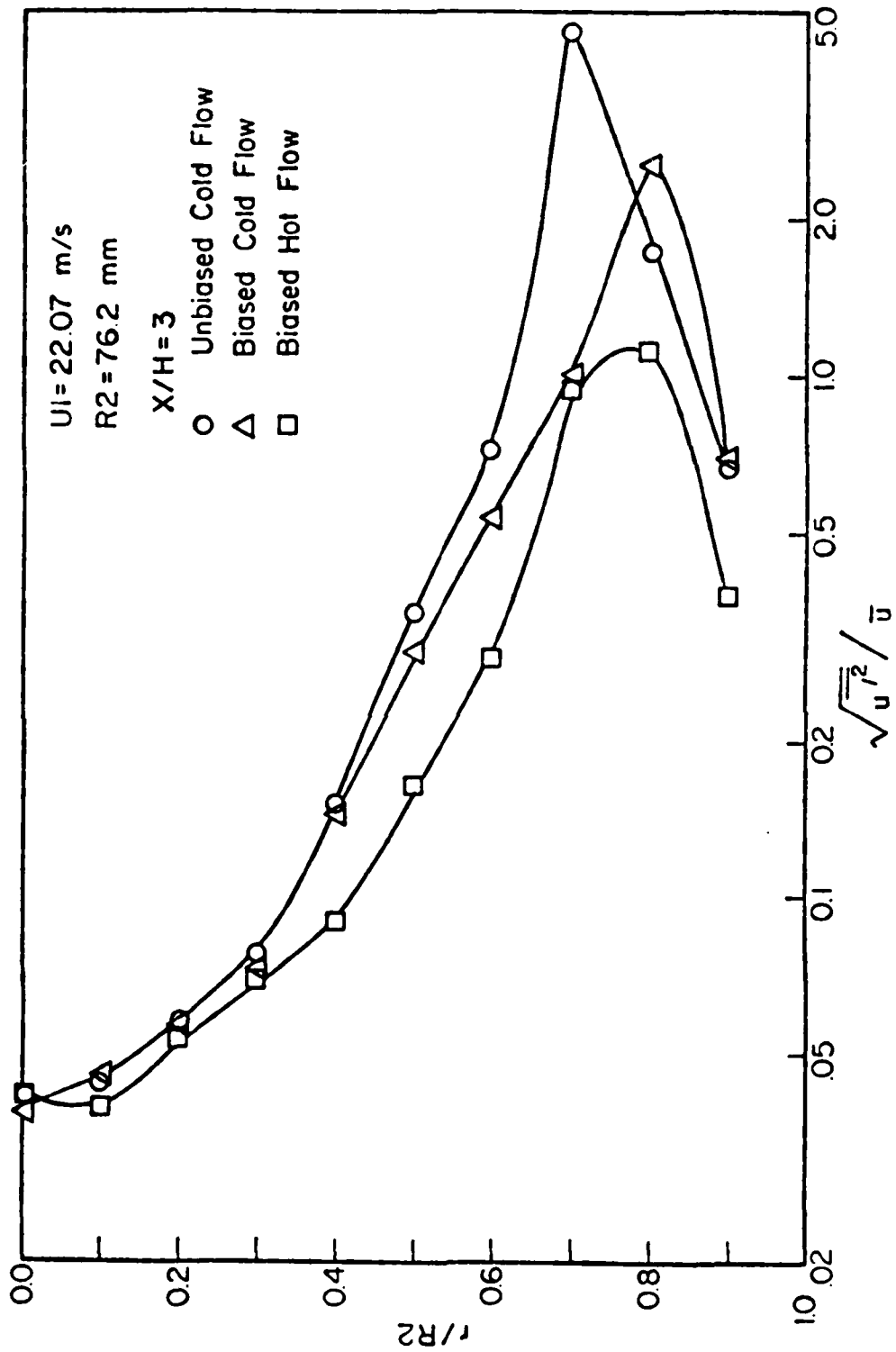


Figure 31. Measured Local Streamwise Turbulence Intensity Profiles at  $x/H = 3$

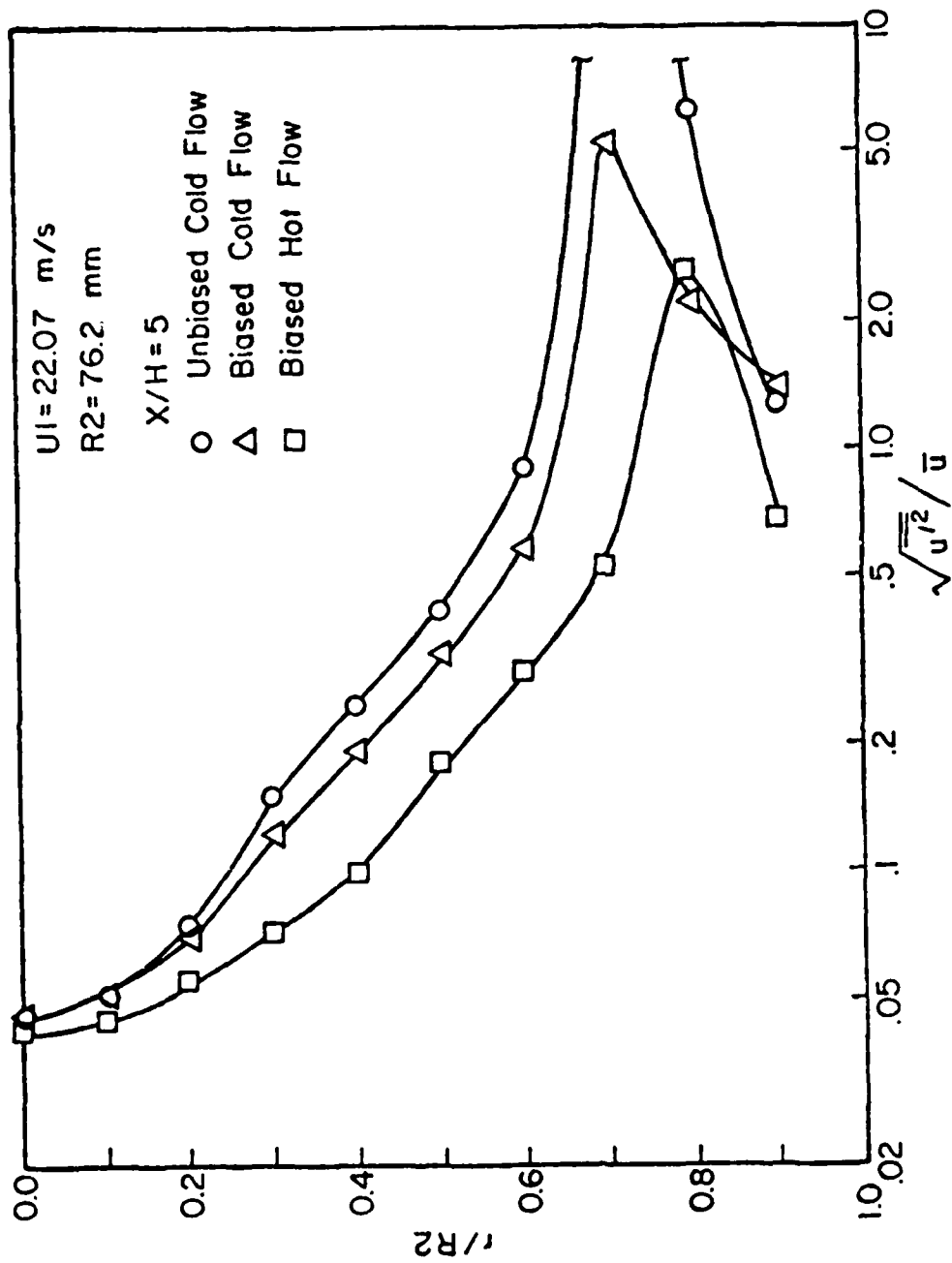


Figure 32. Measured Local Streamwise Turbulence Intensity Profiles at  $x/H = 5$

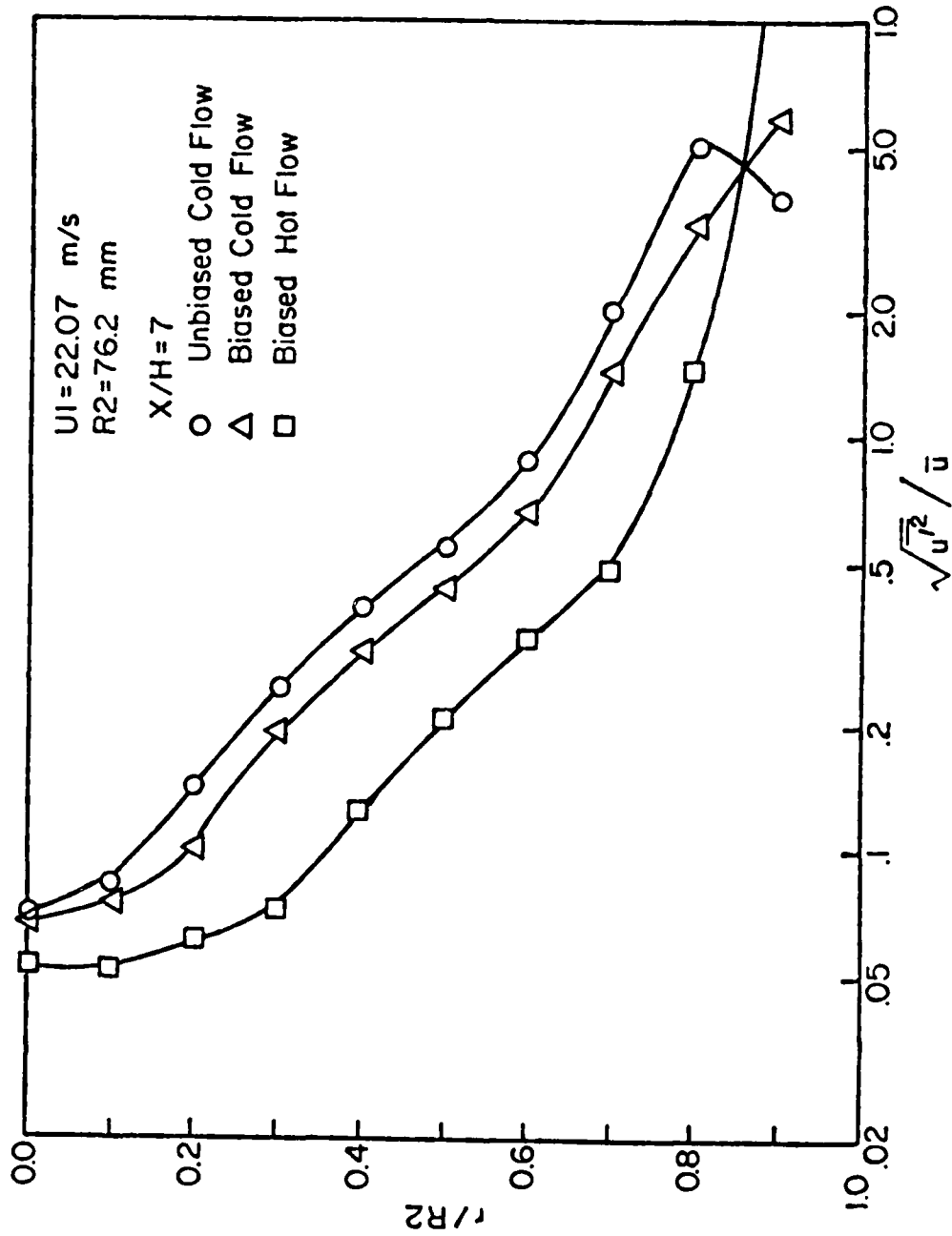


Figure 33. Measured Local Streamwise Turbulence Intensity Profiles at  $x/H = 7$

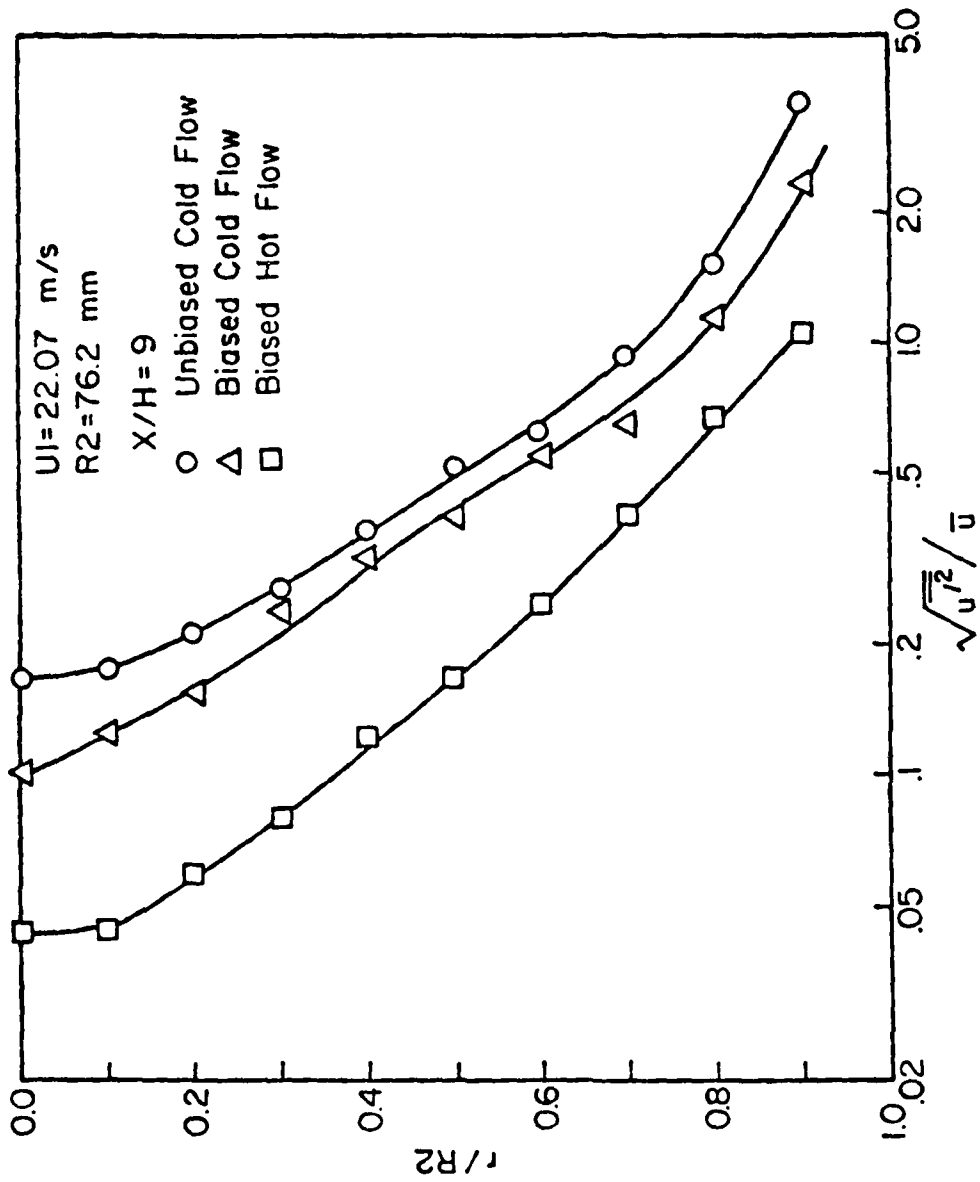


Figure 34. Measured Local Streamwise Turbulence Intensity Profiles at  $x/H = 9$

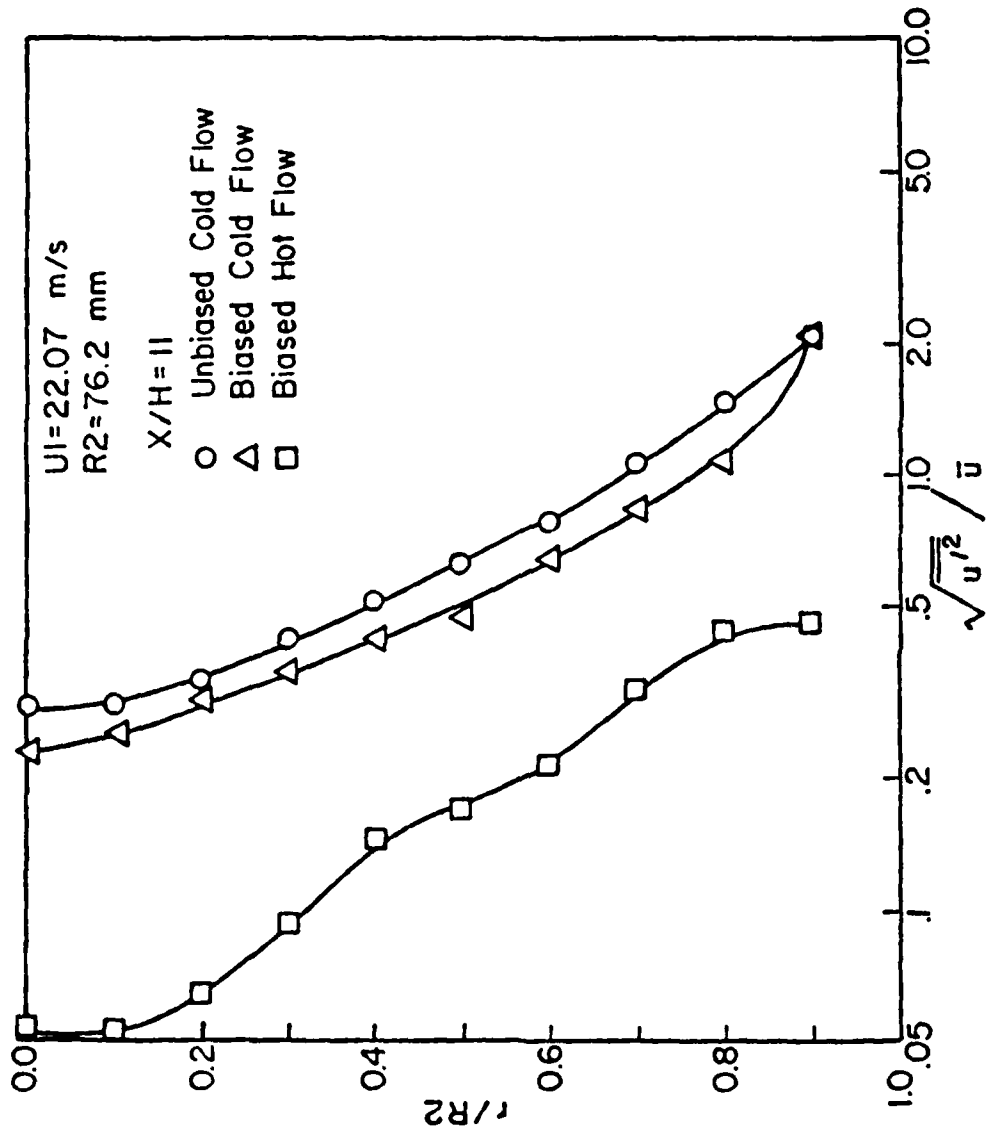


Figure 35. Measured Local Streamwise Turbulence Intensity Profiles at  $x/H = 11$

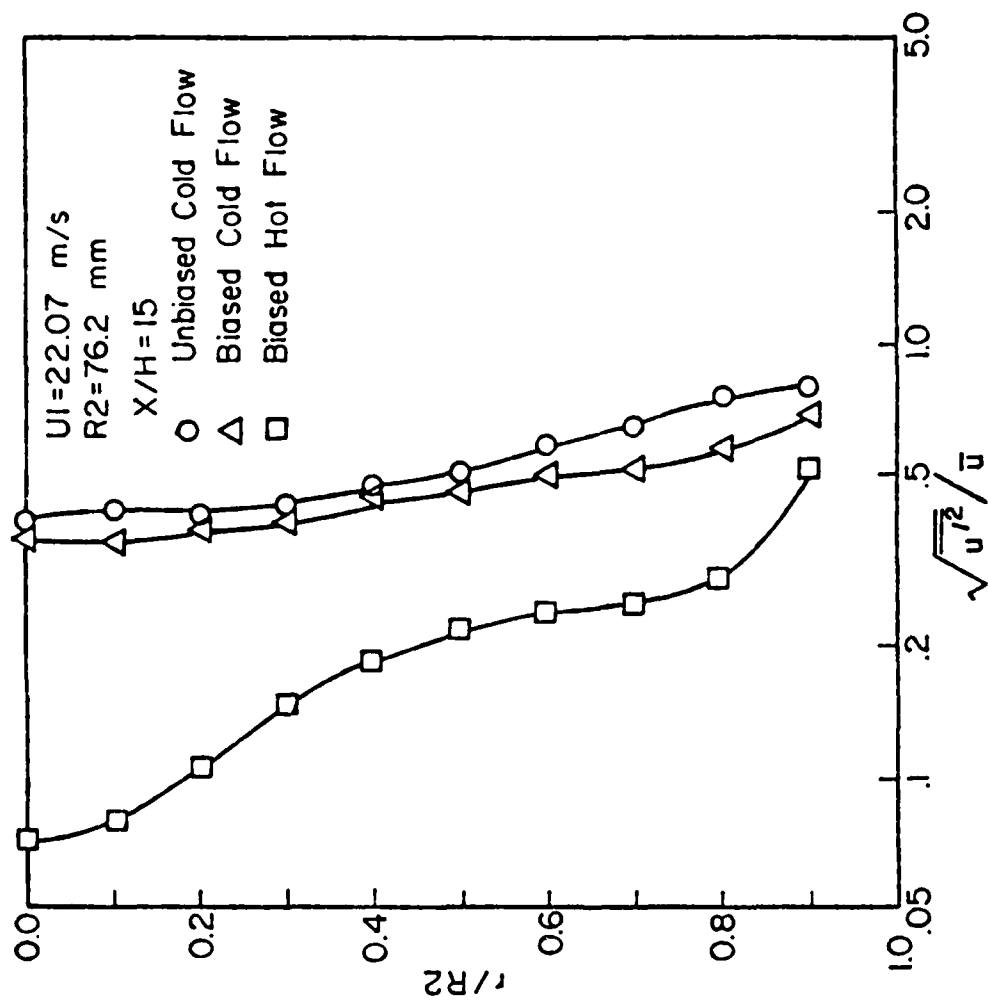


Figure 36. Measured Local Streamwise Turbulence Intensity Profiles at  $x/H = 15$

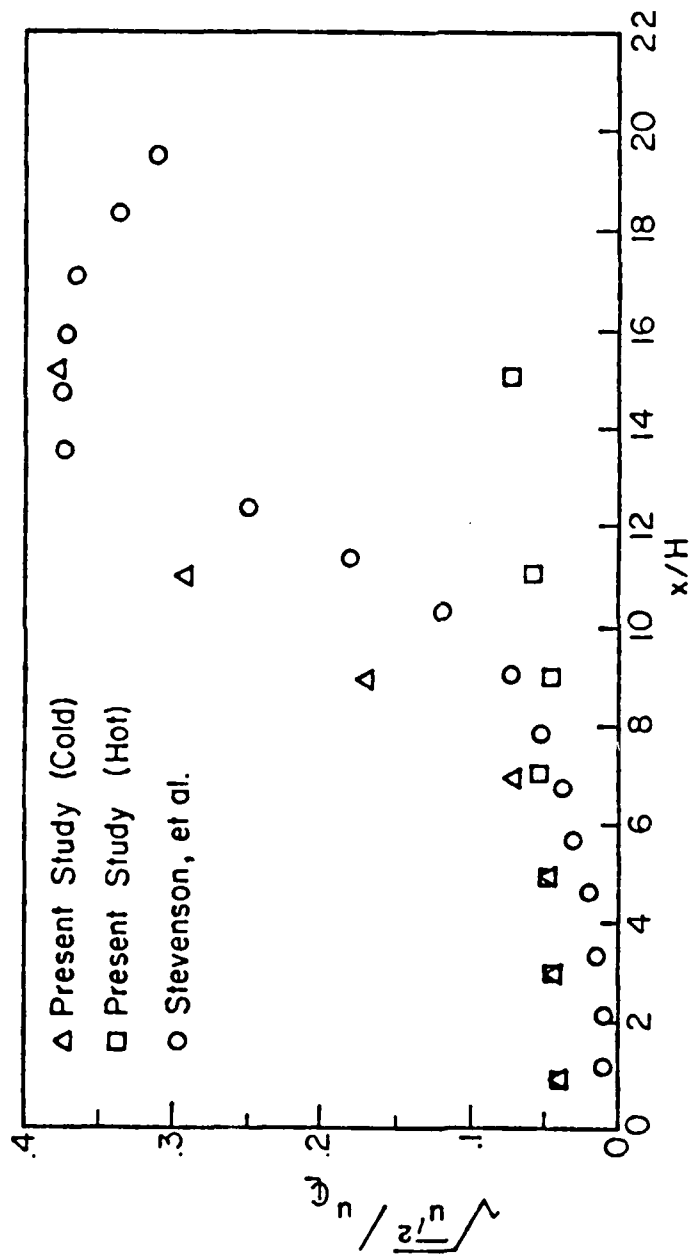


Figure 37. Measured Local Centerline Turbulence Intensity Profiles

Comparisons between the biased hot and cold flow normalized turbulence intensities show that the recirculation zone is narrower and shorter in the hot flow case. This result was also found in the two-dimensional rearward facing step study by Pitz [29]. Maximum normalized turbulence intensities for the hot flow case were approximately 22%. This is the same maximum value found in the cold flow case. It is interesting to note that the maximum normalized turbulence intensity at  $x/H = 1$  (Figure 22) for the hot flow case was 33% higher than the value found for the cold flow case. Pitz [29] also found that the reacting flow had normalized turbulence intensities 30-35% higher than the isothermal flow at this location. The reason for this is not clear.

Although the normalized turbulence intensities were found to be of the same magnitude for cold and hot flow, the local turbulence intensities were not. Figures 30 through 36 show that the hot flow local turbulence intensities are much lower, typically 40 to 60% of the cold flow values, at planes located greater than three step heights downstream of the sudden expansion. Pitz's data [29] also exhibited this result. Combustion has not affected the flow field at planes upstream of three step heights, especially in the central core region. At the plane located 15 step heights downstream of the sudden expansion the local values of stream-wise turbulence intensity were found to vary from 38% on the

centerline to 77% at the near wall point in the cold flow case, whereas the corresponding values in the hot flow case were 7% and 51%. Figure 37 also shows that hot flow local centerline turbulence intensity was much less than in the cold flow.

The fact that local turbulence levels in the reacting flow were lower than in the isothermal flow may be because dilatation by heat release competed with or dominated turbulence energy production by shear flow, notably in the vicinity of the recirculation boundary. This result was also found by Fujii and Eguchi [22] in their study where LDV measurements were made in a bluff body flame stabilizer.

#### 4. SKEWNESS COEFFICIENTS

The skewness coefficient is a statistical parameter commonly used to help identify the turbulence structure. It is a measure of the symmetry or asymmetry of the velocity probability distribution and is calculated by using Equation 6. By definition biased velocity distributions are more negatively skewed (a greater number of high velocity realizations) than unbiased velocity distributions. This was indeed found to be the case as shown in the skewness coefficient profiles plotted in Figures 38 and 39. Note that for values of  $r/R_2$  less than 0.55, the skewness coefficient (which indicates distribution shape) is similar for both the

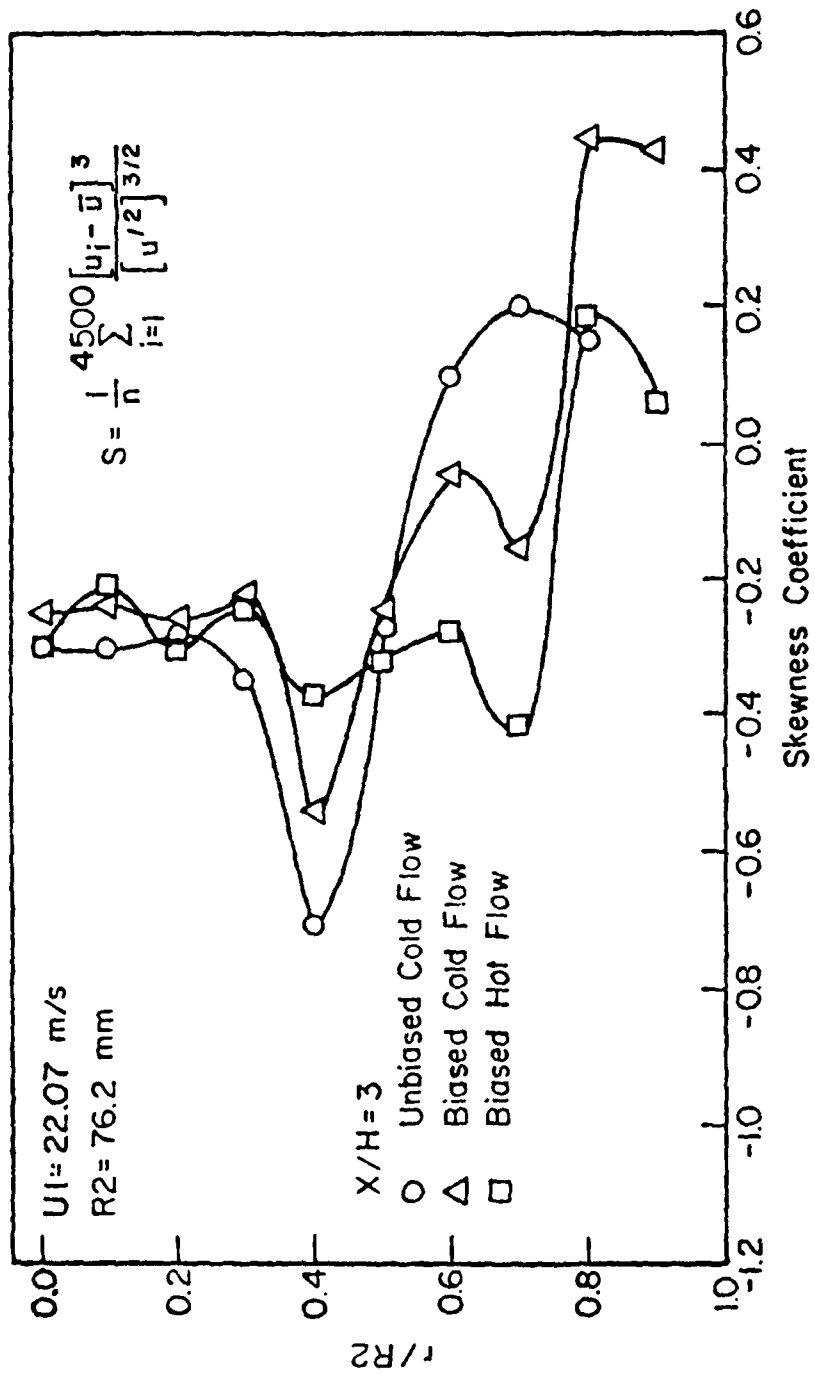


Figure 38. Measured Skewness Coefficient Profiles at  $x/H = 3$

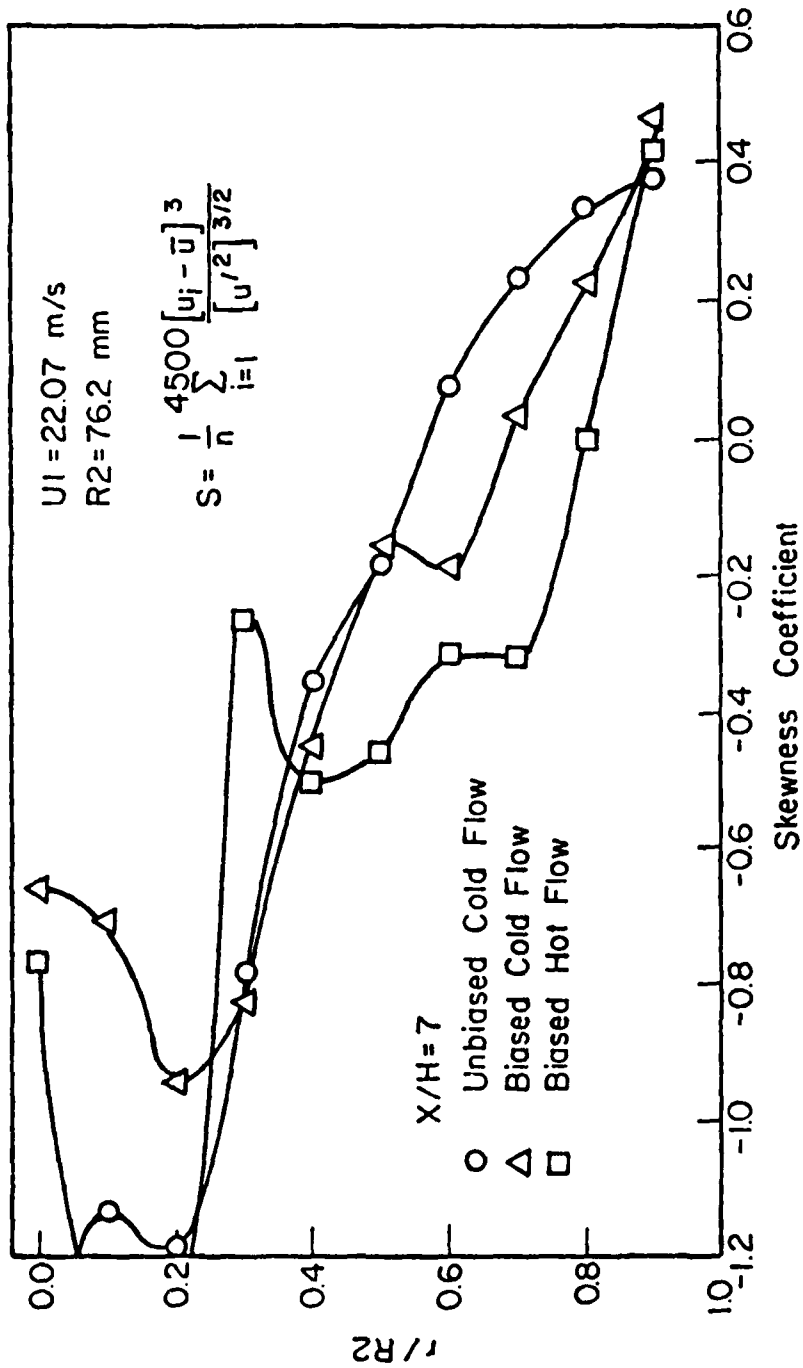


Figure 39. Measured Skewness Coefficient Profiles at  $x/H = 7$

unbiased and biased measurements. This would indicate that the shapes of the histograms constructed from the two sampling techniques were similar. That is, the effect of biasing in the central core, where low turbulence exists, is minimal. However, as one moves radially outward toward the point where the normalized turbulence intensity profiles cross, the distributions start to deviate significantly from one another.

The skewness of the reacting flow measurements looks quite different from that in the cold flow at first glance. However there are similarities when one considers that the reacting shear layer is shifted closer to the test section wall. This is the case before reattachment occurs and can be seen at  $x/H = 3$  and  $7$  in Figures 38 and 39, respectively. If the shift in the shear layer location for hot flow versus cold flow is taken into account Figures 38 and 39 show that shapes of the histograms are very similar, although non-gaussian, at  $x/H = 3$  and  $7$ . This was not the case at planes downstream from reattachment as shown in Figures 40 and 41. The skewness was much more negative in the reacting flow case indicating different turbulence structure. The skewness tends to be highly negative at the centerline and is zero or slightly positive at the wall in the reacting flow. Since no unbiased hot flow data were taken, it is not known how much of this difference in structure (skewness coefficient) was due to the combustion process and how much was

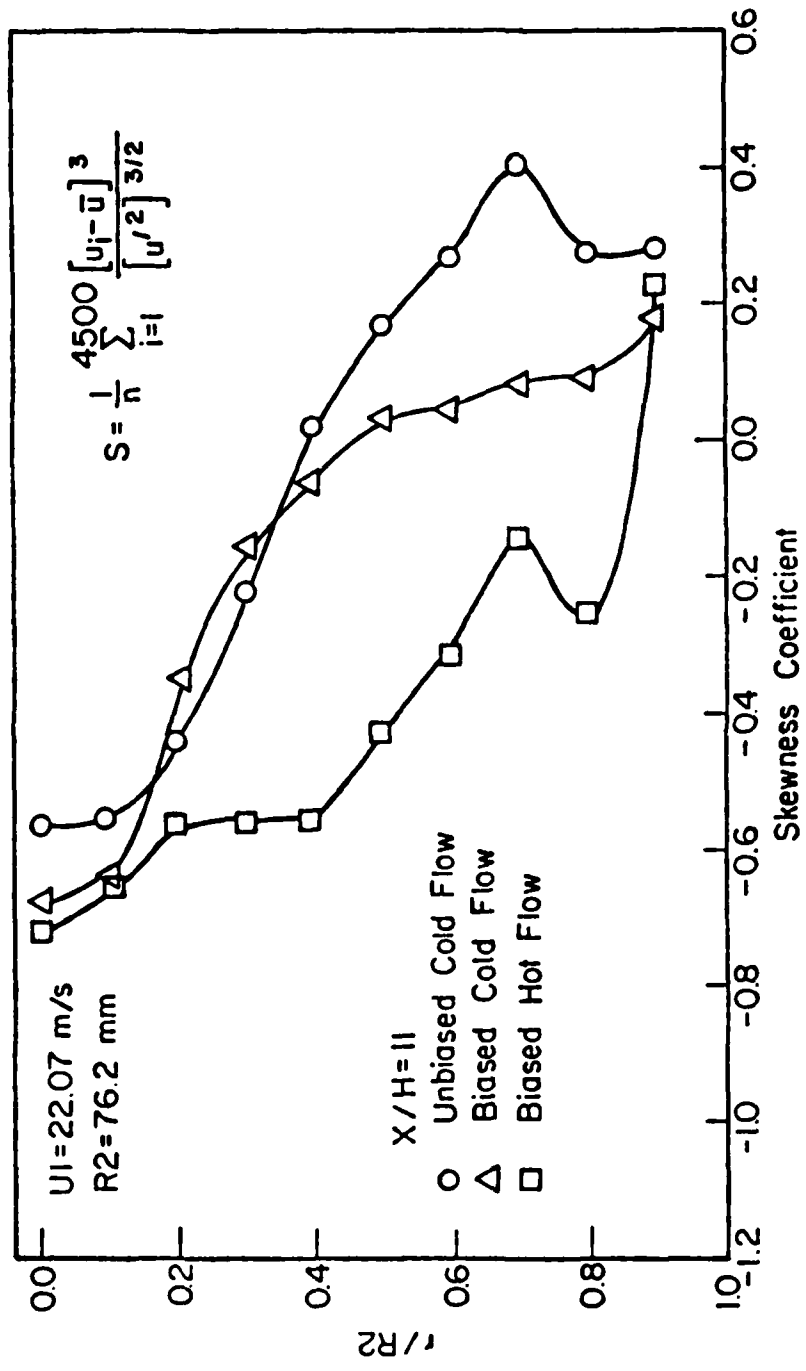


Figure 40. Measured Skewness Coefficient Profiles at x/H = 11

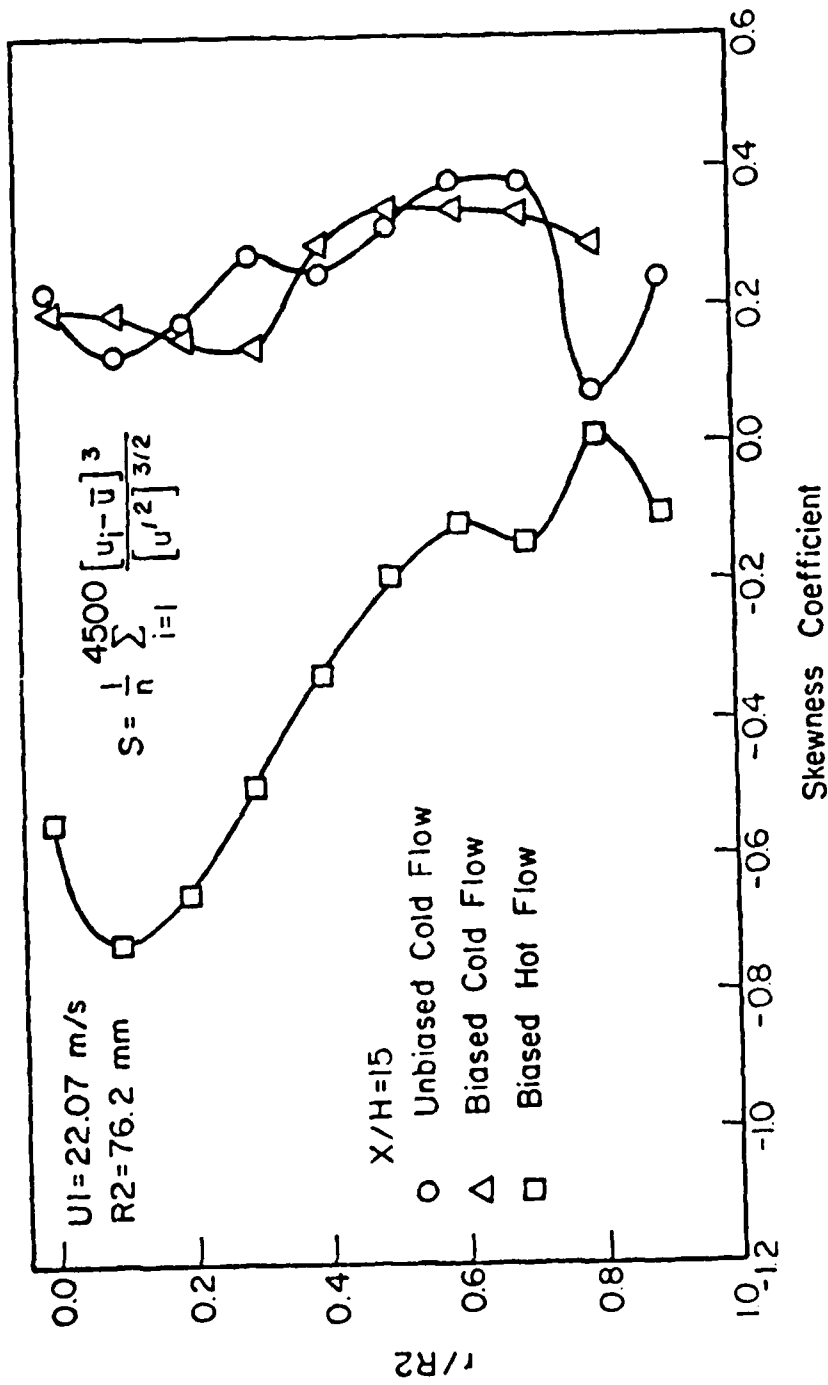


Figure 41. Measured Skewness Coefficient Profiles at  $x/H = 15$

due to sampling technique, although the small difference in skewness observed between the biased and unbiased cold flow data would seem to indicate that combustion was the dominant factor.

#### 5. THE REATTACHMENT LENGTH

The reattachment point was determined by linearly extrapolating the  $\bar{u}=0$  contour to the wall boundary. The measured reattachment length for the unbiased cold flow was found to be 8.62 step heights downstream of the step face. This value is in good agreement with earlier results reported in the literature [11,12,13,15]. The measured reattachment length for the biased hot flow was found to be 7.40 step heights downstream of the step face. The reattachment length for the reacting shear layer was reduced by 15%. Pitz found reductions in reattachment lengths between 20 and 30% in his study.

#### 6. THE STREAM FUNCTION

Figures 42 and 43 show lines of constant volume flow for the unbiased cold flow and the biased hot flow, respectively. These are stream function contours for the cold flow (constant density) case. To partially compensate for slight mass flow discrepancies due to experimental errors, the stream function was non-dimensionalized at each  $x/H$

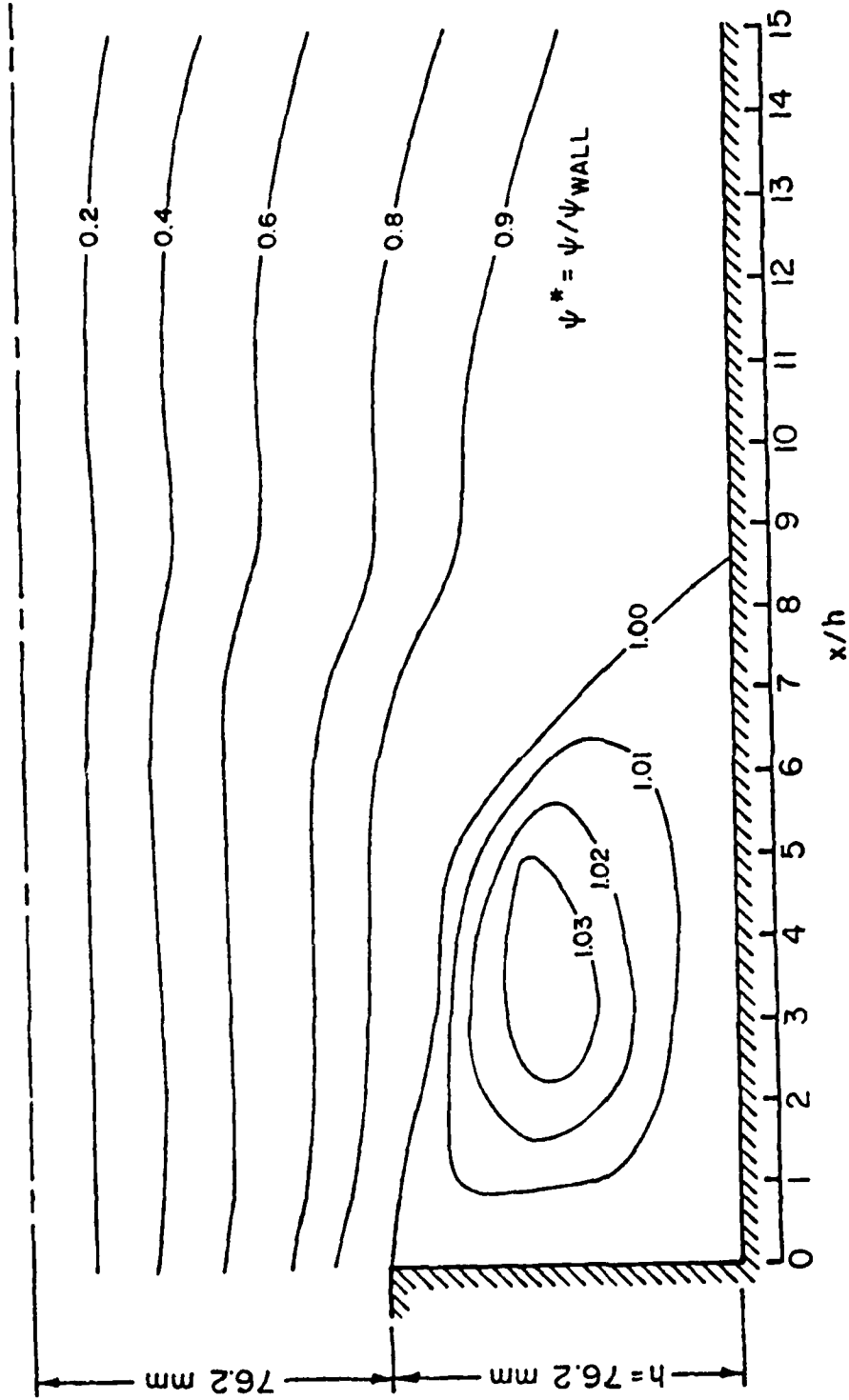


Figure 42. Normalized Stream Function Contours (Unbiased Cold Flow)

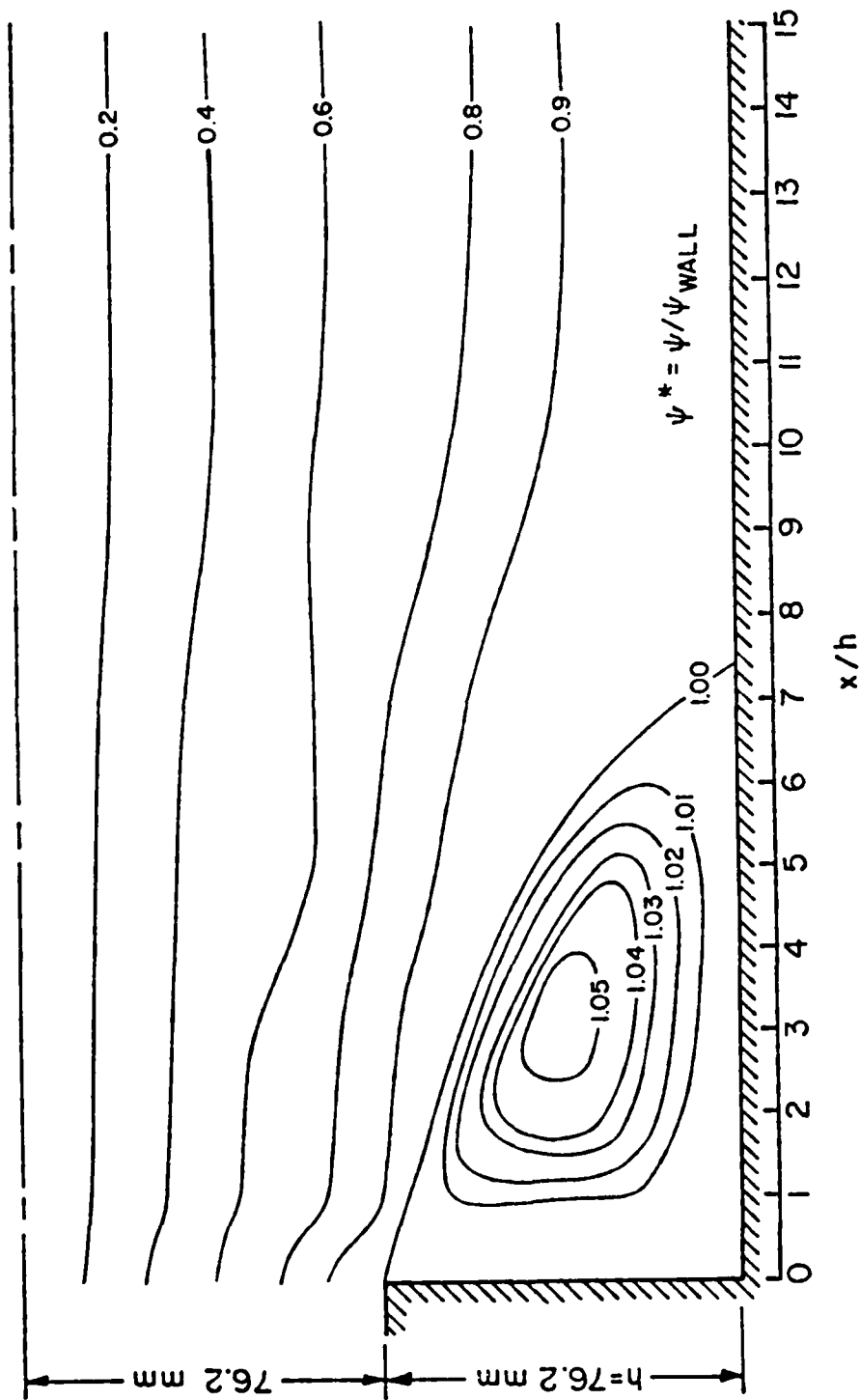


Figure 43. Normalized Stream Function Contours (Biased Hot Flow)

station. That is at each x station

$$\bar{v} = \frac{\bar{v}}{v_{\text{wall}}} \quad (10)$$

The unbiased cold flow measurements showed that the center of the recirculation region was located 3.5 step heights downstream of the step face at a radial distance of  $r/R_2 = 0.725$ . The center of the recirculating region in the hot flow case was located at  $x/H = 3.0$  and  $r/R_2 = 0.750$ . This again illustrates the general shift of the shear layer toward the wall in the hot flow case.

#### 7. THE MASSFLOW RATE

In this study two sets of streamwise velocity measurements for the isothermal flow were taken. As pointed out earlier the first set of measurements, considered isothermal flow were taken. The first set of measurements, considered to be unbiased, was taken with particle arrival rates in excess of 20,000 Hz and a computer sampling rate of 50 samples per second. The second set of data was taken with a particle arrival rate between 500 and 1500 Hz and free sampling, that is, the microcomputer was allowed to sample data as fast as it could (4800 Hz). These two mean velocity data sets were then reduced and integrated using piecewise

integration with forward polynomial fitting to the data points and backward direct integration of the polynomial fit.

Table 5 lists the normalized integrated mass flux at each axial measurement plane for the unbiased and biased measurements. The mass flux was normalized with the inlet mass flux which was obtained by analytically integrating a 1/7 power law velocity profile. The measured values indicate that the unbiased integrated mass fluxes agree to within  $\pm 3\%$  from plane to plane. The biased measurements overpredict normalized integrated mass flux by as much as 24%. This result again demonstrates the effect of velocity bias and gives one confidence in the unbiased velocity measurement technique used. Unfortunately, integration of mass flux in the reacting flow was not possible as detailed temperature (density) information was not available.

## 8. TEMPERATURE PROFILES

A temperature traverse in the reacting flow was made at a plane located 17.7 step heights downstream of the sudden expansion. Figure 44 shows the measured stagnation temperature contours. From the contours, one can see that the core region was fairly cool which indicates that the mixing process was far from complete at this location. The temperatures here were, as pointed out earlier, not true gas

TABLE 5. INTEGRATED MASS FLUX IN AN AXISYMMETRIC  
SUDDEN EXPANSION

x/H	Biased Data $\dot{m}/m_{ref}$	Unbiased Data $\dot{m}/m_{ref}$
0.33	1.07	1.00*
1.00	1.07	1.04
3.0	1.20	1.06
5.0	1.13	1.00
7.0	1.21	1.01
9.0	1.24	1.03
11.0	1.21	1.02
15.0	1.12	1.03

\* $m_{ref}$  based on biased inlet velocity profile at  $x/H = 0.33$

Top  
(Looking Downstream)

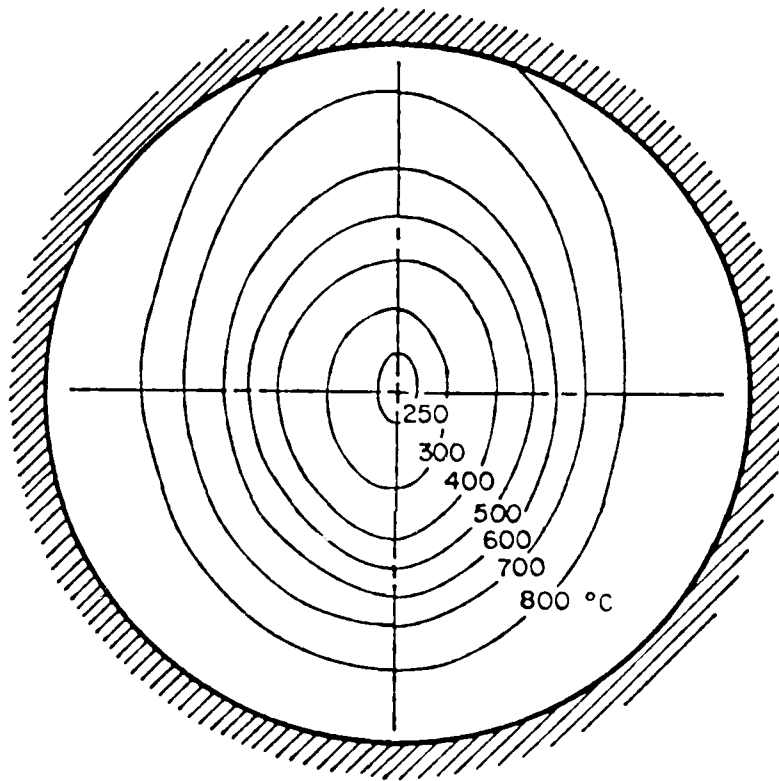


Figure 44. Temperature Contours at  $x/H = 17.7$

temperatures but "equilibrium" temperatures, because no effort was made to correct the thermocouple readings for heat transfer losses. The main purpose for this temperature traverse was to determine profile symmetry. Figure 44 shows that the temperature profile was symmetric across the measurement axis but was not symmetric from top to bottom. The reason for this asymmetry is not known, but it may be due to fuel injection imbalances. An attempt was made to improve symmetry by adjusting the flow in the four fuel inlets, but Figure 44 represents the best result obtainable. The asymmetry was believed not severe enough to cause significant errors in the velocity data taken on the horizontal central plane, however.

SECTION VI  
COMPARISON OF NUMERICAL ANALYSIS  
WITH ISOTHERMAL EXPERIMENTAL RESULTS

1. INTRODUCTION

In order to provide a basis for comparison of analytically predicted and experimentally measured isothermal flow parameters, the computer code CHAMPION 2/E/FIX of Pun and Spalding [52] was adapted to the flow geometry and run. This code uses the  $k - \epsilon$  turbulence model of Launder and Spalding [18] along with a modified version of the SIMPLE algorithm described by Pantankar and Spalding [52]. Unfortunately, a prediction code capable of modeling the combustion process was not available for use in the present study. Therefore only isothermal comparisons will be made in this section.

The 2/E/FIX code, when adapted for an axisymmetric geometry, solves the partial differential equation

$$\frac{\partial}{\partial x} (\rho \bar{u} \Phi) + \frac{1}{r} \frac{\partial}{\partial r} (\rho r \bar{v}_r \Phi) = S_\Phi + \frac{\partial}{\partial x} \left[ \Gamma_\Phi \frac{\partial \Phi}{\partial x} \right] + \frac{1}{r} \frac{\partial}{\partial r} \left( \Gamma_\Phi r \frac{\partial \Phi}{\partial r} \right) \quad (10)$$

where  $r$  is the coordinate in the radial direction,  $x$  is the coordinate in the streamwise direction,  $\bar{u}$  is the mean velocity in the streamwise direction,  $\bar{v}_r$  is the mean velocity in the radial direction,  $\phi$  is the dependent variable,  $\Gamma_\phi$  is the exchange coefficient and  $s_\phi$  is the source term. Equation (10) represents the time averaged Navier-Stokes equations along with a supplemental transport equation. The  $k - \epsilon$  model assumes isotropic diffusion with the effective viscosity,  $\mu_{eff}$ , being the sum of the laminar and turbulent contributions. That is,

$$\mu_{eff} = \mu_{lam} + \mu_t. \quad (11)$$

When appropriate expressions for  $\phi$ ,  $s_\phi$  and  $\Gamma_\phi$  as listed in Table 6 are substituted into the general Equation (10), the equation takes on the form of continuity, axial and radial momentum, turbulent kinetic energy and rate of energy dissipation equations.

The 2/E/FIX code solves this set of simultaneous differential equations, with appropriate boundary conditions, using upwind differencing. The matrix equation obtained

TABLE 6. CONSERVATION EQUATIONS CORRESPONDING TO EQUATION 10

Conservation of	$\phi$	$\Gamma_\phi$	$S_\phi$
Mass	1	0	0
Axial momentum	$\bar{u}$	$\nu_{eff}$	$\frac{\partial}{\partial x} (\nu_{eff} \frac{\partial \bar{u}}{\partial x}) + \frac{1}{r} \frac{\partial}{\partial r} (\nu_{eff} r \frac{\partial \bar{v}}{\partial x}) - \frac{\partial p}{\partial x}$
Radial momentum	$\bar{v}$	$\nu_{eff}$	$\frac{\partial}{\partial x} (\nu_{eff} \frac{\partial \bar{v}}{\partial x}) + \frac{1}{r} \frac{\partial}{\partial r} (\nu_{eff} r \frac{\partial \bar{v}}{\partial r}) - 2\nu_{eff} \frac{\bar{v}}{r^2} - \frac{\partial p}{\partial r}$
Turbulent kinetic energy	k	$\frac{\nu_{eff}}{\sigma_k}$	$G_k - \rho \epsilon$
Turbulent dissipation rate	$\epsilon$	$\frac{\nu_{eff}}{\sigma_\epsilon}$	$\frac{\epsilon}{k} (C_1 G_k - C_2 \rho \epsilon)$

$$G_k = \nu_{eff} \left\{ 2 \left[ \frac{\partial \bar{u}}{\partial x} \right]^2 + \left[ \frac{\partial \bar{v}}{\partial r} \right]^2 + \frac{\bar{v}}{r^2} \right\} + \left( \frac{\partial \bar{u}}{\partial r} + \frac{\partial \bar{v}}{\partial x} \right)^2$$

from the numerical approximations is then solved using a tridiagonal algorithm along with under relaxation to achieve numerical stability.

Inputs to the code include inlet velocity, inlet turbulent kinetic energy, relaxation factors, and five constants used in the expressions listed in Table 6. The numerical values of these five constants recommended by Launder and Spalding [20] are given in Table 7.

TABLE 7. RECOMMENDED TURBULENCE CONSTANTS FROM REF. [20]

Constant	Value
$C_D$	0.09
$C_1$	1.43
$C_2$	1.92
$\sigma_K$	1.00
$\sigma_\epsilon$	1.30

Although the constant  $C_D$  is in none of the expressions in Table 6, it is used in the following two equations

$$\mu_{\text{turb}} = C_D \rho \frac{k^2}{\epsilon} \quad (12)$$

$$\bar{u} C_D^{\frac{1}{4}} k^{\frac{1}{2}} / \left[ \frac{\tau_w}{\rho} \right] = \frac{1}{\kappa} \ln \left[ C_p^{\frac{1}{4}} k^{\frac{1}{2}} y_1 \frac{\rho}{\mu_{lam}} \right] \quad (13)$$

Equation 12 is the equation from which the turbulent contribution to viscosity is evaluated. Equation 13 represents a modified "log law" used to link the first node from the wall to the wall boundary condition where  $\kappa$  is a constant equal to 0.4,  $E$  is a constant equal to 9.0 for smooth walls,  $\tau_w$  is the wall shear stress,  $\bar{u}$  is the mean axial velocity at point  $y_1$ , and  $y_1$  is the distance from the wall to the first node from the wall.

A 21 x 41 grid was used for the computations. The 21 radial increments covered the tube radius while the 41 axial grid planes were located at each integer value of  $x/H$  (downstream distance normalized to step height) from  $x/H = 0$  to 40. At  $x/H = 40$  the flow is essentially fully developed and an exit boundary condition of zero axial velocity gradient is valid.

The velocity profile measured as close as physically possible to the plane of the sudden expansion ( $x/H = 0.33$ ) was used as the inlet boundary condition. The convergence criterion, built into the code, on  $\bar{u}$ ,  $\bar{v}_r$ , turbulent kinetic energy (TKE) and turbulent energy dissipation (TED) was  $10^{-3}$ .

## 2. MATCHING REATTACHMENT LENGTH

Reattachment length was chosen as a common flow field parameter for comparison of the numerical analysis to experimental results. Moon and Rudinger [12] matched their experimental results in terms of reattachment length by setting the coefficients  $C_1=1.43$  and  $C_2=1.70$ . In the study by Stevenson, et al. [15], only  $C_2$  was iterated upon to match the experimental value of reattachment length. A value of  $C_2=1.94$  was used in that study. In the present study  $C_2$  was also the only coefficient iterated upon. A least square linear fit was then applied to the data, yielding the following equation.

$$C_2 = 0.059 \left( \frac{x_r}{H} \right) + 2.4305 \quad (14)$$

where  $x_r$  is the reattachment length and  $H$  is the step height. Since the observed reattachment length was approximately 8.6 step heights, a value of 1.92 was chosen for  $C_2$  based on this equation. This is, in fact, the value suggested by Pun and Spalding.

## 3. MEAN STREAMWISE VELOCITY

Figures 45 through 51 show streamwise mean velocity profile comparisons of the experimental unbiased cold flow

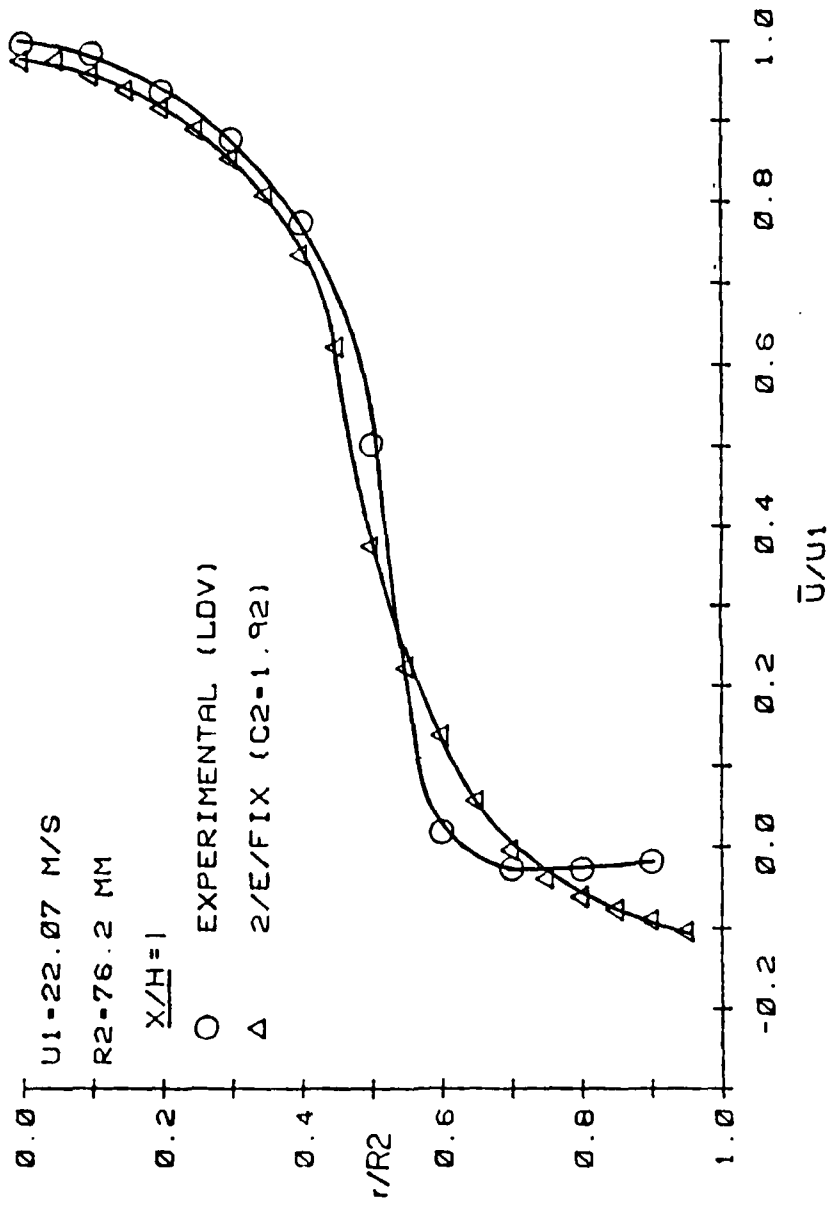


Figure 45. Comparison of Predicted and Measured Mean Streamwise Velocity Profile at  $x/H = 1$

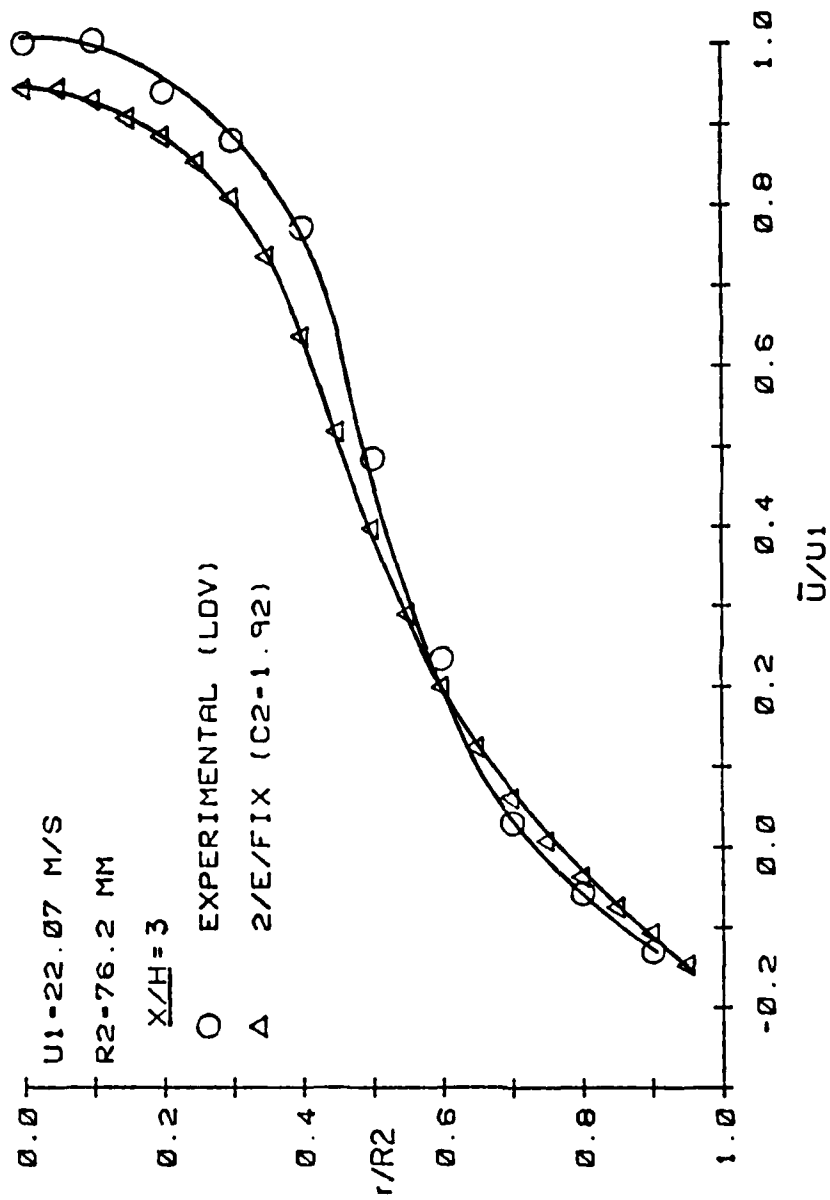


Figure 46. Comparison of Predicted and Measured Mean Streamwise Velocity Profile at  $x/H = 3$

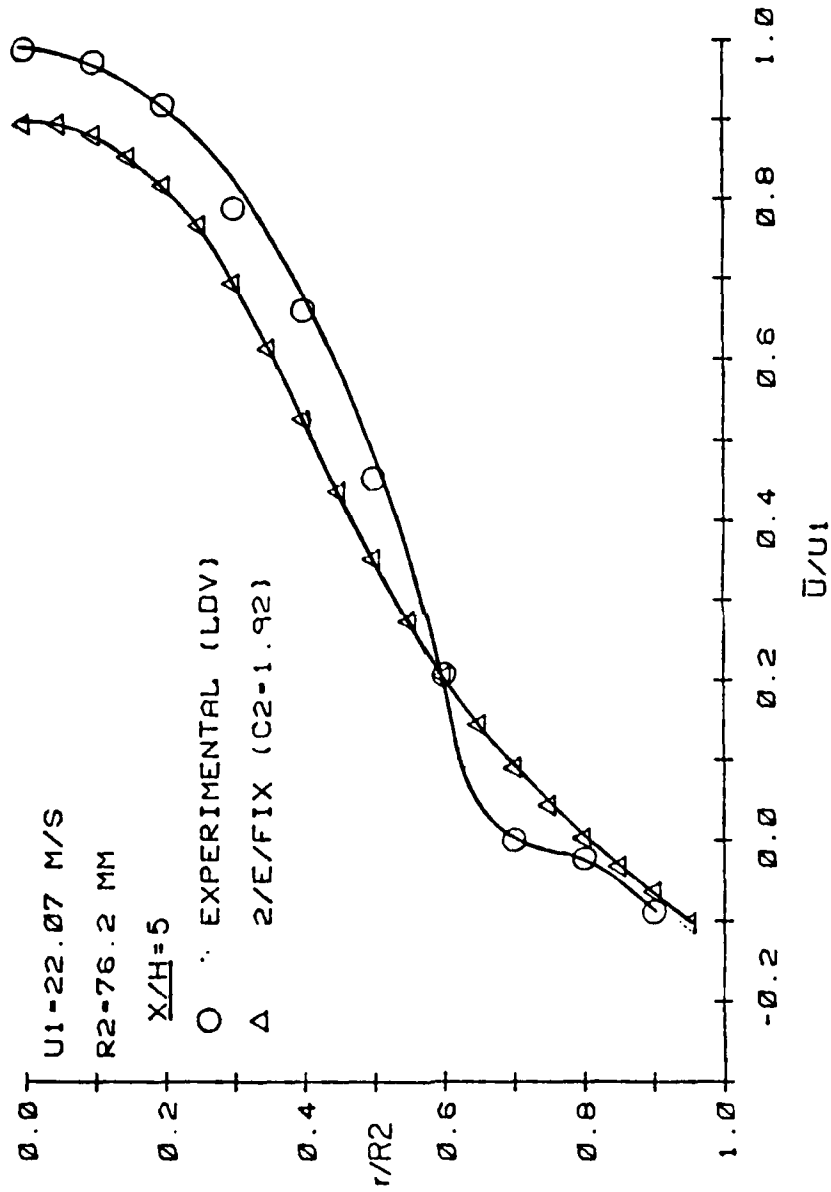


Figure 47. Comparison of Predicted and Measured Mean Streamwise Velocity Profile at  $x/H = 5$

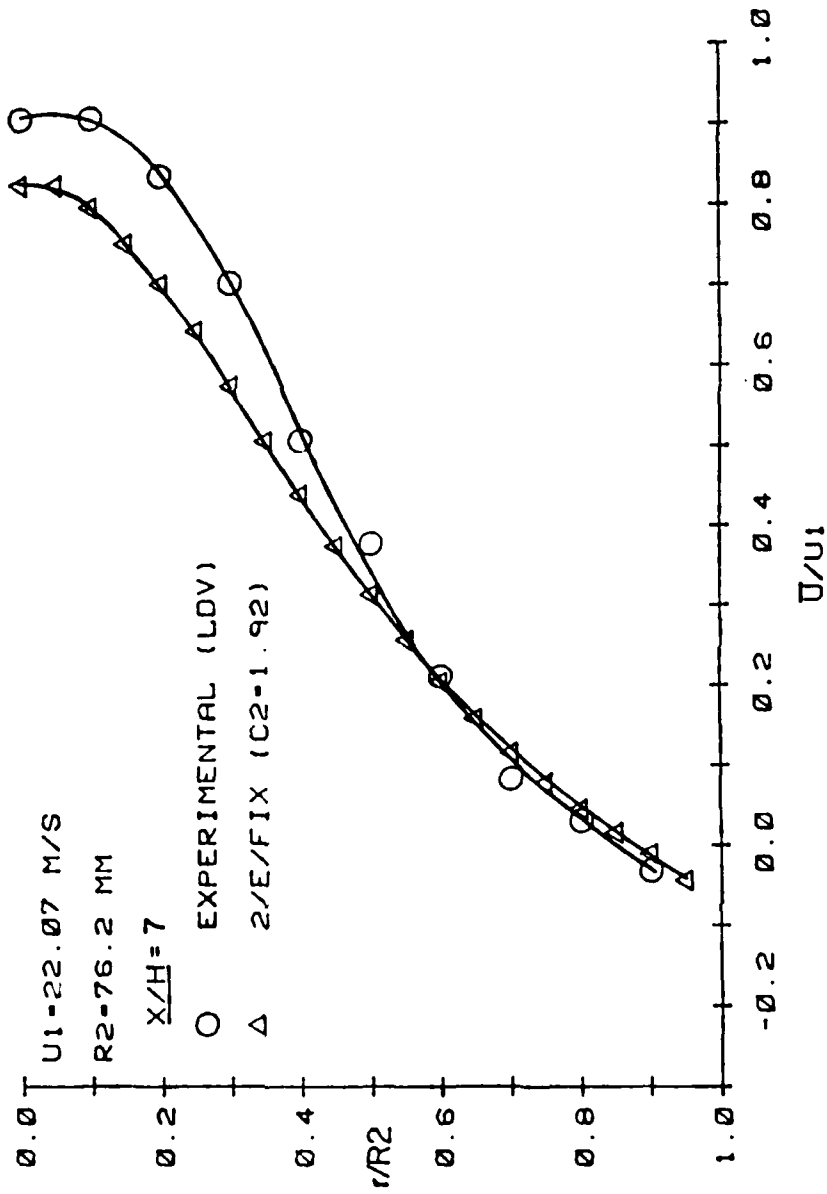


Figure 48. Comparison of Predicted and Measured Mean Streamwise Velocity Profile at  $x/H = 7$

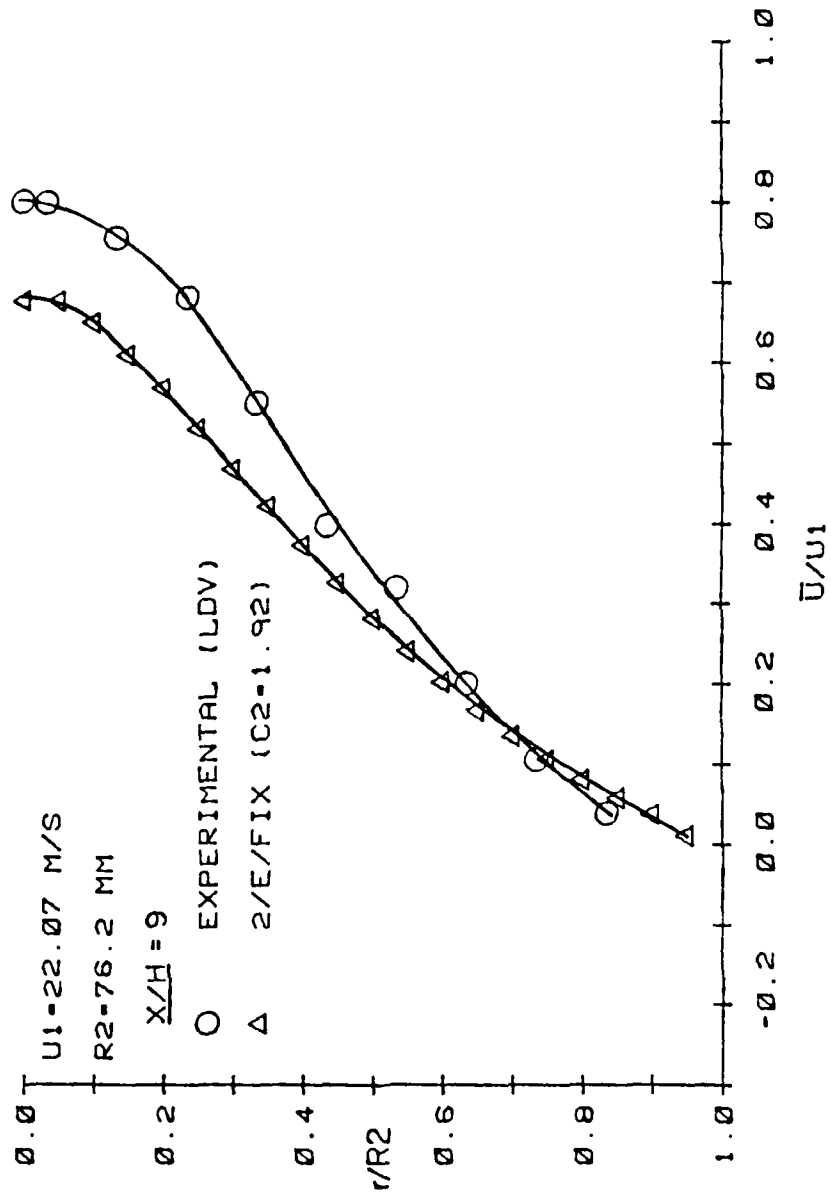


Figure 49. Comparison of Predicted and Measured Mean Streamwise Velocity Profile at  $x/H = 9$

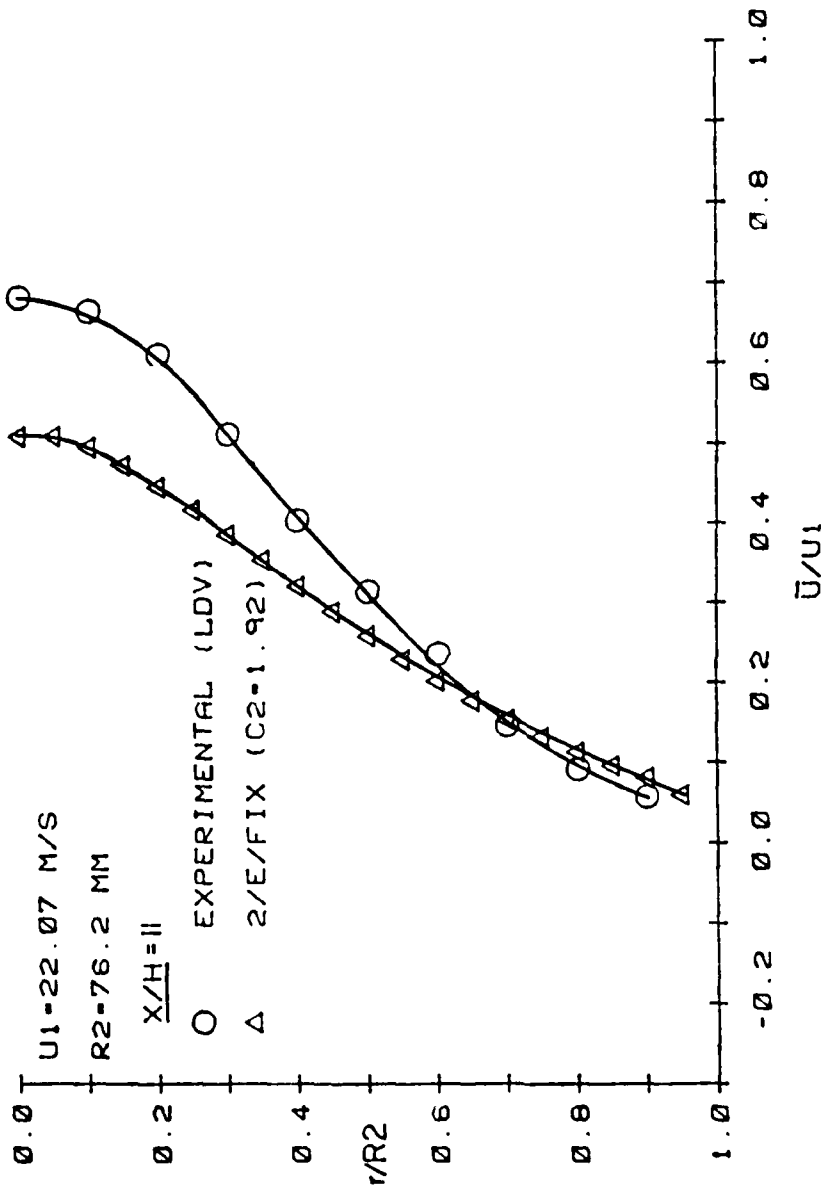


Figure 50. Comparison of Predicted and Measured Mean Streamwise Velocity Profile at  $x/H = 11$

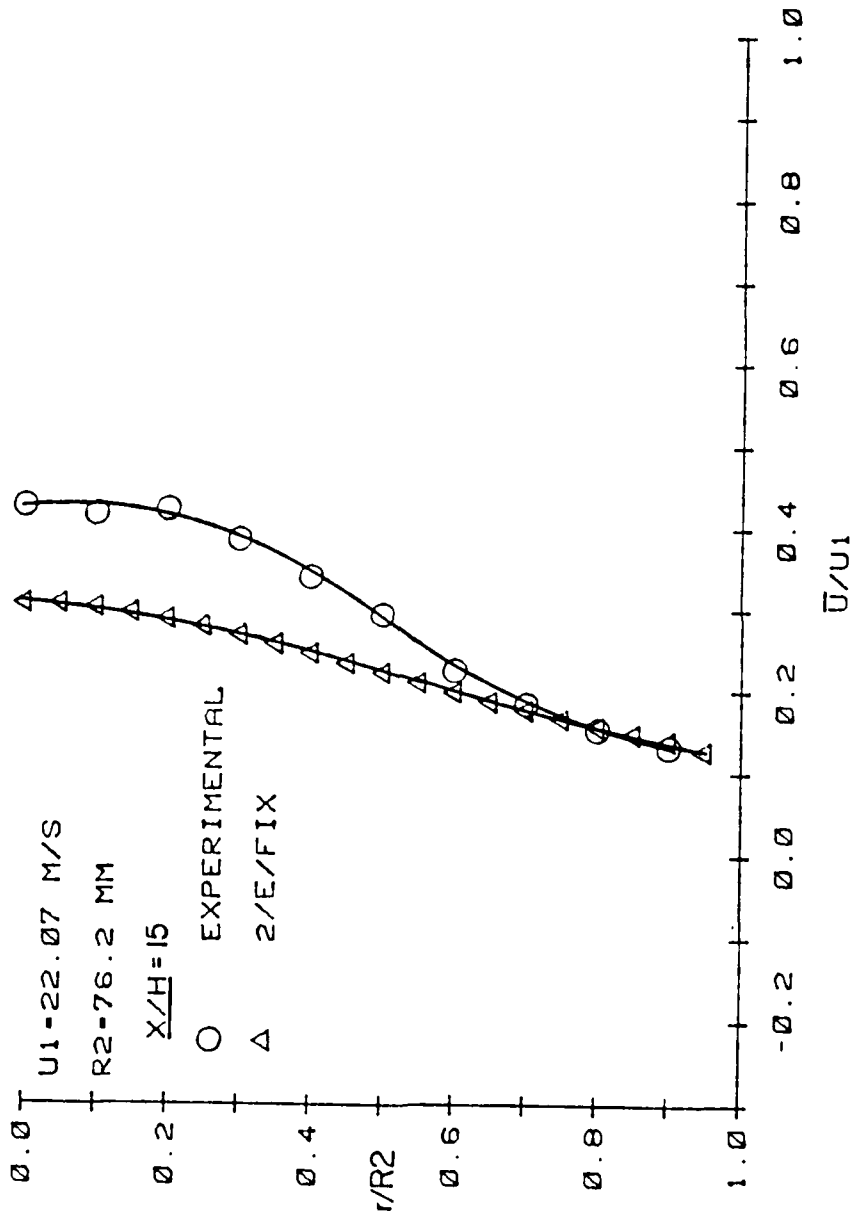


Figure 51. Comparison of Predicted and Measured Mean Streamwise Velocity Profile at  $x/H = 15$

data and the numerically predicted results at different axial locations. Figure 52 shows the normalized stream function contours. It can be seen that the computational results are in fairly good agreement with the unbiased data, although some discrepancies exist in the recirculation zone and the predicted velocities in the center of the flow are consistently low at downstream locations. This agrees with earlier results [15]. The figures also show that as the flow develops the profiles begin to deviate more. Although there is a large difference in the experimental and predicted velocities in the center of the flow, the difference in mass flow rate is small since cross-sectional flow area in this region is small. In order to check the code, the integrated mass flux was calculated using the predicted velocities at each grid line. Mass conservation was satisfied experimentally by the unbiased measurements as shown earlier in Table 5, but the computer code did not conserve mass. Typically, 3.2% of the inlet mass flux was "lost" by the  $x/H = 15$  grid line. This was true for all values of  $C_2$  tested. The mass flux loss was attributed to truncation and convergence errors in the finite difference scheme. The method used to link the pressure field with the velocity field may have also caused slight errors.

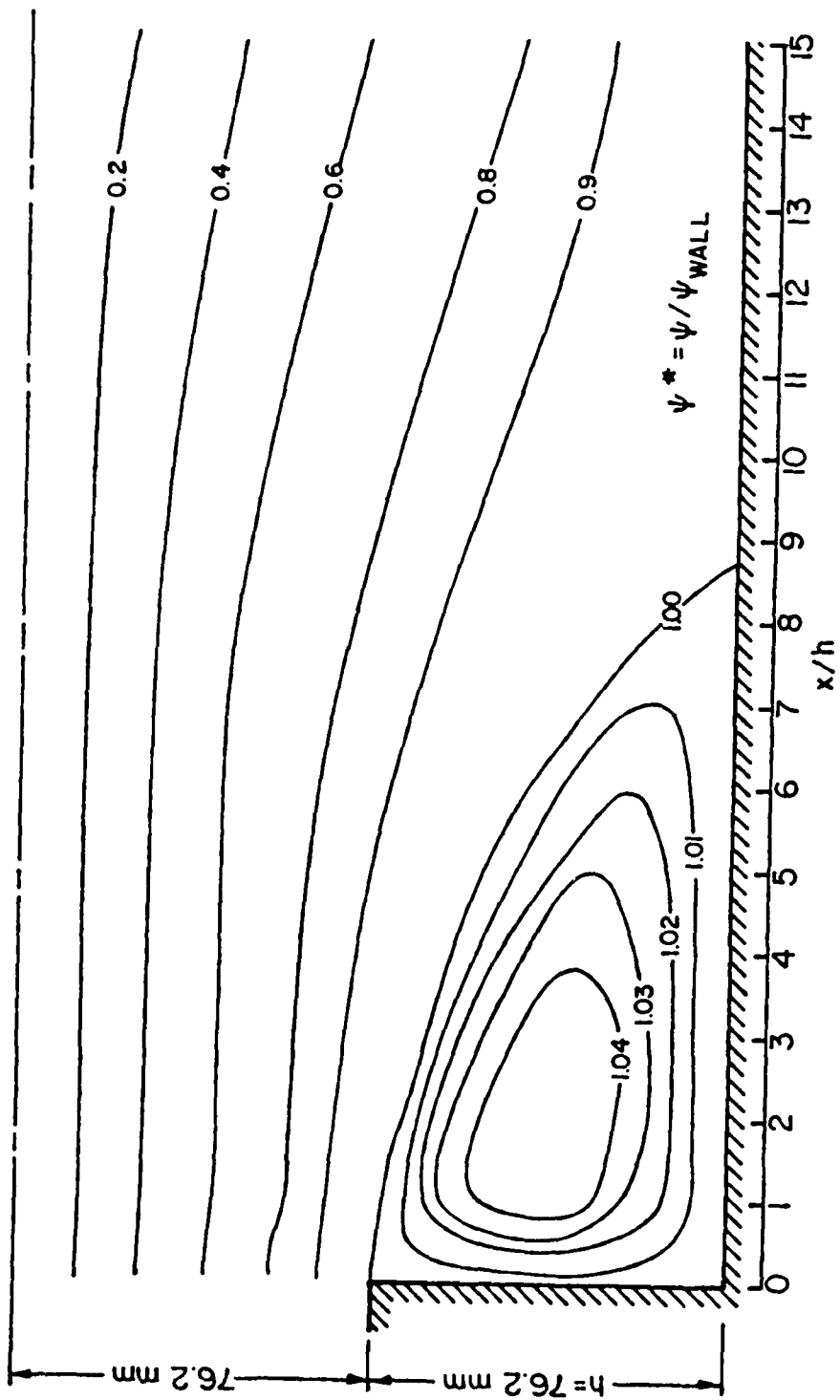


Figure 52. Predicted Normalized Stream Function Contours

## SECTION VII

### CONCLUSIONS AND RECOMMENDATIONS

Several conclusions can be drawn from the results of this investigation. Measurements of the mean streamwise velocity field in the presence of combustion showed the anticipated changes relative to the cold flow case. Those changes include higher mean velocities due to heat release and a shorter, stronger recirculation zone. The effects of combustion were not influential at planes upstream of three step heights.

Turbulence intensity measurements indicated significant differences in shear layer position and rate of turbulence decay for the hot flow case, but relatively small differences in peak normalized turbulence levels. Maximum normalized turbulence intensities were found to be approximately 22% in both the hot and cold flows, while local turbulence intensities were found to be much lower in the hot flow case, typically, 40 to 60% of the cold flow values. This seems to indicate that the turbulence production mechanism due to shear is similar in both flow cases, but that combustion tends to suppress the turbulence in regions away from the shear layer.

The results obtained in this study have again verified the fact that the velocity bias elimination method based on high seeding density and fixed interval data sampling is effective for highly turbulent internal flows. Normalized mass flux values calculated using unbiased mean velocity data agreed throughout the flow field to within  $\pm 3\%$ , while the calculations using the biased mean velocity data over-predicted the mass flux by as much as 24%. The sampling technique itself was also found to "bias" the statistical turbulent quantities (i.e. turbulence intensity and skewness) significantly in highly turbulent regions.

Numerical prediction of the mean velocity field using the CHAMPION 2/E/FIX code was reasonably accurate, although computed velocities in the center of the flow were substantially below those measured at downstream locations. A major deficiency in this code was the lack of mass flow conservation which may have led to the poor prediction of mean centerline velocities.

Some areas which need further investigation are as follows:

- 1) unbiased reacting flow measurements to determine directly the velocity bias
- 2) an effective velocity bias correction or elimination scheme that could be applied to flow measurements in sparsely seeded flow fields including those with significant density fluctuations
- 3) LDV measurements of tangential and radial mean velocities and turbulence intensities along with Reynolds stress correlations in both isothermal

and reacting flows; knowing these values and using the Favre averaged turbulent kinetic energy equation for this type of flow could explain the combustion-turbulence interaction in more detail

- 4) the effect of axial pressure gradient on the turbulence structure of the flow field also seems to be important and its effects need to be investigated systematically.

As a final comment it should be noted that no special problems were encountered when using the LDV in this combustion study. No observable degradation in signal quality was caused by refractive index fluctuations in the flow.

APPENDIX  
EXPERIMENTAL DATA

Table A1. Experimental Velocity and Turbulence Data (x/H=1)

R (mm)	R/R2	$\bar{U}$ (m/s)	$\bar{U}/U_1$	$\sqrt{\bar{U}'^2}/U_1$	$\sqrt{\bar{U}'^2}/U$
COLD FLOW (UNBIASED)					
0	0	21.963	.995	.038	.038
7.620	.100	21.701	.983	.044	.045
15.240	.200	20.661	.936	.053	.057
22.860	.300	19.332	.876	.063	.072
30.480	.400	17.060	.773	.075	.097
38.100	.500	11.049	.501	.151	.301
45.720	.600	.390	.018	.089	5.049
53.340	.700	-.612	-.028	.057	-2.055
60.960	.800	-.616	-.028	.067	-2.403
68.580	.900	-.411	-.019	.075	-4.010
COLD FLOW (BIASED)					
0	0	22.015	.998	.038	.038
7.620	.100	21.892	.992	.045	.045
15.240	.200	20.777	.941	.054	.058
22.860	.300	19.641	.890	.061	.069
30.480	.400	17.361	.787	.076	.096
38.100	.500	11.523	.522	.142	.271
45.720	.600	2.129	.096	.127	1.319
53.340	.700	-1.064	-.048	.070	-1.452
60.960	.800	-1.013	-.046	.067	-1.463
68.580	.900	-.821	-.037	.073	-1.970
HOT FLOW (BIASED)					
0	0	22.254	1.008	.040	.040
7.620	.100	22.221	1.007	.042	.041
15.240	.200	21.446	.972	.051	.052
22.860	.300	19.886	.901	.062	.069
30.480	.400	18.026	.817	.074	.090
38.100	.500	14.629	.663	.102	.153
45.720	.600	3.810	.173	.146	.844
53.340	.700	.904	.041	.202	4.928
60.960	.800	-.924	-.042	.084	-2.002
68.580	.900	-.250	-.011	.068	-6.001
Z/E/FIX					
0	0	22.575	1.023	-	-
3.810	.050	22.575	1.023	-	-
7.620	.100	22.155	1.004	-	-
11.430	.150	21.735	.985	-	-
15.240	.200	21.210	.961	-	-
19.050	.250	20.580	.932	-	-
22.860	.300	19.740	.894	-	-
26.670	.350	18.690	.847	-	-
30.480	.400	17.010	.771	-	-
34.290	.450	14.385	.652	-	-
38.100	.500	8.673	.393	-	-
41.910	.550	5.145	.233	-	-
45.720	.600	3.202	.145	-	-
49.530	.650	1.302	.059	-	-
53.340	.700	-.109	-.005	-	-
57.150	.750	-.930	-.042	-	-
60.960	.800	-1.428	-.065	-	-
64.770	.850	-1.785	-.081	-	-
68.580	.900	-2.079	-.094	-	-
72.390	.950	-2.415	-.109	-	-

Table A1.cont. Experimental Velocity and Turbulence Data (x/H=3)

R (mm)	R/R2	$\bar{U}$ (m/s)	$\bar{U}/U_1$	$\sqrt{\bar{u}^2}/U_1$	$\sqrt{\bar{u}^2}/U$
COLD FLOW (UNBIASED)					
0	0	22.040	.999	.041	.041
7.620	.100	22.112	1.002	.044	.044
15.240	.200	20.719	.979	.054	.058
22.860	.300	19.397	.879	.071	.080
30.480	.400	16.903	.770	.114	.149
38.100	.500	10.652	.483	.170	.352
45.720	.600	5.149	.233	.166	.711
53.340	.700	.648	.029	.137	4.662
60.960	.800	-1.289	-.050	.100	-1.705
68.580	.900	-2.901	-.131	.089	-.674
COLD FLOW (BIASED)					
0	0	22.100	1.001	.039	.039
7.620	.100	21.503	.979	.045	.046
15.240	.200	20.744	.940	.054	.057
22.860	.300	19.487	.883	.065	.074
30.480	.400	16.477	.747	.108	.144
38.100	.500	11.906	.539	.162	.300
45.720	.600	6.771	.307	.159	.519
53.340	.700	3.262	.149	.149	1.003
60.960	.800	-1.203	-.055	.139	-2.547
68.580	.900	-2.925	-.136	.094	-.689
HOT FLOW (BIASED)					
0	0	22.275	1.000	.042	.042
7.620	.100	22.471	1.018	.040	.039
15.240	.200	21.597	.979	.053	.054
22.860	.300	20.307	.920	.063	.069
30.480	.400	16.354	.632	.073	.088
38.100	.500	15.190	.688	.112	.162
45.720	.600	10.726	.486	.140	.288
53.340	.700	3.824	.173	.165	.955
60.960	.800	-2.605	-.118	.132	-1.119
68.580	.900	-4.819	-.218	.082	-.376
Z/E/FIX					
0	0	21.840	.990	-	-
3.810	.050	21.640	.970	-	-
7.620	.100	21.525	.975	-	-
11.430	.150	21.000	.952	-	-
15.240	.200	20.475	.928	-	-
19.050	.250	19.740	.894	-	-
22.860	.300	18.600	.847	-	-
26.670	.350	17.010	.771	-	-
30.480	.400	14.700	.666	-	-
34.290	.450	11.970	.542	-	-
38.100	.500	9.156	.415	-	-
41.910	.550	6.065	.303	-	-
45.720	.600	3.009	.209	-	-
49.530	.650	2.376	.130	-	-
53.340	.700	1.307	.064	-	-
57.150	.750	.163	.008	-	-
60.960	.800	-.876	-.040	-	-
64.770	.850	-1.753	-.079	-	-
68.580	.900	-2.927	-.113	-	-
72.390	.950	-3.923	-.155	-	-

Table A1.cont. Experimental Velocity and Turbulence Data (x/H=5)

R (mm)	R/R2	$\bar{U}$ (m/s)	$\bar{U}/U_1$	$\sqrt{\bar{U}'^2}/U_1$	$\sqrt{\bar{U}'^2}/\bar{U}$
COLD FLOW (UNBIASED)					
0	0	21.763	.966	.045	.046
7.620	.100	21.434	.971	.051	.052
15.240	.200	20.241	.917	.067	.073
22.860	.300	17.380	.787	.119	.151
30.480	.400	14.563	.660	.163	.247
38.100	.500	9.966	.452	.190	.420
45.720	.600	4.581	.208	.187	.903
53.340	.700	.014	.001	.150	231.105
60.960	.800	-1.501	-.023	.144	-6.343
68.580	.900	-1.951	-.088	.116	-1.308
COLD FLOW (BIASED)					
0	0	21.968	.995	.045	.045
7.620	.100	21.563	.977	.051	.052
15.240	.200	20.404	.925	.064	.069
22.860	.300	18.181	.824	.100	.122
30.480	.400	16.144	.731	.140	.191
38.100	.500	11.474	.520	.172	.330
45.720	.600	7.018	.318	.184	.578
53.340	.700	.819	.037	.195	5.252
60.960	.800	-1.502	-.072	.163	-2.269
68.580	.900	-2.000	-.091	.127	-1.400
HOT FLOW (BIASED)					
0	0	22.162	1.004	.042	.042
7.620	.100	21.927	.996	.044	.044
15.240	.200	21.533	.976	.054	.055
22.860	.300	20.255	.918	.066	.072
30.480	.400	18.119	.821	.081	.093
38.100	.500	14.675	.665	.119	.180
45.720	.600	10.922	.495	.147	.297
53.340	.700	7.005	.317	.169	.533
60.960	.800	1.829	.086	.225	2.628
68.580	.900	-4.372	-.198	.135	-1.680
2/E/FIX					
0	0	20.625	.937	-	-
3.810	.050	20.685	.937	-	-
7.620	.100	20.370	.923	-	-
11.430	.150	19.740	.894	-	-
15.240	.200	18.900	.856	-	-
19.050	.250	17.745	.804	-	-
22.860	.300	16.065	.728	-	-
26.670	.350	14.175	.642	-	-
30.480	.400	12.180	.552	-	-
34.290	.450	10.090	.457	-	-
38.100	.500	8.137	.369	-	-
41.910	.550	6.363	.288	-	-
45.720	.600	4.767	.216	-	-
49.530	.650	3.260	.152	-	-
53.340	.700	2.110	.096	-	-
57.150	.750	1.018	.046	-	-
60.960	.800	.006	.003	-	-
64.770	.850	-.760	-.034	-	-
68.580	.900	-1.420	-.067	-	-
72.390	.950	-2.383	-.108	-	-

Table A1.cont. Experimental Velocity and Turbulence Data (x/H=7)

R (mm)	R/R2	$\bar{U}$ (m/s)	$\bar{U}/U1$	$\sqrt{\bar{U}'^2}/U1$	$\sqrt{\bar{U}'^2}/U$
COLD FLOW (UNBIASED)					
0	0	13.915	.902	.063	.070
7.620	.100	19.945	.904	.075	.083
15.240	.200	18.377	.833	.110	.141
22.860	.300	15.435	.699	.171	.244
30.480	.400	11.132	.504	.196	.390
38.100	.500	8.295	.376	.205	.545
45.720	.600	4.643	.210	.106	.684
53.340	.700	1.817	.082	.167	2.025
60.960	.800	.662	.030	.151	5.035
68.580	.900	-.711	-.032	.123	-3.827
COLD FLOW (BIASED)					
0	0	20.851	.945	.064	.067
7.620	.100	20.445	.926	.070	.076
15.240	.200	19.755	.895	.031	.102
22.860	.300	16.531	.749	.146	.196
30.480	.400	12.810	.580	.178	.307
38.100	.500	9.233	.418	.179	.428
45.720	.600	6.722	.305	.203	.665
53.340	.700	3.061	.139	.203	1.462
60.960	.800	1.168	.053	.175	3.306
68.580	.900	-.639	-.029	.158	-5.462
HOT FLOW (BIASED)					
0	0	21.534	.976	.051	.052
7.620	.100	21.746	.985	.049	.050
15.240	.200	20.568	.932	.055	.059
22.860	.300	19.997	.906	.065	.071
30.480	.400	16.974	.769	.095	.124
38.100	.500	14.039	.636	.134	.210
45.720	.600	10.307	.467	.152	.326
53.340	.700	7.455	.338	.167	.494
60.960	.800	3.133	.142	.210	1.478
68.580	.900	-.350	-.017	.176	-10.209
Z/E/FIX					
0	0	19.005	.861	-	-
3.810	.050	19.005	.861	-	-
7.620	.100	18.375	.833	-	-
11.430	.150	17.325	.785	-	-
15.240	.200	16.170	.733	-	-
19.050	.250	14.805	.671	-	-
22.860	.300	13.230	.599	-	-
26.670	.350	11.655	.520	-	-
30.480	.400	10.122	.459	-	-
34.290	.450	8.631	.391	-	-
38.100	.500	7.224	.327	-	-
41.910	.550	5.922	.260	-	-
45.720	.600	4.725	.214	-	-
49.530	.650	3.643	.165	-	-
53.340	.700	2.667	.121	-	-
57.150	.750	1.795	.081	-	-
60.960	.800	1.028	.047	-	-
64.770	.850	.351	.016	-	-
68.580	.900	-.253	-.011	-	-
72.390	.950	-1.029	-.047	-	-

Table A1.cont. Experimental Velocity and Turbulence Data (x/H=9)

R (mm)	R/R2	$\bar{U}$ (m/s)	$\bar{U}/U_1$	$\sqrt{U'^2}/U_1$	$\sqrt{U'^2}/\bar{U}$
COLD FLOW (UNBIASED)					
0	0	17.600	.797	.134	.168
2.620	.034	17.583	.797	.138	.173
10.240	.134	16.639	.754	.160	.212
17.860	.234	14.991	.679	.182	.268
25.480	.334	12.095	.540	.203	.370
33.100	.434	8.758	.397	.205	.517
40.720	.534	7.037	.319	.202	.633
48.340	.634	4.442	.201	.188	.933
55.960	.734	2.350	.106	.162	1.525
63.580	.834	.665	.039	.139	3.552
COLD FLOW (BIASED)					
0	0	18.300	.829	.082	.099
2.620	.034	19.272	.828	.104	.126
10.240	.134	17.633	.799	.125	.157
17.860	.234	15.202	.689	.169	.245
25.480	.334	12.881	.584	.184	.316
33.100	.434	10.214	.463	.184	.399
40.720	.534	8.184	.371	.195	.527
48.340	.634	6.185	.280	.182	.650
55.960	.734	3.560	.162	.186	1.149
63.580	.834	1.647	.075	.176	2.355
HOT FLOW (BIASED)					
0	0	20.000	.942	.041	.043
2.620	.034	20.725	.939	.042	.044
10.240	.134	20.046	.908	.053	.059
17.860	.234	18.681	.856	.068	.080
25.480	.334	17.216	.780	.094	.121
33.100	.434	15.590	.706	.115	.163
40.720	.534	12.557	.569	.140	.245
48.340	.634	9.210	.417	.167	.400
55.960	.734	5.564	.252	.168	.666
63.580	.834	3.766	.172	.174	1.015
2/E/FIX					
0	0	15.645	.709	-	-
3.810	.050	15.645	.709	-	-
7.620	.100	15.015	.680	-	-
11.430	.150	14.070	.638	-	-
15.240	.200	13.125	.595	-	-
19.050	.250	11.970	.542	-	-
22.860	.300	10.815	.490	-	-
26.670	.350	9.733	.441	-	-
30.480	.400	8.620	.391	-	-
34.290	.450	7.549	.342	-	-
38.100	.500	6.531	.296	-	-
41.910	.550	5.586	.253	-	-
45.720	.600	4.704	.213	-	-
49.530	.650	3.885	.176	-	-
53.340	.700	3.150	.143	-	-
57.150	.750	2.478	.112	-	-
60.960	.800	1.879	.085	-	-
64.770	.850	1.354	.061	-	-
68.580	.900	.893	.040	-	-
72.390	.950	.496	.012	-	-

Table A1.cont. Experimental Velocity and Turbulence Data (x/H=11)

R (mm)	R/R2	$\bar{U}$ (m/s)	$\bar{U}/U_1$	$\sqrt{\bar{U}'^2}/U_1$	$\sqrt{\bar{U}'^2}/\bar{U}$
COLD FLOW (UNBIASED)					
0	0	15.016	.000	.190	.291
7.620	.100	14.640	.663	.197	.297
15.240	.200	13.437	.609	.203	.333
22.860	.300	11.261	.510	.214	.419
30.480	.400	8.077	.402	.203	.504
38.100	.500	6.925	.314	.195	.620
45.720	.600	5.219	.236	.170	.753
53.340	.700	3.245	.147	.156	1.059
60.960	.800	2.023	.092	.133	1.446
68.580	.900	1.205	.057	.118	2.066
COLD FLOW (BIASED)					
0	0	15.942	.722	.165	.228
7.620	.100	15.374	.697	.177	.254
15.240	.200	13.375	.607	.185	.305
22.860	.300	11.049	.537	.189	.351
30.480	.400	10.043	.455	.192	.421
38.100	.500	8.718	.395	.187	.473
45.720	.600	6.236	.283	.181	.640
53.340	.700	4.603	.209	.172	.826
60.960	.800	3.330	.151	.161	1.065
68.580	.900	1.489	.057	.130	2.071
HOT FLOW (BIASED)					
0	0	20.081	.910	.048	.053
7.620	.100	20.000	.936	.047	.050
15.240	.200	19.184	.869	.056	.064
22.860	.300	18.211	.825	.076	.092
30.480	.400	16.268	.737	.105	.142
38.100	.500	15.022	.681	.116	.170
45.720	.600	13.014	.590	.125	.213
53.340	.700	10.135	.499	.147	.320
60.960	.800	7.926	.361	.159	.440
68.580	.900	5.415	.245	.111	.453
2/E/FIX					
0	0	11.760	.533	-	-
3.810	.050	11.760	.533	-	-
7.620	.100	11.445	.519	-	-
11.430	.150	10.920	.495	-	-
15.240	.200	10.290	.466	-	-
19.050	.250	9.618	.436	-	-
22.860	.300	8.893	.403	-	-
26.670	.350	8.153	.370	-	-
30.480	.400	7.413	.336	-	-
34.290	.450	6.673	.303	-	-
38.100	.500	5.935	.272	-	-
41.910	.550	5.203	.241	-	-
45.720	.600	4.693	.213	-	-
49.530	.650	4.116	.186	-	-
53.340	.700	3.570	.162	-	-
57.150	.750	3.076	.139	-	-
60.960	.800	2.625	.119	-	-
64.770	.850	2.226	.101	-	-
68.580	.900	1.869	.085	-	-
72.390	.950	1.575	.062	-	-

Table A1.cont. Experimental Velocity and Turbulence Data (x/H=15)

R (mm)	R/R2	$\bar{U}$ (m/s)	$\bar{U}/U_1$	$\sqrt{\bar{U}'^2}/U_1$	$\sqrt{\bar{U}''^2}/U_1$
<b>COLD FLOW (UNBIASED)</b>					
0	0	9.368	.424	.163	.384
7.620	.100	9.156	.415	.171	.412
15.240	.200	9.297	.421	.165	.393
22.860	.300	8.406	.365	.162	.421
30.480	.400	7.502	.320	.154	.454
38.100	.500	6.408	.274	.149	.507
45.720	.600	4.974	.205	.129	.572
53.340	.700	4.009	.184	.117	.636
60.960	.800	3.393	.153	.116	.753
68.580	.900	2.914	.132	.102	.773
<b>COLD FLOW (BIASED)</b>					
0	0	9.911	.449	.160	.356
7.620	.100	9.945	.451	.154	.341
15.240	.200	9.679	.439	.160	.365
22.860	.300	8.754	.397	.154	.387
30.480	.400	7.136	.323	.146	.452
38.100	.500	6.930	.314	.142	.453
45.720	.600	5.377	.244	.129	.493
53.340	.700	4.926	.223	.113	.507
60.960	.800	4.440	.201	.108	.535
68.580	.900	3.900	.177	.104	.590
<b>HOT FLOW (BIASED)</b>					
0	0	19.342	.876	.062	.071
7.620	.100	19.629	.889	.070	.079
15.240	.200	19.330	.881	.069	.106
22.860	.300	16.998	.770	.112	.145
30.480	.400	14.763	.669	.122	.182
38.100	.500	12.949	.587	.128	.218
45.720	.600	11.799	.535	.127	.237
53.340	.700	10.761	.488	.120	.246
60.960	.800	8.962	.405	.114	.291
68.580	.900	5.179	.235	.120	.510
<b>2/E/FIX</b>					
0	0	7.093	.322	-	-
3.810	.050	7.093	.322	-	-
7.620	.100	6.993	.317	-	-
11.430	.150	6.656	.311	-	-
15.240	.200	6.678	.303	-	-
19.050	.250	6.408	.293	-	-
22.860	.300	6.237	.283	-	-
26.670	.350	5.985	.271	-	-
30.480	.400	5.722	.259	-	-
34.290	.450	5.439	.246	-	-
38.100	.500	5.166	.234	-	-
41.910	.550	4.882	.221	-	-
45.720	.600	4.609	.209	-	-
49.530	.650	4.347	.197	-	-
53.340	.700	4.095	.186	-	-
57.150	.750	3.864	.175	-	-
60.960	.800	3.633	.165	-	-
64.770	.850	3.403	.156	-	-
68.580	.900	3.234	.147	-	-
72.390	.950	2.950	.134	-	-

Table A2. Experimental Temperature Data

r/R	THERMOCOUPLE RAKE LOOKING DOWNSTREAM *			
	TOP	LEFT	BOTTOM	RIGHT
0.9	705	820	834	861
0.8	682	809	785	868
0.7	630	785	721	848
0.6	552	671	595	750
0.5	471	560	482	647
0.4	397	441	385	527
0.3	322	350	313	414
0.2	275	293	275	332
0.1	250	260	246	271
0.0	232	235	232	235

\*Thermocouple rake located at  $x/H=17.7$  and all temperatures are in degrees Centigrade

REFERENCES

## REFERENCES

- [1] Stevenson, W.H., Experimental Diagnostics in Gas Phase Combustion Systems, Progress in Astronautics and Aeronautics, Vol. 53, AIAA Publication, New York, 1977.
- [2] Thompson, H.D., and Flack, R., Jr., "An Application of Laser Velocimetry to the Interpretation of Turbulent Structure," Proceedings of the ISL/AGARD Workshop on Laser Anemometry, German-French Research Institute, Pfeifer, H., and Haertig, J., editors, St.-Louis, France, 1976.
- [3] Bremner, R., Thompson, H.D., Stevenson, W.H., "An Experimental and Numerical Comparison of Turbulent Flow Over a Step," APWL-TR-80-2105, December 1980.
- [4] Roesler, T., Stevenson, W.H., and Thompson, H.D., "Investigaion of Bias Errors in Laser Doppler Velocimeter Measurements," APWAL-TR-80-2108, December 1980.
- [5] Stevenson, W.H., Thompson, H.D., and Roesler, T.C., "Direct Measurement of Laser Velocimeter Bias Errors in a Turbulent Flow," AIAA Journal, 1982. (To be published)
- [6] Eaton, J.K., and Johnston, J.P., "Turbulent Flow Reattachment: An Experimental Study of the Flow and Structure Behind Backward-Facing Step," Report MD-39, Mechanical Engineering, Stanford University, 1980.
- [7] Eaton, J.K., and Johnston, J.P., "An Evaluation of Data for Backward-Facing Step Flow: Report prepared for the 1980/81 Conferences on Complex Turbulent Flows," Dept. of Mechanical Engineering, Stanford University, 1980.
- [8] Macagno, E.O., and Hung, T.K., "Computational and Experimental Study of a Captive Annular Eddy," Journal of Fluid Mechanics, Vol. 28, pt. 1, pp. 43-63, 12 April, 1967.

REFERENCES (con'd)

- [9] Zemanick, P.P., and Dougall, R.S., "Local Heat Transfer Downstream of an Abrupt Circular Channel Expansion," ASME Journal of Heat Transfer, Vol. 92, pp. 53-60, February, 1970.
- [10] Back, L.H., and Roschke, E.J., "Shear-Layer Flow Regimes and Wave Instabilities and Reattachment Lengths Downstream of an Abrupt Circular Channel Expansion," ASME Journal of Applied Mechanics, Vol. 945, pp. 677-681, September, 1972.
- [11] Freeman, A.R., "Laser Anemometer Measurements in the Recirculating Region Downstream of a Sudden Pipe Expansion," In Proceedings of the LDA-Symposium Copenhagen, pp. 704-709, 1975.
- [12] Moon, L.F., and Rudinger, G., "Velocity Distribution in an Abruptly Expanding Circular Duct," ASME Journal of Fluids Engineering, Vol. 99, pp. 226-230, March, 1977.
- [13] Drewry, J.E., "Fluid Dynamic Characterization of Sudden-Expansion Ramjet Combustor Flowfields," AIAA Journal, Vol. 16, No. 4, pp. 313-319, April, 1979.
- [14] Kangovi, S., and Page, R.H., "Subsonic Turbulent Flow Past a Downstream Facing Annular Step," ASME Journal of Fluids Engineering, Vol. 101, pp. 230-236, June, 1979.
- [15] Stevenson, W.H., Thompson, H.D., and Luchik, T.S., "Laser Velocimeter Measurements and Analysis in Turbulent Flows with Combustion, AFWAL-TR-82-2076, Part I, September, 1982.
- [16] Logan, S.E., "A Laser Velocimeter for Reynolds Stress and Other Turbulence Parameters," AIAA Journal, Vol. 19, No. 7, pp. 933-935, 1972.
- [17] Eaton, J.K., Johnston, J.P., and Jeans, A.H., "Measurements in a Reattachment Turbulent Shear Layer," 2nd Symposium on Turbulent Shear Flows, Imperial College, London, 2-4 July, 1979.
- [18] Kuehn, D.M., "Effects of Adverse Pressure Gradient on the Incompressible Reattaching Flow over a Rearward-Facing Step," AIAA Journal, Vol. 18, No. 3, pp. 343-344, March, 1980.

REFERENCES (cont'd)

- [19] Harlow, F.H., and Nakayama, P., "Transport of Turbulence Decay Rate," Los Alamos Science Laboratory, University of California Report LA-3854, 1968.
- [20] Launder, B.E., and Spalding, D.B., "The Numerical Computation of Turbulent Flows," Computer Methods in Applied Mechanics and Engineering, Vol. 3, pp. 269-289, 1974.
- [21] Launder, B.E., Morse, A., Rodi, W., and Spalding, D.B., "The Prediction of Free Shear Flows - A Comparison of the Performance of Six Turbulence Models," In: Proceedings of NASA Conference on Free Shear Flows, Lagley, 1972.
- [22] Gosman, A.D., Khalil, E.E., and Whitelaw, J.H., "The Calculation of Two-Dimensional Turbulent Recirculating Flows," Turbulent Shear Flows I, Springer-Verlag, New York, pp. 13.35-13.45, 1977.
- [23] Teysandier, R.G., and Wilson, M.P., "An Analysis of Flow Through Sudden Enlargements in Pipes," Journal of Fluid Mechanics, Vol. 64, pt. 1, pp. 85-95, 3 June, 1974.
- [24] Fujii, S., and Eguchi, K., "A Comparison of Cold and Reacting Flows Around a Bluff Body Flame Stabilizer," ASME Journal of Fluids Engineering, Vol. 103, pp. 328-334, June, 1981.
- [25] Williams, G.C., Hottel, H.C., and Scurlock, A.C., "Flame Stabilization and Propagation in High Velocity Gas Streams," 3rd Symposium on Combustion and Flame, and Explosion Phenomena, p. 21, 1949.
- [26] Durao, D.P.G., and Whitelaw, J.H., "Velocity Characteristics of Disc-Stabilized Diffusion and Premixed Flames," AIAA Paper 76-34, 1976.
- [27] Hartmann, V., "LDA Measurements of Velocity and Turbulence Characteristics in Enclosed Turbulent Diffusion Flames," Proceedings Appl. LDA to Fluid Mechanics, Lisbon, 1982.
- [28] Baker, R.J., Hutchinson, P., Khalil, E.E., and Whitelaw, J.H., "Measurements of Three Velocity Components in a Model Furnace with and without Combustion," Proceedings of the 15th Symposium (International) on Combustion, The Combustion Institute, p. 553, 1974.

REFERENCES (cont'd)

- [29] Pitz, R.W., "An Experimental Study of Combustion: The Turbulent Structure of a Reacting Shear Layer Formed at a Rearward-Facing Step," NASA Contractor Report 165427, 1981.
- [30] Starner, S.H., and Bilger, R.W., "LDA Measurements in a Turbulent Diffusion Flame with Axial Pressure Gradient," Combustion Science and Technology, Vol. 21, pp. 259-276, 1980.
- [31] Glass, M. and Bilger, R.W., "The Turbulent Jet Diffusion Flame in a Co-flowing Stream - Some Velocity Measurements," Combustion Science and Technology, 18, pp. 165-177, 1978.
- [32] Bray, K.N.C., "The Interaction Between Turbulence Combustion," Proceedings of the 17th Symposium (International) on Combustion, The Combustion Institute, p. 223, 1978.
- [33] Khalil, E.E., Spalding, D.B., and Whitelaw, J.H., "Calculation of Local Flow Properties in Two Dimensional Furnaces," International Journal of Heat and Mass Transfer, Vol. 18, p. 775, 1975.
- [34] Hutchinson, P., Khalil, E.E., and Whitelaw, J.H., "Measurement and Calculation of Furnace Flow Properties," AIAA Journal of Energy, Vol. 1, No. 4, pp. 212-219, August, 1977.
- [35] Gosman, A.D., Lockwood, F.C., and Salooja, A.P., "The Prediction of Cylindrical Furnaces Gaseous Fueled with Premixed and Diffusion Burners," Proceedings of the 17th Symposium (International) on Combustion, The Combustion Institute, pp. 747-760, 1978.
- [36] Baker, R.J., Hutchinson, P., and Whitelaw, J.H., "Preliminary Measurements of Instantaneous Velocity in a 2m Square Furnace Using Laser Anemometry," Journal of Heat Transfer, Vol. 96, p. 410, August, 1974.
- [37] Barlow, S.M., "Laser Doppler Anemometry Measurements in a Large Gas-Fired Furnace," Proceedings Appl. LDA to Fluid Mechanics, Lisbon, 1982.

REFERENCES (cont'd)

- [38] McLaughlin, D.K., and Tiederman, W.G., "Bias Correction for Individual Realization Laser Anemometry Measurements in Turbulent Flows," Physics of Fluids, Vol. 16, No. 12, p. 2082, 1973.
- [39] Barnett, D., and Bentley, H., "Statistical Bias of Individual Realization Laser Velocimeters," Proceedings of the Second International Workshop on Laser Velocimetry, Purdue University, p. 428, 1974.
- [40] Dimotakis, P.E., "Single Scattering Particle Laser Doppler Measurements of Turbulence," Proceedings of the ISL/AGARD Workshop on Laser Anemometry, German-French Research Institute, St.-Louis, France, p. 189, 1976.
- [41] Buchhave, P., "Biasing Errors in Individual Particle Measurements with the LDA-Counter Signal Processor," Proceedings LDA-Symposium, Copenhagen, p. 258, 1975.
- [42] Edwards, R.V., and Jensen, A.S., "Output Statistics of Laser Anemometers in Sparsely Seeded Flows," Proceedings Appl. LDA to Fluid Mechanics, Lisbon, 1982.
- [43] Hoesel, W., and Rodi, W., "New Biasing Elimination Method for Laser Doppler Velocimeter Counter Processing," Review of Scientific Instruments, Vol. 48, No. 7, p. 910, 1977.
- [44] Durao, D.F.G., Laker, J., and Whitelaw, J.H., "Bias Effects in Laser Doppler Anemometry," Journal of Physics E, Vol. 13, p. 442, 1980.
- [45] Erdmann, J.C., and Tropea, C.D., "Statistical Bias of the Velocity Distribution Function in Laser Anemometry," Proceedings Appl. LDA to Fluid Mechanics, Lisbon, 1982.
- [46] Johnson, D.A., Modarress, D., and Owen, F.K., "An Experimental Verification of Laser-Velocimeter Sampling Bias Correction," Proc. of the Symp. on Engr. Appl. of Laser Velocimetry, ASME Winter Annual Meeting, Phoenix, AZ, Nov. 1982.
- [47] Tiederman, W.G., "Interpretation of Laser Velocimeter Measurements in Turbulent Boundary Layers and Regions of Separation," Symposium on Turbulence, Edited by G.K. Patterson and J.L. Zakin, Science Press, pp. 153-161, 1977.

REFERENCES (cont'd)

- [48] McVey, R., "The Design of a Laser Doppler Velocimeter for use in Studying Turbulent and Mixing Flows," Master's Thesis, Purdue University, 1979.
- [49] Instruction Manual for TSI Model 1980 Counter, Thermo-Systems Incorporated, St. Paul, Minnesota.
- [50] Baker, R.J., Hutchinson, P., and Whitelaw, J.H., "Velocity Measurements in the Recirculation Region of an Industrial Burner Flame by Laser Anemometry with Light Frequency Shifting," Combustion and Flame, Vol. 23, pp. 57-71, 1974.
- [51] Karpuk, M.E., and Tiederman, W.G., "Effect of Finite Size Probe Volume Upon Laser Doppler Anemometer Measurements," AIAA Journal, Vol. 14, No. 8, pp. 1099-1105, Aug. 1976.